# SYNTHESIS OF SMART NANOMATERIALS FOR PRECONCENTRATION AND DETECTION OF E.COLI IN WATER

by

THEMBISILE PATIENCE MAHLANGU

submitted in accordance with the requirements
for the degree of

MAGISTER TECHNOLOGIAE

in the subject

Chemical Engineering

at the

UNIVERSITY OF SOUTH AFRICA

SUPERVISOR: PROF. A MAITY

CO-SUPERVISOR: DR A CHETTY

JUNE 2015

**DECLARATION**

I declare that this dissertation titled “Synthesis of smart nanomaterials for preconcentration and detection of *E. coli* in water”, is my own work and that the sources that I have used have been indicated and acknowledged by means of complete references.

I further declare that I have not previously sumbitted this work, or part of it, for examination at UNISA for another qualification or at any other higher education institution.

_____ on this _____ day of _____

(Candidate)

_____ on this _____ day of _____

(Supervisor)

_____on this _____ day of _____

(Co-supervisor)

## DEDICATION

I dedicate this dissertation to my late grandmother, Hester Nofanezile Masemola, and my loving family (Daniel Mahlangu, Shirley Mahlangu and Busisiwe Mahlangu). The tremendous support and encouragement during the course of my studies was not in vain.

**ACKNOWLEDGMENTS**

I would like to thank God for granting me the strength and wisdom to pursuit this study. I would not have been here should He had not permitted me to walk in this path.

I would like to extend my gratitude to the following people, insitutions and organisations for their contributions towards the completion of this study:

Prof Arjun Maity for his supervision and invaluable insight and guidance througout this study.

Dr Avashnee Chetty for her supervision, technical input and continuous support throughtout this study.

Dr Ilse du Preez for her unwithering support and assistance with the biological aspect of this study.

Dr James Wesley-Smith and Dr David Motaung for their assistance and training with TEM and spectrofluorometry respectively.

Mrs Charity Maepa and Mrs Antoinette Buys for their assistance with SEM.

Mrs Andri Swanepoel (my shoulder to cry on) for being there for me through all the challenges I have face with this study and for the moral support.

CSIR (Polymers and Composites) and staff, thank you for trusting me with this project and for the financial support.

To my lovely family and friends, I appreciate the words of encouragement, your support and for always being there for me.

My best friend Samuel Monama, thank you for all the love, support and encouragement throughout this period. I am truly grateful.

## EXECUTIVE SUMMARY

It is common knowledge that water is one of the basic needs for human beings. However, the consumption of contaminated water can lead to waterborne diseases and fatalities. It is, therefore imperative to constantly monitor the quality of potable water. There are numerous technologies used for water quality monitoring. These technologies are relatively effective however these tests are expensive and complex to use, which then require experienced technicians to operate them. Other tests are not rapid, making consumers of water susceptible to waterborne diseases. In this study, dye-doped, surface functionalized silica nanoparticles (SiNPs) and surface-functionalized magnetic nanocomposites (MNCs) were proposed as materials that can be applied in order to reduce the time taken to get results as well as to make the processes less complex and portable.

The aim of this study was to synthesize and characterize surface functionalized dye-doped SiNPs and surface functionalized MNCs for detection and preconcentration of in water. Additionally, proof of concept had to be shown using the synthesized materials.

SiNPs were the materials of choice due to their easily functionalized surfaces and their strong optical properties. SiNPs are photostable and they do not leach in solution due to the inert nature of the silica matrix in aqueous media. MNCs were chosen as materials of choice for preconcentration of *E. coli* in water because they are easy to synthesize and they can be applied in various biological applications due to their functional groups.

SiNPs were synthesized using the water-in-oil microemulsion. The SiNPs were further functionalized with amine and carboxyl groups and avidin. Thereafter, they were bioconjugated with biotinylated anti-*E. coli* antibodies. The pure and surface functionalized SiNPs were characterized using ATR-FTIR spectroscopy, FE-SEM, HR-TEM, Zeta Sizer, UV-vis spectroscopy and spectrofluorometry. The application of the dye—doped surface functionalized SiNPs in *E. coli* detection was characterized using the fluorescence plate reader. The SiNPs were spherical and uniform in size. They increased in size as they were being functionalized, ranging from 21.20 nm to 75.06 nm. The SiNPs were successfully functionalized with amine and carboxyl groups as well as with avidin and antibodies. Two methods were

investigated for carboxyl group attachment (direct and indirect attachment) and the direct attachment method yielded the best results with a surface charge of -31.9 mV compared to -23.3 mV of the indirect method. The dye loading was found to be 1% after particle synthesis. The optical properties of the Ru(Bpy) dye were enhanced 3 fold when they were encapsulated in the Si matrix. The SiNPs were binding to the *E. coli* cells and enabled detection.

MNCs were synthesized through in-situ polymerization. The MNCs were characterized using ATR-FTIR spectroscopy, SEM, TEM and XRD. The MNCs were successfully functionalized with carboxyl groups. The increase in size of the nanocomposites as seen in SEM images proved that the $Fe_3O_4$ was successfully encapsulated in the polymer matrix. The MNCs were proven to be magnetic by a simple magnetism test whereby they were separated in an aqueous solution using an external magnetic field. The antibody-labelled MNCs were binding to the *E. coli* cells as shown in TEM images. *E. coli* cells were removed from water at varying concentrations of $1x10^6$ CFU/mL to $1x10^9$ CFU/mL at 10 mL volumes.

This study has demonstrated that dye-doped SiNPs amplify the signal of *E. coli* cells using fluorescence. The study has also demonstrated that the MNCs can be applied in sample preconcentration and enrichment for *E. coli* detection. However, further studies should investigate and optimize the combination of the two techniques in a point of use device for water quality testing of 100 mL-samples as per the requirement of the SANS 241 standard.

## PRESENTATIONS AND PUBLICATIONS

The work featured in this dissertation has been presented in the following conferences and is in preparation for submission to scientific journals for publication.

### Conference presentations

T. Mahlangu, A. Chetty and A. Maity, Synthesis of Dye-doped Amine Functionalized SiNPs for Rapid Bacteria Detection in Water. Oral presentation, 12th International Chemistry Conference Africa, University of Pretoria, South Africa, 8 - 12 July 2013.

T. Mahlangu, A Chetty and A Maity, Synthesis of Dye-doped Surface Functionalized SiNPs for Rapid Bacteria Detection in Water. Poster presentation, Young Water Professionals Conference, University of Stellenbosch, South Africa, 16 - 18 July 2013.

T. Mahlangu, A. Chetty, I. duPreez and A. Maity, Synthesis of Dye-doped Surface Functionalized SiNPs for Rapid Bacteria Detection. Oral presentation, Fourth CSIR Emerging Researchers Symposium, CSIR, South Africa, 29 - 30 October 2013 (Best Oral presentation award).

T. Mahlangu, A. Chetty, I. duPreez and A. Maity, Synthesis of smart nanomaterials for preconcentration & detection of *E. coli* in water. Oral presentation, International Symposium on Macro-and Supramolecular Architectures and Materials, Emperors Palace Hotel Casino, Johannesburg, South Africa, 23 - 27 November 2014

T Mahlangu, Making the invisible visible, FameLab competition, Grahamastown, 16 – 20 March 2015.

### Manuscripts in Preparation

T. Mahlangu, I. du Preez, A. Swanepoel, A. Maity and A. Chetty, Dye-doped Silica Nanoparticles: Synthesis and application. The manuscript is in preparation for submission to a scientific journal.

T. Mahlangu, I. du Preez, A. Swanepoel, A. Maity and A. Chetty, Immunomagnetic Separation of *E. coli* from water using poly(1-(2-carboxyethyl)pyrrole) magnetic nanocomposites. The manuscript is in preparation for submission to a scientific journal.

**Table of Contents**


**DECLARATION** ..... I

**DEDICATION** ..... II

**ACKNOWLEDGMENTS** ..... III

**EXECUTIVE SUMMARY** ..... IV

**PRESENTATIONS AND PUBLICATIONS** ..... VI

**CHAPTER 1: INTRODUCTION** ..... 1

**a. Preconcentration** ..... 3
**b. Detection and signal amplification** ..... 4
**c. Hypothesis** ..... 6
**d. Objectives** ..... 6

**CHAPTER 2: LITERATURE REVIEW** ..... 8

**2.1. Conventional detection methods** ..... 8
2.1.1. Culturing and plating method ..... 8
2.1.2. Laboratory-based biochemical methods for pathogen detection ..... 9
**2.2. Nanoparticles as bioprobes** ..... 12
**2.3. Bioconjugation of nanoparticles** ..... 12
2.3.1. Antibodies ..... 12
2.3.2. Carbodiimide Chemistry ..... 14
2.3.3. Preconcentration or enrichment of pathogens ..... 15
**2.4. Fluorescence Detection** ..... 25
**2.5. Conclusions and recommendations** ..... 31

**CHAPTER 3: INSTRUMENTATION AND CHARACTERIZATION** ..... 32

**3.1. Infrared Spectroscopy** ..... 32
**3.2. X-ray diffraction technique** ..... 33
**3.3. Scanning Electron microscopy** ..... 34
**3.4. Transmission electron microscopy** ..... 35
**3.5. Ultraviolet and visible spectroscopy** ..... 35
**3.6. Dynamic light scattering** ..... 36
**3.7. Fluorescence Spectroscopy (Spectrofluorometer)** ..... 37

**CHAPTER 4: SYNTHESIS AND CHARACTERIZATION OF SURFACE FUNCTIONALIZED SILICA NANOPARTICLES** ..... 39

**4.1. Introduction** ..... 39
**4.2. Experimental Design** ..... 39
4.2.1. Materials ..... 39
4.2.2. Synthesis of silica nanoparticles (SiNPs) ..... 40
4.2.3. Chemical modification of SiNPs ..... 41
4.2.3.1. Attachment of amine groups to the SiNPs ..... 41
4.2.3.2. Carboxyl surface functionalization ..... 42
4.2.4. Immobilization of avidin to nanoparticles ..... 44
4.2.5. Attachment of biotinylated-antibodies to avidin-functionalized SiNPs ..... 45
4.2.6. Culture of *E. coli* ..... 45
4.2.7. Avidin Quantification ..... 45
4.2.8. Dye-loading of Ru(Bpy) dye in SiNPs ..... 48
*4.2.9.* SiNPs-labelled *E. coli* fixing for TEM analysis ..... 48
*4.2.10.* *E. coli* detection through fluorescence microscopy ..... 49
4.2.11. Application of SiNPs for *E. coli* detection ..... 49
**4.3. Material characterisation** ..... 50
**4.4. Results and Discussions** ..... 50

4.4.1. Synthesis of dye-doped SiNPs....50
4.4.2. Mass yield....55
4.4.3. Surface charge....56
4.4.4. Attenuated Total Reflection Fourier Transform Infrared (ATR-FTIR) analysis 62
4.4.5. Absorbance studies using Ultraviolet-Visible Adsorption Spectroscopy....68
4.4.6. Fluorescence properties of the Ru(Bpy) dye and dye-doped SiNPs....69
4.4.7. Fluorescamine assay to determine primary amine groups on SiNPs....71
4.4.8. Quantitation of avidin immobilized on SiNPs....73
4.4.9. Application of SiNPs for *E. coli* detection....76
4.4.10. Microscopic detection of *E. coli*....80
**4.5. Conclusions....83**

**CHAPTER 5: SYNTHESIS AND CHARACTERIZATION OF MAGNETIC NANOCOMPOSITES FOR *E. COLI* PRECONCENTRATION....85**

**5.1. Introduction....85**
**5.2. Experimental....85**
5.2.1. Materials....85
5.2.2. Synthesis of magnetic carboxyl-functionalized polypyrrole monomer....86
5.2.3. Preparation of the carboxyl-functionalized polypyrrole magnetic nanocomposites (MNCs) by *in-situ* polymerization....86
5.2.4. Bioconjugation of MNCs....87
5.2.5. Attachment of biotinylated-antibodies to avidin-functionalized MNCPs....88
5.2.6. Culture of *E. coli*....88
5.2.7. Magnetism testing and preconcentration....88
5.2.8. Material Characterization....89
**5.3. Results and discussions....90**
5.3.1. Synthesis of MNCs....90
5.3.2. ATR-FTIR analysis of MNCs....91
5.3.3. X-ray diffraction (XRD) study....93
*5.3.4.* Application of MNCs for preconcentration of *E. coli*....94
**5.4. Conclusions....96**

**CHAPTER 6: CONCLUSIONS AND RECOMMENDATIONS....98**

**6.1. Conclusions....98**
6.1.1. SiNPs....98
6.1.2. MNCs....99
**6.2. Recommendations....100**

**REFERENCES....101**

## Table of Figures

*Figure 1: Pie chart showing a high prevalence of diarrhoea cases among children <5 years old, in developing countries .* ..... 2
*Figure 2: A) A pictorial of one E.coli cell and B) an example of a water source that is potentially contaminated with E.coli .* ..... 2
*Figure 3: A schematic diagram illustrating the process followed in an ELISA .* ..... 10
*Figure 4: Schematic diagram of the Colilert testing process .* ..... 11
*Figure 5: The structure of the IgG antibody* ..... 13
*Figure 6: A schematic diagram illustrating the use of membrane filtration in the enumeration of E. coli .* ..... 16
*Figure 7: Immunomagnetic separation of E. coli O157:H7 cells from a complex sample matrix, followed by labeling with electroactive immuno-polyanaline, and magnetic alignment of IMB-E. coli-immuno-polyanaline complexes on an screen printed carbon electrode sensor for amplified electrochemical detection* ..... 19
*Figure 8: Jablonski diagram illustrating the processes involved in the creation of an excited electronic singlet state by optical absorption and subsequent emission of fluorescence.* ..... 25
*Figure 9: Synthesis of SiNPs through a reverse micelle water-in-oil microemulsion.* ..... 41
*Figure 10: Carboxyl surface functionalization of SiNPs using succinic anhydride under inert conditions.* ..... 42
*Figure 11: TEM Images of A) Pure SiNPs, B) Dye-doped SiNPs, C) amine functionalized dye-doped SiNPs and D) carboxyl functionalized SiNPs* ..... 53
*Figure 12: SEM images of A) Dye-doped SiNs and B) Dye-doped $NH_2$-SiNPs.* ..... 55
*Figure 13: SEM image of deformed SiNPs after being synthesized with ammonium hydroxide that had degraded.* ..... 56
*Figure 14: Fluorescent images of dye-doped SiNPs in A) water (no surfactant), B) 0.5% Tween 20 and C) 0.5 % PVA solutions.* ..... 58
*Figure 15: FTIR spectrum of pure SiNPs that are not surface functionalized. The structure of the silica matrix is given in the bottom left.* ..... 62
*Figure 16: FTIR spectra and chemical structure of the Ru(Bpy) dye .* ..... 63
*Figure 17: FTIR spectra of a) Ru(Bpy) dye, b) pure SiNPs and c) dye-doped SiNPs* ..... 64
*Figure 18 : FTIR spectra of a) amine functionalized SiNPs with an amine peak at 1657 $cm^{-1}$ and b) carboxyl functionalized SiNPs with a carboxyl peak at 1702 $cm^{-1}$. The carboxyl groups were attached through the conversion of amine groups using succinic anhydride.* ..... 65
*Figure 19: A comparison between a) the direct and b) indirect attachment of carboxyl groups onto SiNPs. The direct method entails introducing an organosilane with carboxyl groups during the particle synthesis. The indirect method entails making use of succinic anhydride to convert the amine groups to carboxyl groups.* ..... 66
*Figure 20: FTIR spectra of pure SiNPs (a), carboxyl functionalized SiNPs (b) and antibody-functionalized SiNPs (c).* ..... 67
*Figure 21: UV analysis of 0.27 mg/mL Ru(Bpy) dye, 0.27 mg/mL dye in dye-doped SiNPs and pure SiNPs.* ..... 68
*Figure 22: The calibration graph of the Ru(Bpy) dye obtained from the absorption spectra of the UV Vis at 450 nm by serial dilution of a stock solution of 6.5 mg/mL.* ..... 69
*Figure 23: Fluorescence excitation obtained using UV-vis and emission spectra obtained using spectrofluorometer of SiNPs (blue and purple dashed lines) and RuBpy dye (red and green solid lines).* ..... 70
*Figure 24: A graph showing the results of a fluorescamine assay performed on pure, amine – and carboxyl surface functionalized SiNPs (n=3).* ..... 72
*Figure 25: A graph showing results for a fluorescamine assay performed on SiNPs synthesized using the direct carboxylation method (n=3).* ..... 73
*Figure 26: Chemical structure of biotin (5-florescein) conjugate.* ..... 74
*Figure 27: Calibration curve indicating the difference in fluorescence intensity of biotin (5-fluorescein) and avidin concentrations present in the supernatant.* ..... 75
*Figure 28: Titration of biotin (5-fluorescein) conjugate in the presence of avidin in the supernatant of the SiNPs samples (n=3).* ..... 75
*Figure 29: Fluorescence intensity of the detection of E. coli using bioconjugated, dye-doped SiNPs as a function of particle mass (n=3).* ..... 77

*Figure 30: Fluorescence intensity of the detection of E. coli using bioconjugated, dye-doped SiNPs as a function of particle mass with positive controls (particles that are retained in order to obtain maximum fluorescence intensity) (n=3).* ..... *78*
*Figure 31: Fluorescence intensity of the detection of E. coli using bioconjugated, dye-doped SiNPs as a function of E. coli concentration with positive controls (n=3).* ..... *79*
*Figure 32: TEM images of A) Cross-sectional image of E. coli that was not contacted with SiNPs and B) & C) Cross-sectional images of antibody-conjugated SiNPs bound to E.coli cells.* ..... *81*
*Figure 33: Fluorescent field images of A) dye-doped SiNPs and B & C) E. coli cells (the cells are in the direction arrows) incubated with dye-doped antibody-labelled SiNPs.* ..... *82*
*Figure 34: SEM images of A) $Fe_3O_4$ nanoparticles, B) PPy-COOH homopolymer and C) PPy-COOH MNCs with a magnetite core.* ..... *91*
*Figure 35: FTIR spectra of a) pyrrolecyanide monomer, b) PPy-COOH homopolymer and c) PPy-COOH/ $Fe_3O_4$* ..... *92*
*Figure 36: XRD powder pattern of a) PPy-COOH, b) $Fe_3O_4$ and c) MNCs.* ..... *93*
*Figure 37: Images of a) MNCs in suspension before magnetic separation and b) MNCs that have been separated by a magnetic force.* ..... *94*
*Figure 38: TEM images of A) an E. coli cell without MNCs. and B) an E. coli cell labelled with MNCs* *95*

## *Table of Schemes*

*Scheme 1 : A schematic diagram of a polymerase chain reaction cycle . ..... 10*
*Scheme 2: A schematic representation of the mechanism of carbodiimide chemistry . ..... 15*
*Scheme 3: Schematic diagram indicating the ATR-FTIR principle ..... 33*
*Scheme 4: Schematic diagram of an x-ray diffractometer ..... 34*
*Scheme 5: A schematic illustration of electron beam interactions with sample ..... 35*
*Scheme 6: A schematic representation of the UV-vis principle ..... 36*
*Scheme 7: Schematic diagram showing the basic principle of dynamic light scattering . ..... 37*
*Scheme 8: Schematic drawing of a spectrofluorometer . ..... 38*
*Scheme 9: Schematic diagram of surface modification of SiNPs with amine groups. ..... 42*
*Scheme 10: Schematic diagram of the indirect attachment of carboxyl groups onto SiNPs. ..... 43*
*Scheme 11: Schematic diagram of the direct attachment of carboxyl groups onto SiNPs. ..... 44*
*Scheme 12: A schematic diagram illustrating the immobilization of avidin onto SiNPs and the attachment of biotinylated antibodies. ..... 45*
*Scheme 13: Schematic diagram illustrating the way in which SiNPs form in a microemulsion . ..... 51*
*Scheme 14: A schematic diagram of the fluorescamine reacting with primary amines to form a fluorescent product. ..... 71*
*Scheme 15: A schematic diagram of the formation of Poly (1(2-carboxyethyl)pyrrole)) homopolymer . ..... 86*
*Scheme 16: A schematic diagram of the synthesis of MNCs. ..... 87*
*Scheme 17: A schematic diagram illustrating the immobilization of avidin onto SiNPs and the attachment of biotinylated antibodies. ..... 88*

## List of Tables

*Table 1: Preconcentration studies combining IMS and a variety of detection methods* ..... 21
*Table 2: Silica nanoparticles applied to various detection methods* ..... 30
*Table 3: Reagents that were used in the experimental section* ..... 39
*Table 4: A list of reagents used in the bioconjugation process of SiNPs.* ..... 40
*Table 5: Composition of data points used for the avidin-biotin(5-fluorescein) standard curve.* ..... 46
*Table 6: Composition data points used to determine the avidin concentration present in the supernatant of SiNPs after avidin conjugation* ..... 47
*Table 7: Comparison of the size of the different particles that were synthesized.* ..... 54
*Table 8: Comparison of the zeta potential of the different particles that were synthesized.* ..... 59
*Table 9: Surface charge of fluorescent dye-doped SiNPs-COOH in other studies synthesized using the same experimental procedure.* ..... 61
*Table 10: Materials used to synthesize magnetic nanocomposites.* ..... 85
*Table 11: Capture efficiency of MNCs to E. coli cells.* ..... 96

**List of abbreviations**

ATP: Adenosine triphosphate

Au: gold

BSA: Bovine serum albumin

CETS: Carboxyethylsilanetriol sodium salt

CV: Cyclic voltammetry

DETA: Trimethoxysilyldiethylenetriamine

ELISA: Enzymatic-linked immunosorbent assay

*E. coli: Escherichia coli*

EDC: 1-ethyl-3-(3-dimethlyaminopropyl) carbodiimide

FE-SEM: Field emission scanning electron microscope

HR-TEM: High resolution transmission electron microscopy

IMS: Immunomagentic separation

MES: 2-(N-morpholino)ethanesulfonic acid

MNC: Magnetic nanocomposite

MNP: Magnetic nanoparticle

NHS: N-hydroxysuccinimide

PANI: Polyaniline

PBS: Phosphate buffer silane

PEG: Poly(ethyleneglycol)

PFP: Pentafluorophenol

PPy: Polypyrrole

Py: Pyrrole

QD: Quantum dot

$Ru(Bpy)_3^{2+}$: Tris (2,2' bipyridyl)dichlororutheum (II) hexahydrate

SAM: Self-assembled molecular monolayer

SEM: Scanning electron microscopy

SERS: Surface enhanced Raman scattering

SiNPs: Silica nanoparticles

$SiO_2$: Silicon dioxide

SPCE: Screen printed carbon electrode

Sulfo-NHS: N-hydroxysulfosuccinimide sodium salt

TEOS: Tetraethylorthosilicate

XRD: X-ray Diffraction

## Chapter 1: Introduction

Water is a reusable resource but it is not renewable. Water resources are finite and the amount of water available for human consumption is decreasing because of wasteful or polluting practices. One of the main concerns in developing countries is the contamination of fresh water sources with faecal matter due to poor sanitation practices.

According to the World Health Organisation (WHO), 768 million people still rely on unimproved drinking water, with the majority being in developing countries (WHO, 2011). Additionally, only 63 % of the global population use toilets and other improved sanitation facilities, while 2.5 billion people still lack improved sanitation. Of these 1.1 billion people (15 % of the global population) practice open defecation, with the majority living in rural areas. As a result, every 20 seconds, a child dies from a disease associated with faecal contamination in water (WHO, 2011). Hence it is essential to identify and treat the contamination source in environmental water to prevent outbreaks of waterborne diseases. In 2004 alone, 696 million cases of children in Africa, under the age of 5 years, were reported to be suffering from diarrhoea (WHO, 2011) (**Figure 1)**.

Faecal-oral transmission is the main route for the cause of disease by pathogens. *Escherichia coli* (*E. coli*) and other coliforms form 0.1 % of the flora in the intestines of humans and warm blooded animals (WHO, 2011). Most of the *E. coli* strains are non-pathogenic but some serotypes can cause severe illnesses in human beings.

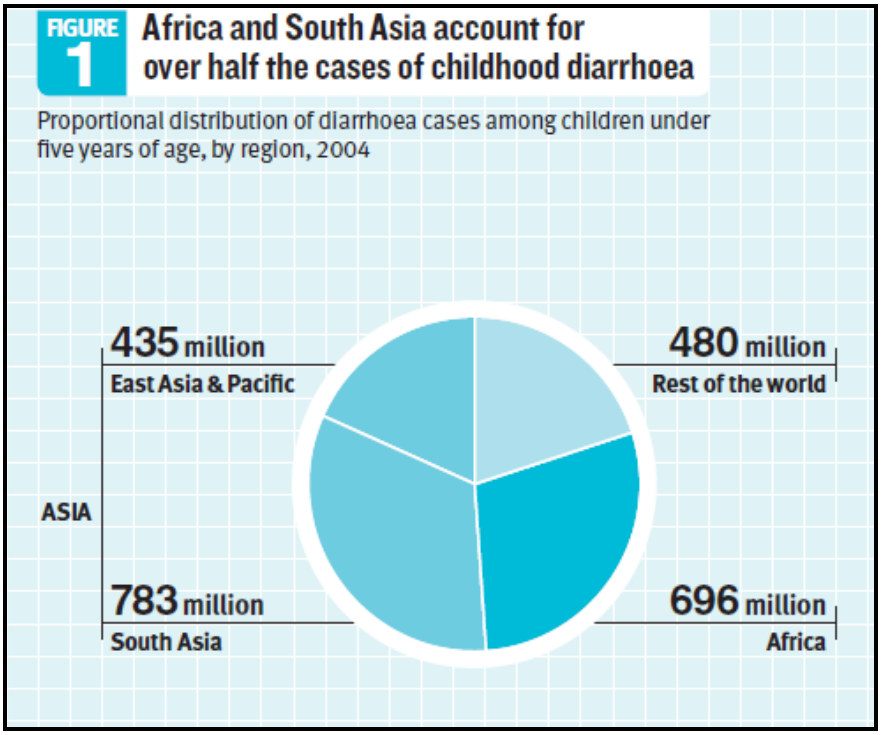


Figure 1: Pie chart showing a high prevalence of diarrhoea cases among children <5 years old, in developing countries (WHO, 2011).

The ability for *E. coli* to survive outside the human body makes it a good indicator bacterium to test for faecal contamination (Iqbal *et al*., 2012). **Figure 2** shows an image of **A)** an *E.coli* cell and **B)** an example of a water source used by communities that is potentially infested with pathogens.

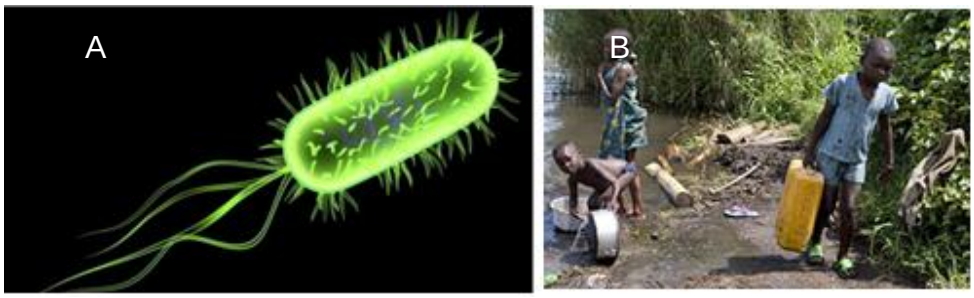


Figure 2: A) A pictorial of one *E.coli* cell (Elite Lawyer Project, 2013) and B) an example of a water source that is potentially contaminated with *E.coli* (WHO, 2011).

The detection of bacteria is a very important aspect in potable water and food safety, as well as in prevention strategies to fight against bioterrorism agents.

It is also essential to have minimal sample manipulation as possible, during detection (Zhao *et al*., 2004b).

The conventional method for *E.coli* detection is based on membrane filtration and culturing. Currently, methods such as Polymerase Chain Reaction (PCR) and enzymatic-linked immunosorbent assay (ELISA) are also used for bacteria detection (Rompre *et al*., 2002).

The current methods which are used for the detection of *E. coli* take long before acquiring a signal. They require pre-enrichment of the samples. They are laborious and they require trained, technical personnel to operate. This makes them expensive to use. Therefore, there is a need for a rapid preconcentration and detection system for *E. coli* in water. Another challenge is the signal amplification of low concentrations of bacteria. Traditionally this involves culturing the bacteria because the signal is not high enough to enable detection.

### a. Preconcentration

According to the SANS 241: 2005 drinking water specification, the standard for drinking water is: “0” (zero) *E.coli* cells or faecal coliform in 100 mL of water (SANS 241-1:2011, 2011). This indicates that the detection methods should use 100 mL sample volumes; therefore, samples have to be preconcentrated or enriched to lower volumes that will enable sample analysis.

Currently, membrane filtration is used as a form of preconcentration (Yang *et al*., 2007). Although convenient, and easy to use, the use of filters leads to the loss of bacteria in the sample due to bacteria not being able to be completely removed from the filters (Yang *et al*., 2007). Hence, membrane filtration restricts one to conducting the analysis or culturing the bacteria on the membrane itself (Yang *et al*., 2007). Recently, immunomagnetic separation has been introduced whereby magnetic nanoparticles (Setterington & Alocilja,

2011; Madonna *et al*., 2001), paramagnetic nanoparticles (Lee & Deininger, 2004; Kell *et al*., 2008) or films (Yang *et al*., 2007; Fredj *et al*., 2008) are used to preconcentrate bacteria, while also allowing bacteria detection through electrochemical detection. Magnetic nanoparticles or nanocomposites have a high surface area, they hold strong magnetic properties and they have low toxicity (Yoza *et al*., 2003; Bai *et al*., 2013). Given these properties, they simplify the enrichment process by eliminating the incubation of lower bacteria concentrations and thus making the process faster.

Immunomagnetic separation however, has primarily been used to preconcentrate samples with a maximum volume of 1-10 mL which only cater for processes such as DNA extraction and protein purification among others. Hence, a need arises for a preconcentration procedure or system that can be applied to 100 mL sample volumes, in order to satisfy the SANS 241 standard.

### b. Detection and signal amplification

Biological methods such as immunoassays make use of fluorophores as bioprobes to enable detection. These immunoassays are based on linking one or many dye molecules to an antibody which then binds the bacteria, in order to get a better signal (Zhao *et al*., 2004a). The conventional fluorophores that are used as fluorescent labels are restricted in some fields of biological applications because of photobleaching and dye instability, which decreases the emission intensity (He *et al*., 2001). This in turn reduces the efficiency of detecting the bacteria and amplifying the signal. It is important to introduce new fluorophores that are capable of high signal amplification in order to address the need of highly sensitive bioassays (Chen *et al*., 2012; Wang *et al.*, 2008a; Wang *et al*., 2008b).

Quantum dots (QDs) and dye-doped nanoparticles are opening new possibilities for developing a new range of luminescent bioprobes (Chen *et al*., 2012; Wittenberg & Haynes, 2009; Chen & Tong, 2012). In recent years, QDs

have gained a lot of interest as fluorescent probes for cell imaging and *in-vivo* cell tracking due to the miniature size of 1 - 10 nm diameters. They are also 20 times brighter than most organic fluorophores, with good photostability and multiplexing ability. Having a higher fluorescence signal makes it possible to push the limits of detection to lower bacteria concentrations (Wittenberg & Haynes, 2009). Quantum dots, however, cannot be used extensively because their core is made of heavy metals, which would be a concern for *in-vivo* studies. QDs are not soluble in water and require to be coated with a polymer in order for them to be used in biological processes. Single colloidal QDs suffer from stochastic blinking (Wang *et al*., 2008a).

In the past few years, there have been advances in the synthesis and characterization of nanomaterials such as hydrogels, silica, carbon nanotubes, magnetic and polymeric nanoparticles. Silica nanoparticles have become an essential part in biomedical applications and bioanalysis (Yang *et al*., 2011). Fluorescent silica nanoparticles (SiNPs) are photostable, robust, easy to prepare and are reactive for chemical modification, making them versatile (Knopp *et al*., 2009).

Recently, many studies have focussed on the use of dye-doped SiNPs as luminescent biosensors (Wang *et al*., 2008b; Chen & Tong, 2012; Tansub *et al*., 2012; Cai *et al*., 2013). This involves encapsulating thousands of fluorophores into the SiNPs matrix, thereby giving a fluorescence intensity that is 10000 times higher than that of organic fluorophores (Zhao *et al*., 2004b). Furthermore the high density of dye-doped SiNP's makes them easy to separate during centrifugation (Yang *et al*., 2011).

Methods that incorporate SiNPs however, face problems where the detection of coliforms is not reproducible. This is due to agglomeration and non-specific binding (Bagwe *et al*., 2006). The surface modification induces agglomeration of the particles because of the low surface charge of the particles, therefore resulting in weak repulsion forces. Recent developments in the field are focussed towards reducing agglomerating by functionalising SiNPs with

functional groups such as -COOH, phosphates, octadecyl and poly(ethylene glycol) (PEG) (Cai *et al*., 2013; Bagwe *et al*., 2006).

### c. Hypothesis

Surface functionalizing SiNPs with anti-*E. coli* antibodies will enable binding of *E. coli* bacteria onto the NP's, and doping the NP's with fluorescent dye molecules, will enable the detection of *E. coli* as well as the amplification of the signal. Part of the amplification of the signal is dependent on the efficacy of the attachment of antibodies onto the surface of the SiNPs, which occurs only when the surface functionalization is done effectively. Therefore, the attachment of more functional groups on the surface of the nanoparticles will enable better antibody attachment resulting in a larger signal.

The attachment of functional groups such as carboxyl groups onto the SiNPs surface will increase the dispersibility of the nanoparticles in suspension.

Preconcentrating the sample using immunomagnetic separation, through magnetic nanocomposites, will enable processing of large volumes of water (i.e. 100 mL), and will also provide sample enrichment and reduce sample preparation.

### d. Objectives

The aims of this study were to synthesize:

i. Dye-doped and surface functionalized SiNPs for the detection of *E. coli* in water and amplify the signal thereof, with emphasis on developing an effective and efficient method for the synthesis of the SiNPs.

ii. To synthesize carboxyethylpolypyrrole magnetic nancomposites (MNCs) to preconcentrate the *E. coli* from larger volumes of 100 mL to small volumes of 300 µL if possible.

The objectives of this study were:

- To synthesize monodispersed, uniform dye-doped SiNPs and conducting polymer based MNCs.
- To functionalize the dye-doped SiNPs with primary amines, carboxyl groups and avidin.
- To synthesis carboxyl-modified MNCs and functionalise with avidin.
- To bioconjugate the SiNPs and MNCs with anti-*E. coli* antibodies
- To characterize the pure and surface functionalized dye-doped SiNPs and MNCs using HR-TEM, FE-SEM, XRD, ATR-FTIR, Zeta Sizer and spectrofluorometer.
- To show proof of concept for the preconcentration, detection and signal amplification of *E. coli* in water.

The scope of this project entails the synthesis and characterization of the nanomaterials and the surface functionalization thereof. The nanomaterials are surface functionalized with various functional groups and antibodies. The scope further extends to preliminary efficacy studies whereby the antibody-labelled nanomaterials are tested in *E. coli* contaminated water samples. Furthermore, the SiNPs and MNCs are referred to as smart nanomaterials because they respond to external stimuli. SiNPs respond fluoresce when they are irradiated and MNCs are magnetic when exposed to an external magnetic field.

## Chapter 2: Literature Review

The rapid and accurate detection of undesirable matter such as pathogens and toxins in food and water has become a necessity in these respective industries. Although the laboratory-based biochemical methods for pathogen detection are well established, there has been a growing interest in easy-to-use biosensors, which could potentially be used as point of care devices.

This review focuses on the different pathogen detection methods with emphasis on biosensors making use of dye-doped SiNPs and preconcentration using magnetic nanoparticles. The specific aspects covered in the literature review include the following: conventional detection methods (**Section 2.1**); nanoparticles a bioprobes (**Section 2.2**); bioconjugation of nanoparticles (**Section 2.3**) and conclusions and recommendations gathered from the literature review (**Section 2.5**).

### 2.1. Conventional detection methods

#### 2.1.1. Culturing and plating method

The culturing and plating method is the oldest bacterial detection technique and it remains the gold standard for detection. Different selective media are used to detect particular bacteria species. They can contain inhibitors (in order to stop or delay the growth of non-targeted strains) or particular substrates, which only the targeted bacteria can degrade, or that confers a particular colour to the growing colonies (rainbow agar from Salmonella detection) (Fratamico, 2003). Thereafter, detection is performed using optical methods like ocular inspection (Gunasekera *et al*., 2000a; Gunasekera *et al*., 2000b).

This method is excessively time consuming. The results are obtained after incubating and culturing the bacteria for 24 hours. After obtaining results, confirmation tests must be done to ensure that the results are accurate. This method requires microscopy and iterations in order to quantify the bacteria. In

the case of Campylobacter, it takes 4–9 days to obtain a negative result and 14 - 16 days to confirm a positive result (Brooks *et al*., 2004). This is an obvious inconvenience in many industrial applications, and particularly unacceptable in the food and water sectors where rapid results are essential. Another significant disadvantage of traditional culture methods is that they fail to isolate viable but non-culturable organisms (Gunasekera *et al*., 2000a).

### 2.1.2. Laboratory-based biochemical methods for pathogen detection

Laboratory-based biochemical methods mainly detect specific nucleotide sequences within the pathogen genome. They also detect pathogen-specific surface epitopes with the aid of antibodies.

Initially, detection methods were limited to immunoassays such as the Polymerase Chain Reaction (PCR)enzymatic-linked immunosorbent assay (ELISA) and nucleic-acid based assays such as the. Then the real-time PCR was introduced, which shifted the focus due to its high specificity and sensitivity (Ozalp *et al*., 2014; Skottrup *et al*., 2008).

#### 2.1.2.1. Polymerase Chain Reaction

The PCR method makes use of nucleic acid sequences as shown in **Scheme 1**. The method is also not cost effective, due to the cost of the equipment as well as the PCR reagents which are required. The method is quite sensitive but using conventional PCR takes about a day to obtain results from the tests. Recently, real-time rapid PCR offer faster analysis, but this method requires skilled personnel due to its complex nature PCR lacks simplicity, as well as complicated, therefore, it is expensive and laborious. Real time PCR reduces the time taken to analyse a sample, however it still requires skilled personnel and of high cost (Rompre *et al*., 2002).

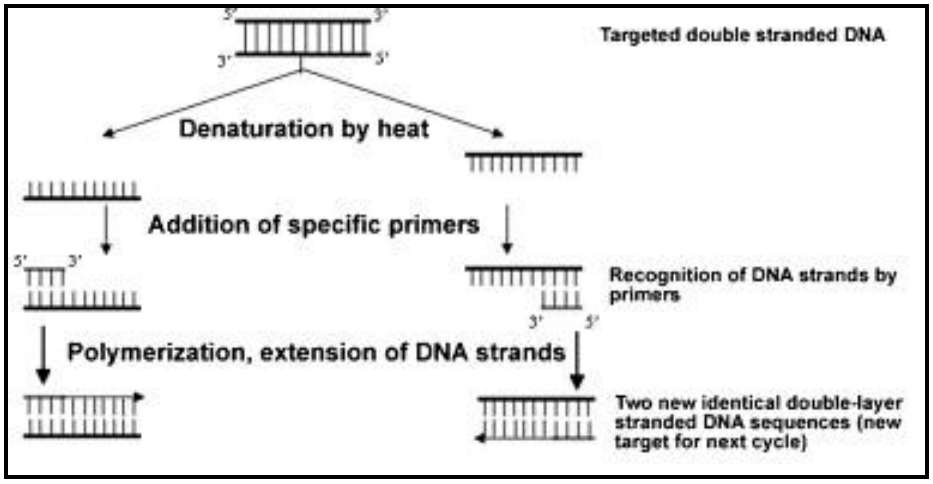


Scheme 1 : A schematic diagram of a polymerase chain reaction cycle (Lazcka *et al*., 2007).

### 2.1.2.2. Enzyme-linked immunosorbent assay (ELISA)

The ELISA (

**Figure** 3) uses antibodies and colour change to identify the species investigated. This method is lab-based and it cannot differentiate between viable and dead bacteria due to the DNA that continues to be present in dead bacteria cells. The amount of bacteria is difficult to quantify and the method is time consuming.

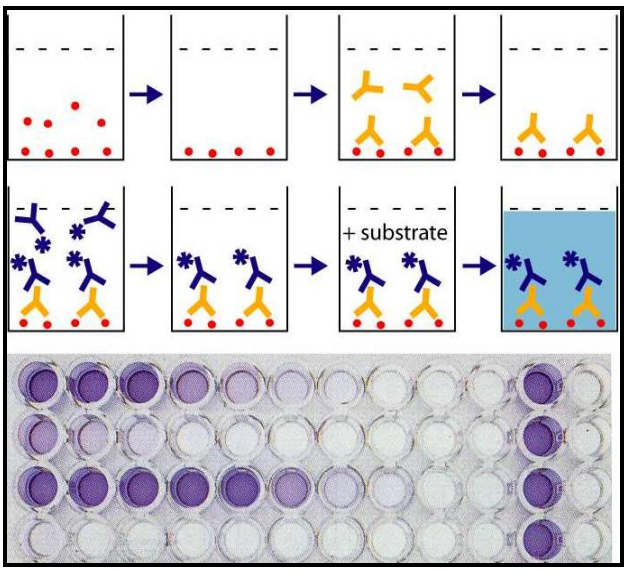


Figure 3: A schematic diagram illustrating the process followed in an ELISA (Trudeau, 2012).

An assay is conducted whereby the antibodies that are specific to the bacteria and the enzymes are oriented in a sandwich form. When the enzymes attach to a specific substrate, a signal is produced in the form of colour. This method is also lab-based and requires skilled operators. The method requires a lot of washing steps, which makes it a tedious process. It takes ~7 hours to get a signal from this method (Rompre *et al*., 2002).

### 2.1.2.3. Colilert

Colilert and Colisure are the current state of the art testing methods used worldwide at water testing facilities to detect *E.coli* and total coliforms in a sample (**Figure 4**).


Figure 4: Schematic diagram of the Colilert testing process (IDEEX Laboratories, 2013).

The reagent is added to the sample and mixed. The mixture is then poured into the Quanti-Tray and sealed in the Quanti-Tray Sealer. The Quanti-Tray is then placed in incubator for 24 hours to allow the enzymatic colour change to occur. The Quanti-Tray results are read, whereby the total coliforms are represented by the yellow colour and the E. coli cells are represented by a yellow fluorescent colour (IDEEX Laboratories, 2013).

A Quanti-Tray, Quanti-Tray sealer, UV light source, and testing reagents are required for testing, which increases the costs of the whole setup, making the process expensive.

## 2.2. Nanoparticles as bioprobes

Nanotechnology entails the creation of materials that are less than 100 nm in size, which are used in fields such as biotechnology, biomedical sciences, material sciences and engineering (Smith *et al*., 2006). Nanomaterials have chemical and physical properties that enable advanced functionalities which are superior to those of conventional materials. The use of nanoparticles and nanoprobes can be used to obtain a much deeper understanding of biological processes (Smith *et al*., 2006). Nanomaterials have a high surface-to-volume ratio, which is different to bulk materials. The compatibility and suitability of nanomaterials towards the relevant applications is determined by their composition (Smith *et al*., 2006). Some of the nanomaterials that are used as bioprobes are quantum dots, gold, polystyrene latex, magnetic nanoparticles and dye-doped nanoparticles (Smith *et al*., 2006).

Sample preparation of complex biological samples includes purification, enrichment and preconcentration. (Turney *et al*., 2004) used nanomaterials in solid-phase extraction of analytes. Although the sample clean-up and preconcentration occur, the analytes are not removed selectively. Herr *et al.,* 2006 prepared magnetic nanomaterials for selective extraction and enrichment of various types of cancer cells. A great deal of research was done using nanomaterials to overcome the inadequacies of separation techniques used for bioseparation and bioanalysis (Herr *et al*., 2006).

## 2.3. Bioconjugation of nanoparticles

### 2.3.1. Antibodies

Biosensor sensitivity relies on the immobilization of antibodies on the surface of the substrates.

Antibodies are protein molecules that bind specifically to antigens (the substance that caused their production). Antigens can be other proteins or

polysaccharides of viral or bacterial origin. The most prevalent type of the antibodies is the immunoglobulin G molecule (IgG). A general structure of IgG is shown in **Figure 5** (Janeway *et al*., 2001).

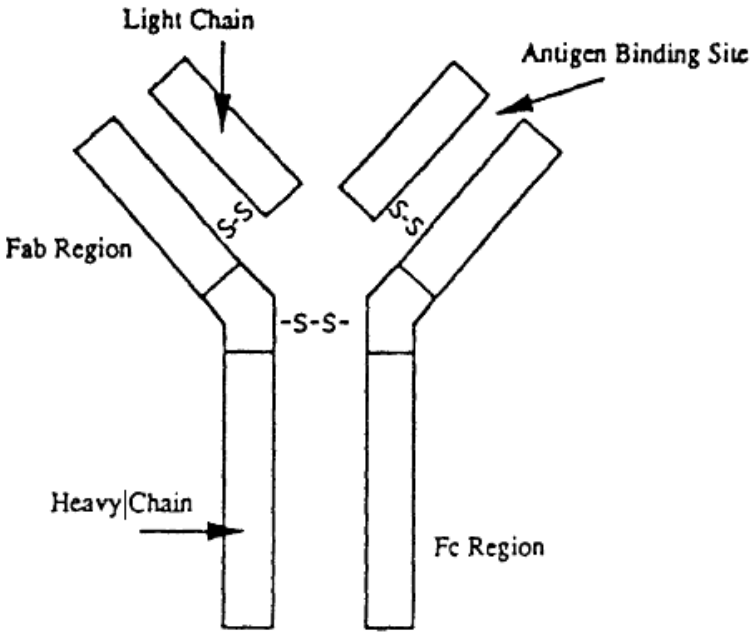


Figure 5: The structure of the IgG antibody (Laffey, 1995)

Each IgG molecule consists of two heavy chains (M.W. - 50 kDa each) and two light chains (M.W. - 25 kDa each). The two heavy chains are linked to each other and to their corresponding light chains by disulfide bonds to form the Y shape structure shown above (**Figure 5**). The two arms on the IgG molecule are named the Fab region. The Fab region is responsible for antigen recognition and binding through amino acid residues. The stem of the IgG is named the Fc region. The Fc region is responsible for the effector functions. There are five types of heavy chains consisting of subtypes and they determine the functional activity of the antibody (Janeway *et al*., 2001).

It is important for the antibodies to be oriented such that the antigen-binding sites face away from the nanoparticle surface; therefore it is crucial to identify a surface chemistry that enables optimum orientation. Antibodies can be immobilised through passive adsorption or covalent attachment (Skottrup *et al*., 2008).

Passive adsorption is a simple process; however, it is an uncontrolled process. The antibodies can denature when hydrophobic surfaces are used (Heredia & Maynard, 2006). Ligand leaching from the nanoparticle surface can occur when there is extensive washing, which can decrease the bioactivity of the nanoparticles (Skottrup *et al*., 2008). Covalent attachment on the other hand is a complex process and it requires stable active products such as an amine reactive ester. However, it enables the ligands to maintain their conformational stability and they do not leach from the nanoparticle surface (Skottrup *et al*., 2008; Heredia & Maynard, 2006).

Affinity biological molecules are used to bioconjugate nanoparticles. Avidin (an egg white glycoprotein) and streptavidin (deglycosylated avidin) are two proteins that bind to biotin (a vitamin). The bond between avidin and biotin forms very rapidly and is so strong (Kd = $10^{-15}$ $M^{-1}$) that it is not affected by pH, denaturing agents or organic solvents. The irreversible bond between biotin and avidin can only be released by denaturing the protein subunits (de Dios & Díaz-García, 2010; Airenne *et al*., 1999; Diamandis & Christopoulos, 1991). Biotin and avidin may be attached to substrates by adsorption (Bashir *et al*., 2001) or covalent bonds (Vermette *et al*., 2003). The attachment of antibody layers may be bound to a substrate surface that has been modified using aldehyde (QI *et al*., 2006), 11-MUA on gold-coated magnetic nanoparticles (Torun *et al*., 2012),1-ethyl-3-(3-dimethlyaminopropyl) carbodiimide (EDC)-activated polystyrene beads (Holmlin *et al*., 2000), or EDC/ N-hydroxysuccinimide (NHS) activated silica nanoparticles (Chen *et al*., 2012) and many other ligands.

### 2.3.2. Carbodiimide Chemistry

Carbodiimide crosslinking is a common method for conjugation of avidin or antibodies to a surface. The zero-length cross-linker (EDC) reacts with carboxyl-modified nanoparticles in the presence of NHS or sulfo-NHS to form amine-reactive NHS esters (**Scheme 2**).

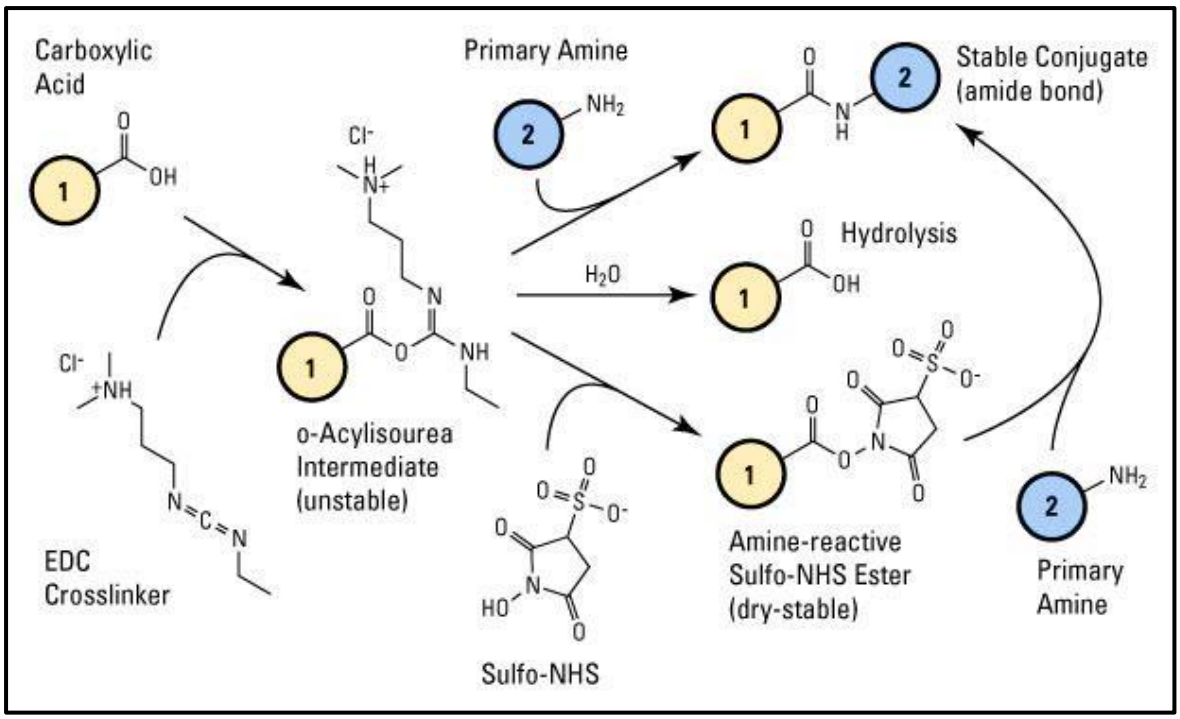


**Scheme 2:** A schematic representation of the mechanism of carbodiimide chemistry (Hermanson, 2013).

Subsequent addition of antibodies results in coupling between the nanoparticles and primary amines on the antibody via a stable amide bond (Thorek *et al*., 2009). Taylor *et al* applied carbodiimide chemistry in order to attach proteins to the surfaces of commercially available carboxyl-modified latex nanoparticles for probing specific sequences on single DNA molecules (Taylor *et al*., 2000). The combination of avidin-biotin affinity coupled with carbodiimide chemistry was found to be more effective than passive adsorption, in *E. coli* capture because of the directed orientation of antibodies on the nanoparticles (Cheng *et al*., 2009).

### 2.3.3. Preconcentration or enrichment of pathogens

Environmental samples contain a number of microorganisms, organic and inorganic matter and other particles. This poses a number of challenges to the development of assays. Waterborne pathogens are usually present in low concentrations in environmental samples, which is an obstacle for detection.

In order to overcome these challenges the development of sample pre-treatment that is compatible with the detection method is essential (Connelly & Baeumner, 2012).

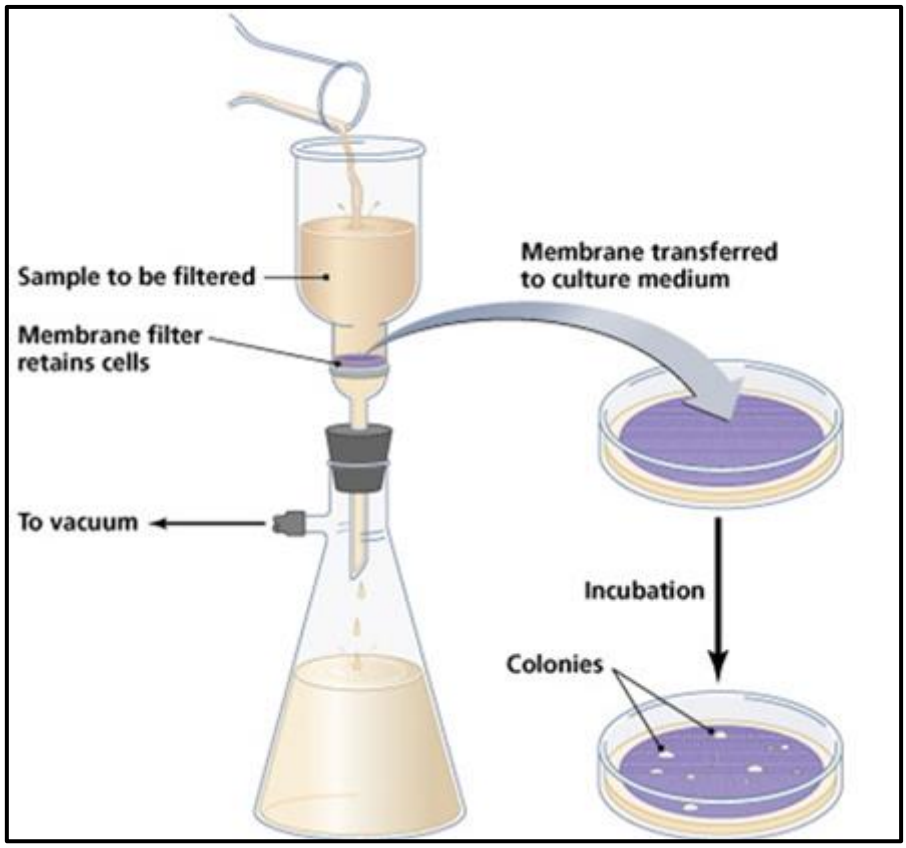


Figure 6: A schematic diagram illustrating the use of membrane filtration in the enumeration of *E. coli* (Lee *at al*., 2003).

Membrane filtration (**Figure 6**) is the current standard for sample concentration of large volumes of water, with various buffer changes required for adsorption and elution of the analyte of interest (Kittigul *et al*., 2005; Katayama *et al*., 2002; Kittigul *et al*., 2001).

### 2.3.3.1. Microfluidic devices for preconcentration

Recently, microfluidic devices have been developed for preconcentration of bacteria. Balasubramanian et al., developed a microfluidic device with an electrostatic trapping compartment that attracts waterborne microbes through the electrostatic force. The device consisted of a microchannel with electrodes

acting as two walls that are capable of concentrating *E. coli*, *Salmonella*, and *Pseudomonas* with a capture efficiency of >99% (Balasubramanian *et al*. , 2007). Size-based microfluidic filtration techniques have also been implemented for pre-concentration. Taguchi et al. developed a size-based microfluidic filtration device. The device incorporated a stainless steel filter with conical pores. The sample was pulled under negative pressure whereby the sample was pulled through the pores and the larger particles were captured. The captured analytes were visualized using fluorescent antibodies (Taguchi *et al*., 2007).

Filtration methods are beneficial when they are used to process large volumes of water (Litres of water) as well as initially when handling environmental sample. However, microfluidic devices that are used for filtration are prone to clogging and fouling as well as limiting the application to real samples. Another disadvantage of using filtration is that it is not analyte-specific.

#### 2.3.3.2. Immunomagnetic Separation

Immunomagnetic separation (IMS) has nowadays become the standard in life sciences for concentrating biological analytes of interest and for purifying biological samples (Connelly & Baeumner, 2012).

Magnetic nanoparticles have become the most popular materials in nanoscience. They have been applied in immobilization of proteins, biotechnology and biomedicine (Yang e*t al*., 2004). These nanoparticles are superparamagnetic, meaning that they are magnetic when they are exposed to a magnetic field but they do not retain their magnetism in the absence of a magnetic field (Yang *et al*., 2004). Thus, the superparamganetic nanoparticles can be used to remove biomaterials of interest from a sample matrix using an external magnetic field.

Preconcentration of water samples using IMS and other antibody-capture techniques makes immunoassays faster (Connelly & Baeumner, 2012). Typically IMS is coupled with a detection method. A number of different

detection methods have been applied using IMS. Lee *et al* 2004 used superparamagnetic polystyrene beads for IMS of *E. coli* in beach water samples coupled with adenosine triphosphate (ATP) bioluminescence as a detection method (Lee & Deininger, 2004). Gold-coated magnetic nanoparticles combined with surface-enhanced Raman scattering (SERS) were developed to enumerate *E. coli.* The authors achieved a capture efficiency of 55% (Guven *et al*., 2011).

Magnetic nanoparticles can be used in conjunction with immunological assays. Fu *et al*., made use of commercial magnetic nanoparticles to preconcentrate *E. coli* and used real-time PCR as a method of detection (Fu *et al*., 2005). Yang and his group used commercially available carboxylic acid functionalized magnetic nanoparticles coupled with PCR for preconcentration and detection of *Listeria monocytogenes* respectively (Yang *et al*., 2007). Huang et al employed amine-functionalized magnetic nanoparticles for the enrichment of Gram positive and Gram negative bacteria by taking advantage of their high binding affinity (Huang *et al*., 2010). Zhu's group developed a method which combined IMS and a fluorescence immunoassay which they named immunomagnetic fluorescence assay (IMFA). This method has been used for the detection of *E. coli*. The cells were initially captured with anti-*E.coli* antibody-coated magnetic beads and then recognized by a fluorescent detector antibody; thereby forming an immune-sandwich complex (Zhu *et al*., 2011).

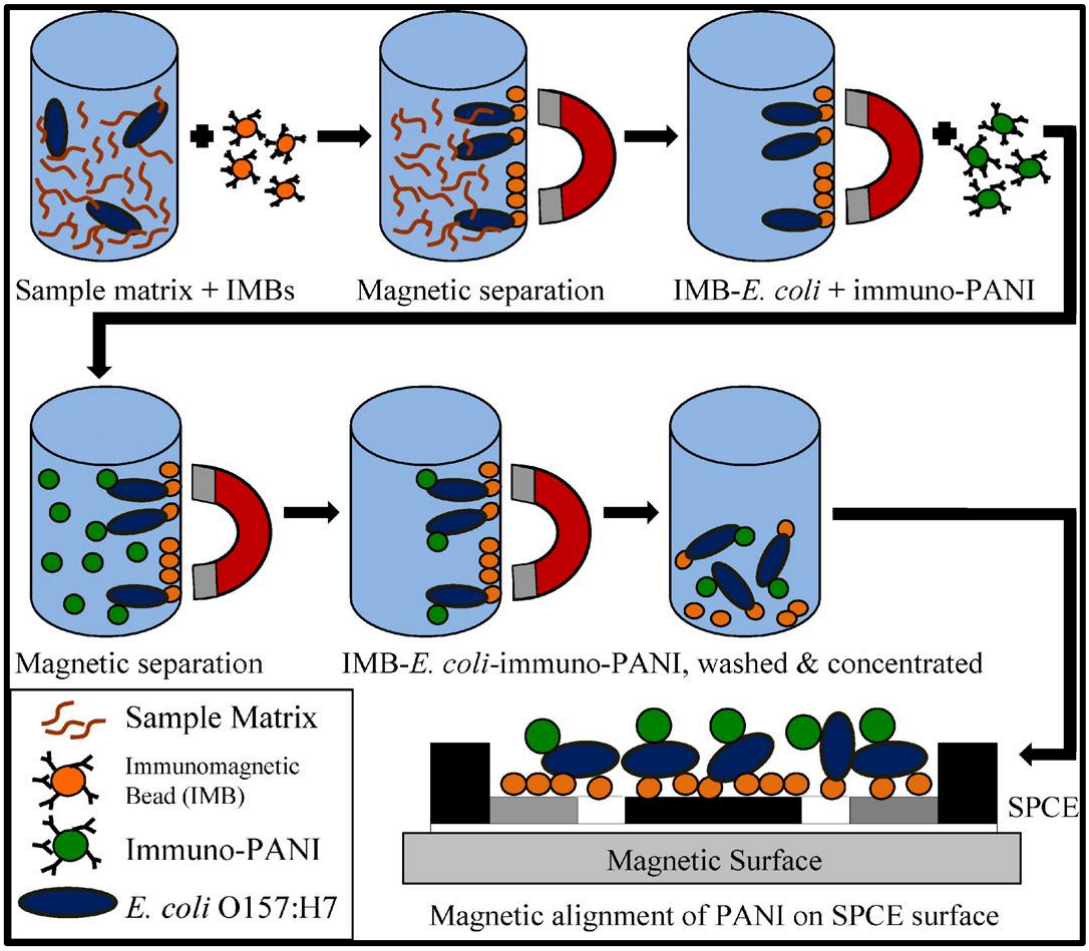


Figure 7: Immunomagnetic separation of E. coli O157:H7 cells from a complex sample matrix, followed by labeling with electroactive immuno-polyanaline, and magnetic alignment of IMB-*E. coli*-immuno-polyanaline complexes on an screen printed carbon electrode sensor for amplified electrochemical detection (Setterington & Alocilja, 2011).

IMS can be combined with electrochemical detection such as cyclic voltammetry and impedance spectroscopy. Setterington and colleagues used electro-active polyaniline nanoparticles to separate and enrich *E. coli* samples. Thereafter, the nanoparticle-bound *E. coli* cells were quantified using cyclic voltammetry (Setterington & Alocilja, 2011) (**Figure 7**). Magnetic nanoparticles can also be coupled with fluorescence. Dudak and colleagues separated cells using IMS (60% capture efficiency) and then the captured cells were incubated in tryptic soy broth with isopropyl-β-D-thiogalactopyranoside, which induces the formation of β-galactosidase in viable bacteria. The bacteria were lysed to release β-galactosidase. β-

Galactosidase converted 4-methylumbelliferyl-β-D-galactoside to 4-methylumbelliferone (4-MU), which was measured by fluorescence spectrophotometry (Dudak *et al*., 2009). Verbag *et al* developed a MagTrap microflow cytometer system whereby magnets rotated in a certain direction. As the magnets turned, the nanoparticles were attracted into the device in the opposite direction as that of the flow. The magnetic beads were retained as they were bioconjugated in the MagTrap device. As the beads are released, they flowed into the flow cytometer where the cells were enumerated (Verbarg *et al*., 2013).

**Table 1** is a summary of preconcentration techniques that are coupled with various detection methods of *E. coli.* The sample volumes used do not exceed 10 mL and the capture efficiency decreases with the increase in bacteria concentrations. The detection methods used to enumerate the *E. coli* cells do not detect whole *E. coli* cells. The *E. coli* cells are lysed prior to enumeration. It is also seen that labelling the magnetic particles with a biorecognition molecule is essential as it permits bacteria capture. Most of the magnetic beads used in the study below are in the micron range, which limits them in terms of surface-to-volume ratio. Some of the detection methods that are used in conjunction with IMS have low detection limits, however, they do not process 100 mL and the systems are lab-based.

Table 1: Preconcentration studies combining IMS and a variety of detection methods

| Material | Detection limit | Detection method | Pre-concentration | Incubation time | Capture Efficiency (%) | Limitations | Comment | Reference |
|---|---|---|---|---|---|---|---|---|
| Nanogold specific probe/ vancomycin coated magnetic beads | - | IMS and microfluidic device | No | 25 min | 99 | saturation above 10^7 CFU/mL | Microfluidic system on a chip using DNA modified probe. *E. coli* captured by vancomycin-magnetic beads. The *E. coli* was lysed in order to detect the target DNA. Detection was by colour change of the aggregated nanogold. | (Chih-Hung Wang *et al*., 2013) |
| Magnetic Beads that fluoresce | 10^4 for *E.coli*, 10^2 for *listeria sp*, 10^6 cells/ mL *Salmonella* and *shigella* | Automated IMS & optical detection (MagTrap-microflow cytometer system at 10 µL/min) | - | 20 min incubation time with beads; | - | 1x10^6 cells/ml | 100 µL sample size containing around 500 beads. Bacteria were heat-inactivated and handled under Biosafety Level 2 conditions.10^2 and 10^6 cells/mL were tested. Rotation of the magnets pulled the beads in an opposite direction to that of the flow, retaining the beads while mixing them. The bioconjugation of the magnetic beads occurs in the MagTrap. The beads | (Verbarg *et al*., 2013) |

| | | | | | | | | |
|---|---|---|---|---|---|---|---|---|
| | | | | | | | were released into the flow cytometer by reversing the rotation. | |
| Electro Active Polyaniline | 7 CFU/mL | IMS and Screen Printed Carbon Electrode (SPCE) sensor and Cyclic Voltammetry | No | 10 min incubation; 70 min from sampling to detection | - | - | 100 µL are used for analysis. The polyaniline nanoparticles were stored in PBS buffer with 0.05% Triton X-100. The nanoparticles were conductive and magnetic at the same time. | (Setterington & Alocilja, 2011) |
| Dyna beads | 10 CFU/mL | IMS & Fluorescence Immunoassay | Not necessarily, but a method of separating the magnetic beads is shown. | 1hr incubation time. Assay is completed in <3hrs | 100% for concentration between 1 and 10^2 cells; 98.8% for 10^3–10^5 cells, and 84.9% for 10^6 cells/mL. | - | Capture efficiency decreased at higher cell concentrations due to limitation of bead capacity. Abs were coated with Cy5 fluorescent dye. Dye-coated Abs were added to the magnetic beads/bacteria complexes. Complexes were separated by suspending them in 100 µL of dissociation buffer by vortexing and incubated at room temperature. | (Zhu *et al*., 2011) |

| | | | | | | | | |
|---|---|---|---|---|---|---|---|---|
| | | | | | | | Fluorescence measurement was done after separation. | |
| Au coated MNPs | 8 - 24 CFU/mL | IMS and Surface-enhanced Ramaan Scattering (SERS) sandwich immunoassay | No (Serial dilution for plate counting method) | 70 min | 55 | saturation above 10^5 | Gold coated magnetic nanoparticles were used to capture *E. coli*. Sandwich immunoassays were used to enumerate bacteria. Confirmed specificity. Tested Lake, stream and puddle water. Confirmed results with plate counting. | (Guven *et al*., 2011) |
| vancomycin-modified NPs | 1x10^6 | IMS | No | 30-60 min | 66 - 83 | saturation above 10^9 CFU/mL | Detection time decreases with the use of larger, highly loaded NPs | (Kell *et al*., 2008) |
| carboxylated magnetic polystyrene beads & Dyna beads | 226 CFU/0.5 mL in milk | IMS & R-PCR | No | Reaction time was 15 min & 60 min was collection time | IMNP-based IMS was 1.4 to 26 times higher than those of Dynabeads®-based IMS | >10^5 CFU/0.5 mL. | The Dyna beads were used as a control. There were no washing steps involved. Milk was used instead of water. | (Yang *et al*., 2007) |

| | | | | | | | | |
|---|---|---|---|---|---|---|---|---|
| | | | | | dependin g on initial cell concentra -tions | | | |
| Biofunction ali-sed MNPs | 5x10 cells/mL | IMS and Real time PCR | No | 2.15 hr | - | - | Make use of commercial magnetic nanoparticles for preconcentration or separation. *E. coli* cells were lysed and quantified using PCR. Preconcentrate 1mL to 50 µL. | (Fu *et al*., 2005) |
| Dyna beads | 20 CFU/g with beads & 2000 CFU/g without beads | IMS as a form of isolation of bacteria | Partial preconcentr ation. The samples are enriched for 18hrs then preconcentr ated (sub-culture) | 30 min saparatio n period | 97 | - | This study was around beef carcass meat, milk & faecal matter. 12/12 strains of *E. coli* 0157 were recovered from the samples. IMS was performed in broth/ growth medium. | (Wright *et al*., 1994) |

## 2.4. Fluorescence Detection

Fluorescence results from a three-stage process that occurs in certain molecules called fluorophores or fluorescent dyes (generally polyaromatic hydrocarbons or heterocycles). A fluorescent probe is a fluorophore that is designed to respond to a specific stimulus or to localize within a specific region of a biological specimen. **Figure 8** illustrates the fluorescence process by an electronic-state diagram (Jablonski diagram).

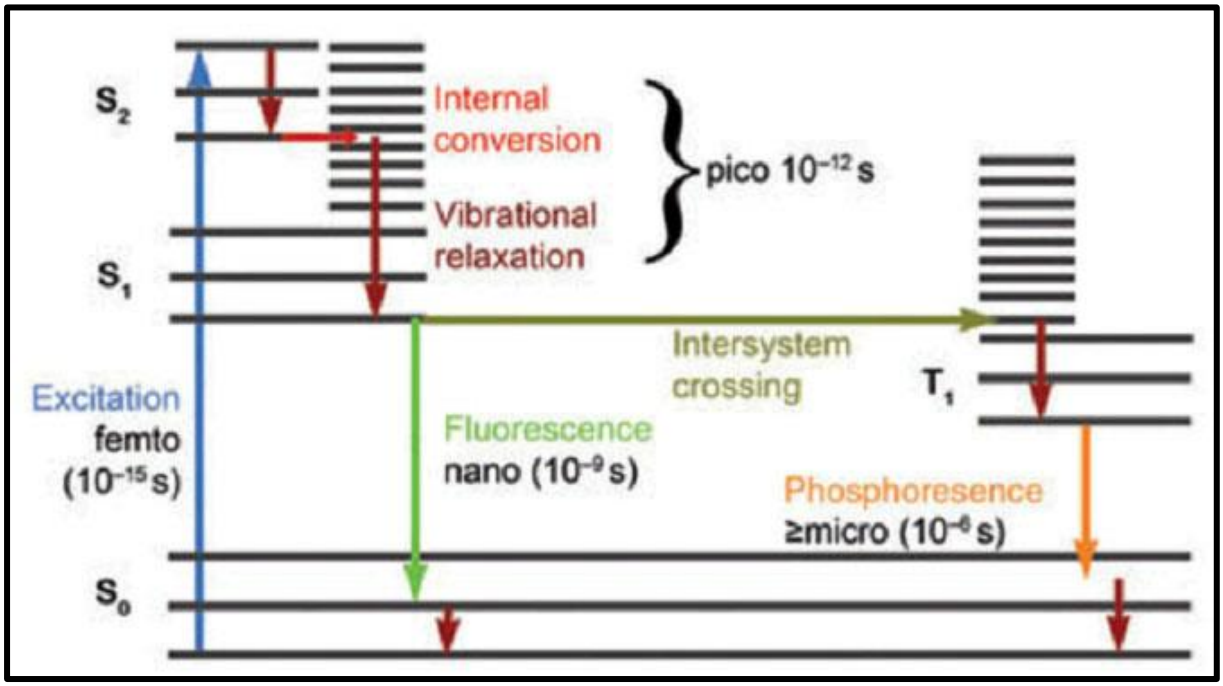


Figure 8: Jablonski diagram illustrating the processes involved in the creation of an excited electronic singlet state by optical absorption and subsequent emission of fluorescence (Life Technologies, 2014).

### 2.4.1.1. Excitation

A photon of energy is supplied by an external source (xenon lamp or a laser) and is absorbed by the fluorophore, creating an excited electronic singlet state ($S_1$). This process distinguishes fluorescence from chemiluminescence, in which for the latter the excited state is populated by a chemical reaction (Life Technologies, 2014).

#### 2.4.1.2. Excited-State Lifetime

The excited state exists for around 1–10 nanoseconds. At this time the conformation of the fluorophore changes. These processes have two important consequences. First, the energy of S1 is partially dissipated, yielding a relaxed singlet excited state (S1) from which fluorescence emission originates. However, not all the molecules that were initially excited by absorption will return to the ground state (S0) by fluorescence emission. S1 may also be depopulated by processes such as collisional quenching, fluorescence resonance energy transfer (FRET) and intersystem crossing. In order to measure the extent to which the process occurs the fluorescence quantum yield is determined (Life Technologies, 2014).

#### 2.4.1.3. Fluorescence Emission

The excited fluorophore is returned to its ground state ($S_0$) by emitting a photon. This produces a longer wavelength than that for excitation due to some of the energy being lost due to vibrations, therefore resulting in lower energy. This process is known as fluorescence. The difference in energy or wavelength between excitation and fluorescence is called the Stokes shift. It is said that," the Stokes shift is fundamental to the sensitivity of fluorescence techniques because it allows emission photons to be detected against a low background, isolated from excitation photons." (Life Technologies, 2014)

#### 2.4.1.4. Fluorescent nanoparticles

The development of dye-doped nanoparticles is a largely studied concept. Dye-doped nanoparticles are typically polymer or silica-based particles containing organic or inorganic dyes. Dyes can either be attached onto the nanoparticle surface or encapsulated inside the particles. Dye-doped nanoparticles are attractive for imaging applications because they are photostable due to the protection of the dye from oxygen and the external environment. This leads to high signal amplification. Their surfaces are also relatively easy to functionalize (Murcia & Naumann, 2005; Zhao *et al*., 2004a).

There have been numerous studies done on dye-doped nanoparticles for different applications including bacteria detection.

#### 2.4.1.5. Quantum dots

Quantum dots (QDs) or semiconductor nanocrystals are composed of group II - VI/V elements of the periodic table. Their size ranges from 1 to 10 nm. QDs are extremely bright whilst they retain their photostability (Roux *et al*., 2010). They have a high quantum yield and they have tunable fluorescence properties which enable them to have multiplex imaging capabilities whilst using a single wavelength (Roux *et al*., 2010). Streptavidin coated CdSe/ZnS QDs were bioconjugated with biotinylated antibodies for the detection of *E. coli* (Hahn *et al.*, 2005). Mannose-labelled CdSe QDs were used to induce fluorescent aggregation and to detect *E. coli* (Mukhopadhyay *et al*., 2009).

#### 2.4.1.6. Polymeric nanoparticles

Polymer-based nanoparticles are mostly prepared from hydrophobic polymers. Hydrophobic dye molecules are retained by hydrophobic interactions that occur between the dye and the polymer matrix. The hydrophobic nature of the dye molecules assists in preventing dye leaching. Hydrophobic polymeric nanoparticles tend to agglomerate and surface functionalization with poly(ethyleneglycol) (PEG), polysaccharides or proteins to reduce agglomeration (Taylor *et al*., 2000). Poly(ethylene glycol-b-trimethylsilyl methacrylate) fluorescent pH-responsive polymeric micelles were bioconjugated with anti-*E. coli* antibodies and used to detect *E. coli* cells (Mouffouk *et al*., 2011).

Amongst polymeric nanoparticles, there are conducting polymeric nanoparticles. Conducting polymers are mostly applied in biosensors and chemical sensors. Conducting polymers are easily modified, they are compatible with biological compounds or molecules and they are not easily reduced, making them environmentally stable. These polymers can also be deposited directly onto electrodes because they can be synthesized electrochemically (Rahman *et al*, 2008). The most commonly used conducting

polymers are polyaniline and polypyrrole because they have good thermal and oxidative stability (Cakmak *et al*, 2005).

#### 2.4.1.7. Silica nanoparticles

Silica nanoparticles are one of the most widely studied carriers for fluorescence. Silica is chemically and physically inert, meaning that the inner core of the particle is protected from any environment (Smith *et al*., 2006). The silica surface is easily modified with various functional groups such as carboxyl, amine, thiol and methacrylate. These nanoparticles can also be modified with biorecognition molecules for biological applications.

Silica nanoparticles are typically synthesized by two methods which are the Stobër method and the reverse micelle method (Smith *et al*., 2006). These methods make use of the “bottom-up” approach, whereby the nanoparticles are formed by self-assembly with an atom-by-atom or molecule-by-molecule motif, which create complex structures. These methods allow the alteration of the nanoparticles to achieve the desirable size (Smith *et al*., 2006).

The Stobër method has been well studied in literature and is used to prepare spherical silica nanoparticles with different sizes (Knopp *et al*., 2009). The method makes use of bulk ethanol solution in the presence of ammonia. Silica nanoparticles form by the hydrolysis of silane alkoxide precursors such as tetraethylorthoslicate (TEOS). The Stobër process can be carried out in a relatively short amount of time and is easy to perform. A number of dye molecules including rhodamine 6G and fluorescein dye molecules can be encapsulated in the silica matrix using the modified Stobër method. However this method produces silica nanoparticle that are not uniform in size (Knopp *et al*., 2009). This method is also not compatible with proteins because of its high alcohol content and basic pH. This leads to partial or complete protein denaturation.

The second method used to form silica nanoparticles is the reverse-micelle system called the water-in-oil microemulsion system. This method comprises

of three primary components: water, oil and surfactant. These components form a single-phase microemulsion system that is isotropic and thermodynamically stable. The particles are formed by water nanodroplets that act as a confined medium. Polar and water soluble dyes can be encapsulated in the SiNPs through this method because of the electrostatic attraction between the dye (positively charged) and the silica matrix (negatively charged) (Santra *et al*., 2001a).

SiNps have been applied in various applications. Thepwiwatjit *et al* used antibody-conjugated dye-doped SiNPs as a signal amplification tool for the detection of *Vibrio Cholerae O1* (Thepwiwatjit *et al*., 2013), whilst Tasnub *et al* used the same nanoparticles, with a different biorecognition molecule, for the rapid single step detection of *Campylobacter jejnu* (Tansub *et al*., 2012).SiNPs have also been applied in lateral flow tests. Bamrungsap and colleagues reported a lateral flow immunoassay for influenza antigen 'A' using fluorescently doped SiNPs as reporters (Bamrungsap *et al*., 2014). Another group reported the use of fluorescent dye-doped SiNPs-based immunochromatographic test strip sensor (lateral flow test) for the quantitative detection of enrofloxacin residues in chicken meat (Huang *et al*., 2013).

MCF-7 breast cancer cells were detected using dye-doped aptamer-conjugated SiNPs (Cai *et al*., 2013). Luminescent Rhodamine B doped SiNPs were used as fluorescent labels for protein microarray detection by (Liu *et al.*, 2013).

Table 2: Silica nanoparticles applied to various detection methods

| **Material** | **Detection method** | **Recognition ligand** | **Detection limit** | **Reference** |
|---|---|---|---|---|
| RuBpy dye-doped SiNPs, (60 nm) | Fluorimetry | Antibody | 25 cells/1.5mL | (Zhao *et al*., 2004b) |
| Core−Shell Fluorescent SiNPs (20-30 nm) | Fluorescence correlation spectroscopy (FCS) | No recognition molecule | - | (Ow *et al*., 2005) |
| Bioconjugated SiNPs (60 nm) | Flow cytometry | Anti-E*. coli* O157:H7 antibody | $1x10^2$-$1x10^3$ cells/mL | (Mechery *et al*., 2006) |
| SiO2 coated CdSe/Zn QD, amino modified ( 100 nm) | Fluorescence microscopy, spectrofluorometry | Glutaraldehyde amine crosslinking between bacteria and SiO2 coated CdSe/Zn QD | $3x10^2$ CFU/mL | (Fu *et al*., 2010) |
| RuBpy-doped silica nanoparticles | Confocal microscopy | Anti-E*. coli* O157:H7 antibody and bacteria stained with SYBR Green | 2.6×103Cell/mL | (Zhou *et al*., 2005) |
| Carboxyl modified, RuBpy dye, (131 nm) | Fluorometer and Fluorescent microscopy | Biotinylated rabbit anti-*E.coli* antibodies | - | (Chen & Tong, 2012) |

## 2.5. Conclusions and recommendations

Conventional methods are sensitive and specific, however they are also time consuming, complex and expensive. They do not bridge the gap between sampling and real-time response. This, therefore, poses as a challenge for safe drinking water and reduction of waterborne diseases. The need for a rapid and efficient detection system is yet to be satisfied.

The use of nanoparticles labelled with antibodies has been studied extensively and the techniques are well established. The use of antibody-labelled nanoparticles in this project will enable us to target the desired analytes. There are a number of techniques for bioconjugating nanoparticles with antibodies. The use of biotin-avidin chemistry ensures the most efficient orientation of the antibodies.

It was evident that magnetic nanoparticles are ideal for IMS, which is required for preconcentration. They can be made specific through the use of biorecognition molecules that are specific to the analyte of interest. They can be applied in a range of applications.

Literature suggests that there is a need for a “lab-on-a-chip” system for the detection of pathogens in food and water. The use of nanomaterials will aid in reaching this goal.

Encapsulating dye molecules into nanoparticles elongates the shelf-life of the dye. Signal intensities are amplified and thus making them beneficial tools for imaging applications. Lateral flow tests are moving from using colloidal gold to fluorescent nanoparticles because of the increased sensitivity that fluorescent nanoparticles provide. Thus, using fluorescent SiNPs for detection of bacteria will be adventitious towards signal amplification and the reduction in detection time. Using the reverse-micelle water-in-oil emulsion to synthesize fluorescent SiNPs will ensure reproducibility because the particle size obtained will be uniform.

## Chapter 3: Instrumentation and characterization

### 3.1. Infrared Spectroscopy

Spectroscopy is defined as the interaction between electromagnetic radiation (EMR) and matter. Infrared (IR) spectroscopy is a technique used for obtaining quantitative and qualitative results from samples of interest. The nature of the samples ranges from inorganic to organic compounds in the form of solids, liquids and gases. IR consists of 3 regions namely: the far infrared (400-10 $cm^{-1}$), mid-infrared (4000 - 400 $cm^{-1}$) and the near infrared (14285 - 4000 $cm^{-1}$) (Chemical Engineering Methods and Technology, 2010).

The mid infrared region is used most frequently because the vibrations of most organic compounds that are light-to-medium weight occur in this region. Fourier transform (FT) spectrometers are used to separated and measure the IR radiation (Chemical Engineering Methods and Technology, 2010).

Attenuated total reflectance-Fourier transform infrared spectroscopy (ATR-FTIR) is a technique used to determine the structure or the identity of a compound. Absorption measurements of different IR frequencies given off by different compounds are provided by this technique. The absorption measurement is generated by positioning a sample in the path of the IR beam. The chemical bonding or molecular structure that is characteristic to a compound is determined by irradiating the compound using IR energy. Therefore, to determine functional groups associated with the compound, ATR-FTIR is one of the techniques used (Chemical Engineering Methods and Technology, 2010).

The basic principle of the ATR-FTIR is shown in **Scheme 3**. The ATR crystal has a high refractive index and a polished surface.

In ATR-FTIR, a sample is placed on the ATR crystal, whereby the crystal has a high refractive index. The infrared beam enters the ATR crystal, which is then internally reflected at the sample-to-crystal interface. Prior to the internal

reflectance, the beam interacts with the sample up to a few microns (0.5 – 3 µm). In the IR region where the sample absorbs energy, this interaction causes attenuation of the beam's intensity. Following a few internal reflections, the IR beam exits the ATR crystal and is directed to the detector (AZom, 2015).

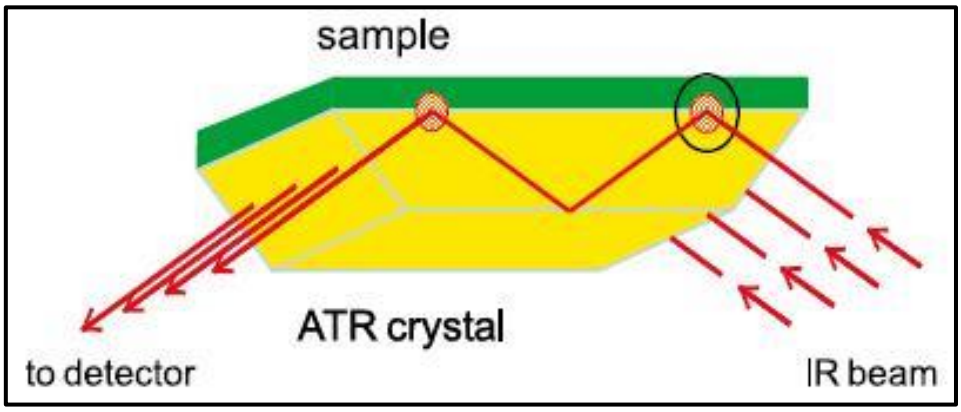


Scheme 3: Schematic diagram indicating the ATR-FTIR principle (AZom, 2015)

### 3.2. X-ray diffraction technique

X-ray powder diffraction (XRD) is a technique that is used to determine the crystallographic structure or phase of a material. X-rays are generated from a cathode ray tube, then they are collimated (concentrated) and directed towards the sample. Bragg's law ($n\lambda=2d\sin\theta$) relates the wavelength of electromagnetic radiation to the diffraction angle and the lattice spacing in a crystalline sample. When Bragg's Law is satisfied, the interaction between the incident ray and the sample causes interference in the form of diffracted rays. The diffracted rays are then detected, processed and counted. The x-ray beam is generated an angle θ, whilst the detector receives the diffracted rays at an angle of 2θ (**Scheme 4**) (Skoog *et al*., 1998; Dutrow & Clark, 2013).

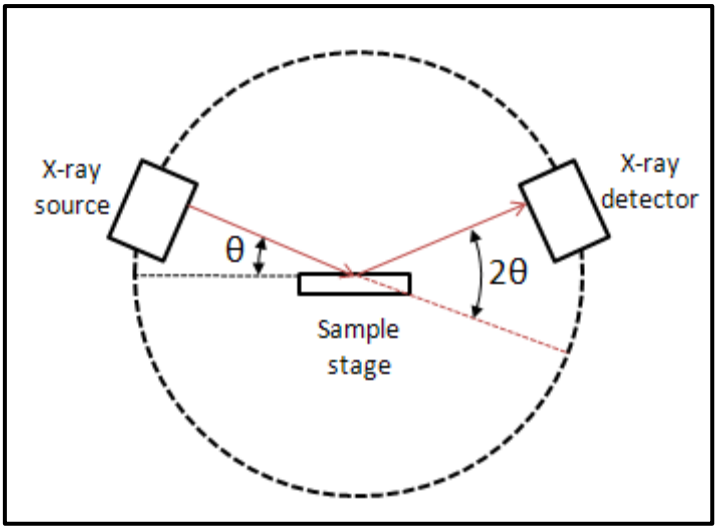


Scheme 4: Schematic diagram of an x-ray diffractometer (Dutrow & Clark, 2013).

### 3.3. Scanning Electron microscopy

Scanning electron microscopes (SEM) make use of a beam consisting of highly energetic electrons (primary electrons of up to 200 keV) to examine objects on a very small scale. When an electron beam strikes a sample, a number of signals are generated (**Scheme 5**). These kinds of signals produce various types of information such as: topographic or crystallographic information, as well as the composition of the sample. When an incident electron excites an electron in the sample, secondary electrons are produced. These secondary electrons move up to the surface and provided they have sufficient energy, they excite the surface. Another type of electrons that are deflected from the original path, are called backscattered electrons. These electrons are scattered primary electrons that rebound from the sample and they do not lose their energy. Alternatively x-rays and light/heat are produced in the sample. An image is generated by the backscattered and secondary electrons that arise from the scanning of the sample. The electros are collected by magnetic or electronic lenses on digital cameras in order to produce highly magnified images (Skoog *et al*., 1998).

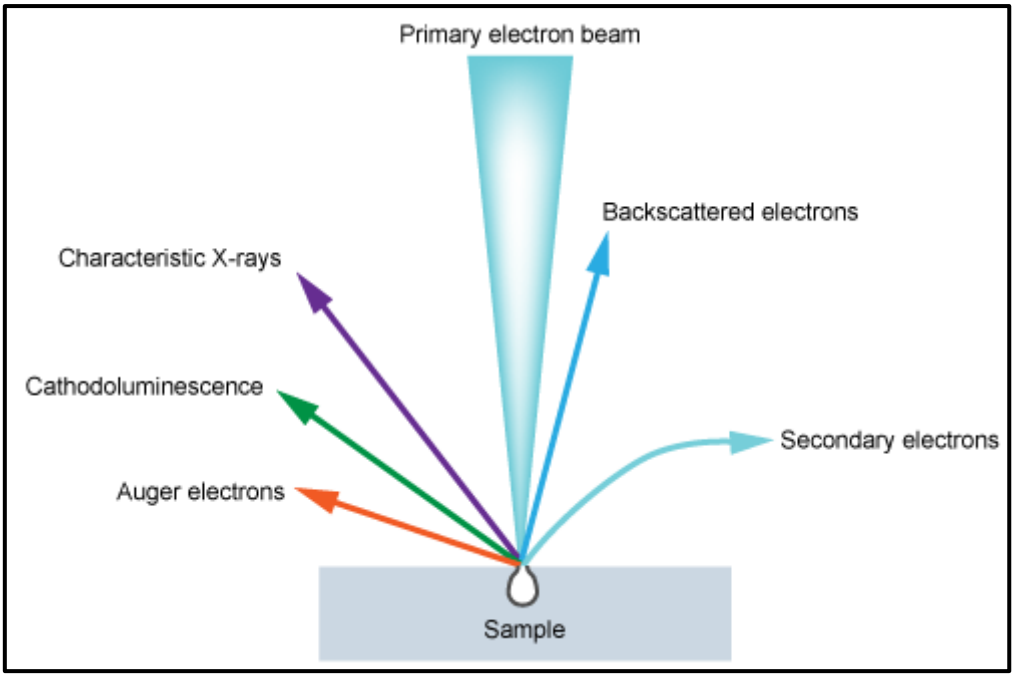


Scheme 5: A schematic illustration of electron beam interactions with sample (My Scope)

### 3.4. Transmission electron microscopy

Transmission electron microscopy (TEM) uses a similar principle as the SEM except the manner in which the electrons are detected. The image is formed by illuminating the sample with an electron beam in a high vacuum. The electrons that are transmitted through the sample are detected from below the sample onto a digital camera or phosphorescent screen. In regions where the electrons did not transmit, the image will be dark. In regions where the electrons are not scattered, the image will be brighter depending on the scattering effects of the sample (Skoog *et al*., 1998).

### 3.5. Ultraviolet and visible spectroscopy

Ultraviolet and visible spectroscopy (UV-vis) is an instrument that is used to measure the concentration of a sample through the measurement of absorbance intensity of a sample at a certain wavelength. The measurement is carried out through the application of Beer-Lambert Law. The Beer-Lambert

law is defined by the linear relationship between concentration and absorbance of an absorbing species. The law is denoted as

A= ***abc*** (**Equation 3.6.1**)

Where ***a*** is the molar absorptivity, ***b*** is the optical path length and ***c*** is the concentration. Quantitative analyses of compounds can therefore be carried out using standard calibration.

A measurement is taken by shining a light source onto the sample passing a monochromator. The electrons are then excited and they give off energy. The energy given off by these interactions is quantified by the detector and a reading is given at certain wavelengths (**Scheme 6**) (Skoog *et al*., 1998; Tissue, 1996).

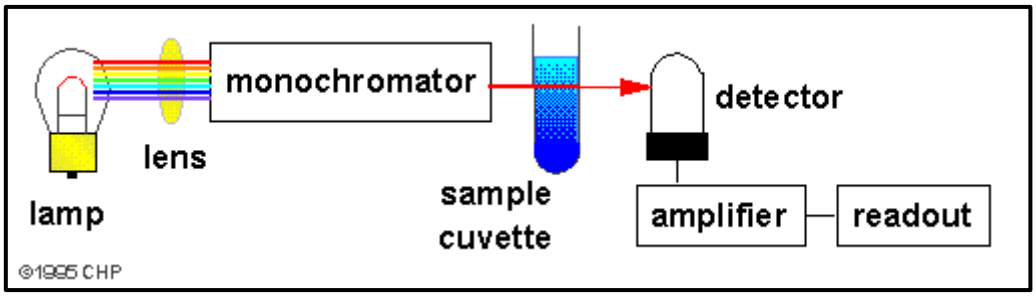


Scheme 6: A schematic representation of the UV-vis principle (Tissue, 1996).

### 3.6. Dynamic light scattering

Dynamic Light Scattering (DLS) is a technique that is widely used to determine particle size of micelles, polymers, proteins, emulsions, colloids and nanoparticles. This technique allows the measurement of particles with a size up to 1 nm. The size is determined by illuminating the sample with a laser beam and the light is scattered as the light hits the particles. The fluctuations of the scattered light are detected by a fast photon detector (**Scheme 7**). The fluctuations give information on the motion of the particles, which is then used to correlate the particle size through the diffusion constant. The diffusion coefficient ***D*** is then related to the radius ***R*** of the particles by means of the Stokes-Einstein Equation:

$$D = \frac{k_B T}{6\pi\eta\alpha}$$ (**Equation 3.6.2**)

Where **k** is the Boltzmann-Konstant, ***T*** the temperature and **η** the viscosity.

The correlation of the intensity can be performed by electronic hardware or software analysis of the photon statistics (Frisken, 2001; Voelker, 2015).

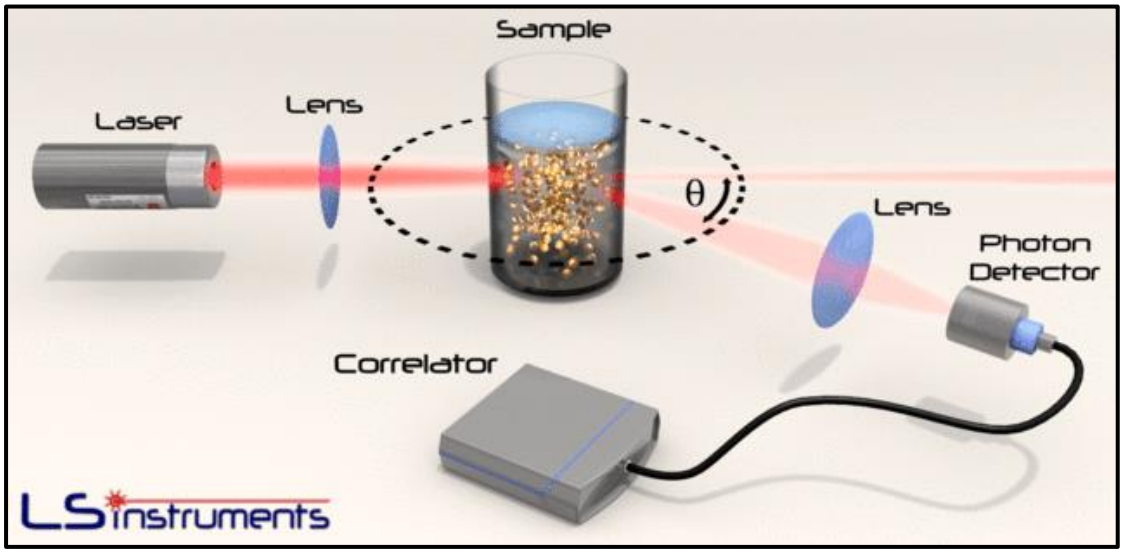


Scheme 7: Schematic diagram showing the basic principle of dynamic light scattering (Voelker, 2015).

The same principle is used to measure the surface charge (zeta potential) of the particles in a suspension. DLS is used in conjunction with electrophoresis whereby an electric field is generated.

## 3.7. Fluorescence Spectroscopy (Spectrofluorometer)

A spectrofluorometer is an instrument that is used to determine the excitation and emission wavelengths of a luminescent substance, as well as their photostability. A spectrofluorometer (**Scheme 8**) is equipped with a xenon lamp, which is used to excite the electrons in the sample. Motorized monochromators are placed to select the excitation and emission wavelengths. The excitation monochromator consists of two gratings that decrease light that has different wavelengths to those selected. Photomultiplier tubes are used to detect fluorescence. Fluorescence

(described in **section 2.4**) is quantified using designated electronic devices. Optical modules surround the sample holder (Lakowicz, 2007).

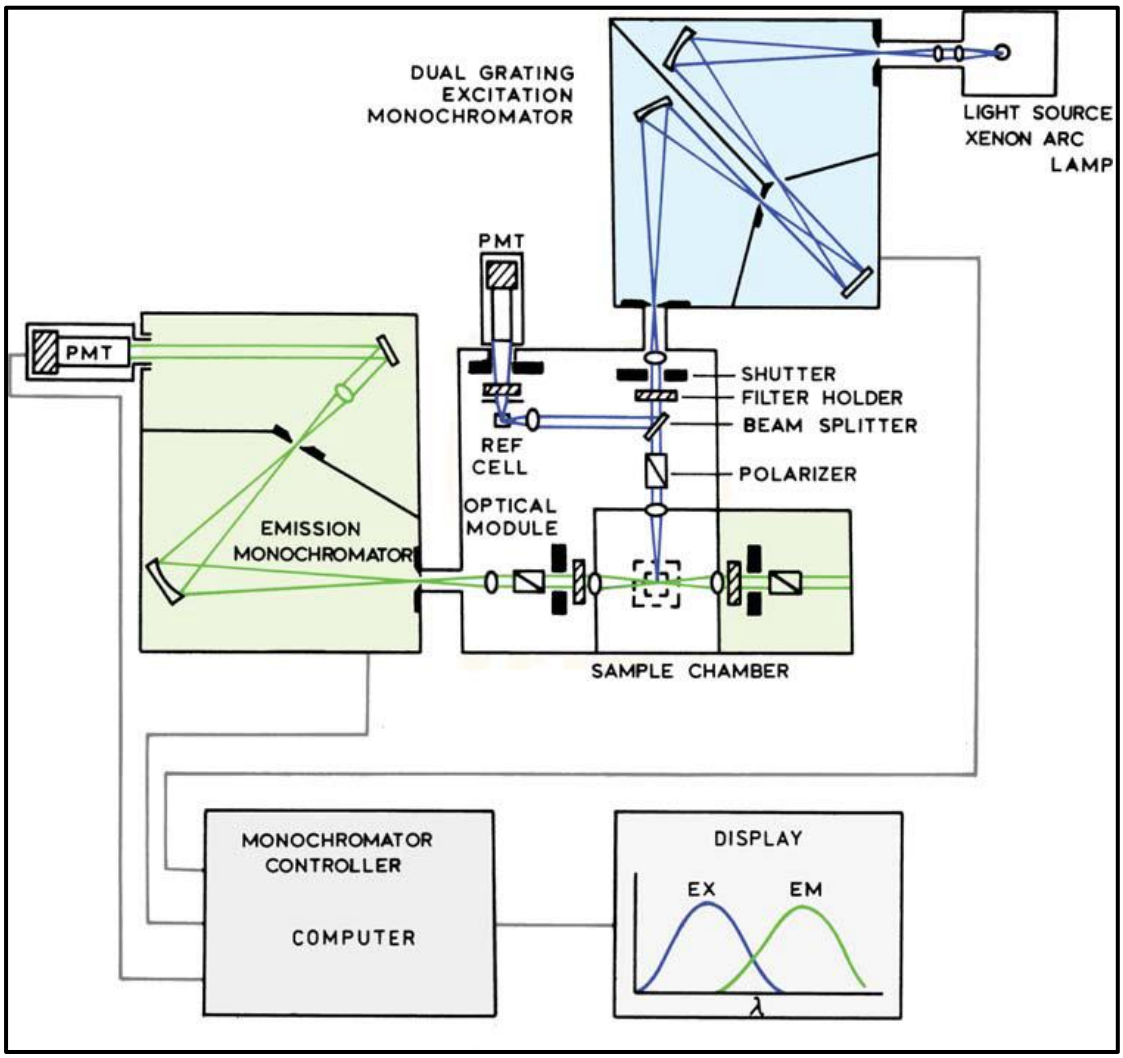


Scheme 8: Schematic drawing of a spectrofluorometer (Lakowicz, 2007).

# Chapter 4: Synthesis and characterization of surface functionalized silica nanoparticles

## 4.1. Introduction

This chapter describes the synthesis and application of SiNPs. The SiNPs were synthesized and surface functionalized with amine and carboxyl groups in order to bioconjugate them to avidin. Bioconjugation was then achieved by attaching biotinylated antibodies to avidin functionalized particles. The particles were then contacted with *E. coli* cells in order to test whether they could detect the *E. coli* as well as amplify the signal

## 4.2. Experimental Design

### 4.2.1. Materials

**Table 3: Reagents that were used in the experimental section**

| Material | Supplier |
|---|---|
| Tetraethylorthosilicate (TEOS) | Sigma Aldrich, USA |
| Tris(2,2'-bipyridyl)dichlororutheum (II) hexahydride (Ru(Bpy)) | Sigma Aldrich, USA |
| Triton X-100 | Sigma Aldrich, USA |
| Cyclohexane | Sigma Aldrich, USA |
| Hexanol | Sigma Aldrich, USA |
| Ammonium Hydroxide | Sigma Aldrich, USA |
| Ethanol | Radchem, SA |
| Trimethoxysilyldiethylenetriamine (DETA) | Sigma Aldrich, USA |
| Succinic Anhydride | Sigma Aldrich, USA |
| N-N'-Dimethylformamide | Sigma Aldrich, USA |
| Carboxyethylsilanetriol disodium | Fluorochem, UK |

| | |
|---|---|
| salt in 25% water (CETS) | |
| Tween 20 | Sigma Aldrich, USA |

Table 4: A list of reagents used in the bioconjugation process of SiNPs.

| | |
|---|---|
| 1-ethyl-3-(3-dimethylaminopropyl) carbodiimide hydrochloride (EDC) | Sigma Aldrich,USA |
| N-hydroxysulfosuccinimide sodium salt (sulfo-NHS) | Sigma Aldrich, USA |
| 2-(N-morhpolino)ethanesulfonic acid (MES) | Sigma Aldrich, USA |
| Avidin | |
| Polyclonal rabbit anti-*E.coli* biotinylated antibodies | AbD Serotec 4329-4906, UK |
| Bovine serum albumin (BSA) | Fluka, USA |

### 4.2.2. Synthesis of silica nanoparticles (SiNPs)

SiNPs were synthesized using the water-in-oil reverse micelle microemulsion (Bagwe *et al*., 2004). 1.77 g of triton X-100 were weighed in four 50 mL-beakers each, and stirred continuously at 450 revolutions per minute (rpm). The following reagents were added in the order in which they are mentioned while continuously stirring: 1.6 mL of hexanol, 7.5 mL of cyclohexane, 400 µL deionized water, 80 µL of 0.1M Ru(Bpy) dye, 100 µL of tetraethylorthosilicate (TEOS) and 60 µL of ammonium hydroxide (**Figure 9**). The mixture was stirred for 24 hours. 20 mL of acetone were added in order to release the particles from the microemulsion. The particles were washed three times, twice with ethanol and once with deionized water. The nanoparticles were then suspended in 10 mL of water.

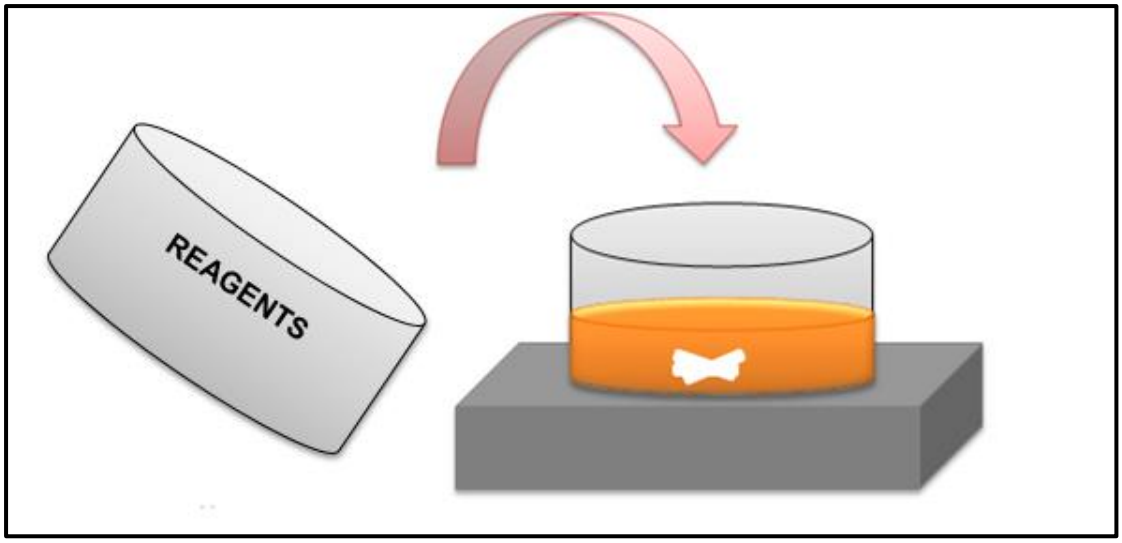


Figure 9: Synthesis of SiNPs through a reverse micelle water-in-oil microemulsion.

### 4.2.3. Chemical modification of SiNPs

The SiNPs were chemically modified with amine and carboxyl groups. Two methods were investigated for the attachment of carboxyl groups onto the SiNPs surfaces.

#### 4.2.3.1. Attachment of amine groups to the SiNPs

During the surface functionalization process, the particles were post coated in order to have the functional groups on the exterior particle surfaces. Therefore, before the washing step as indicated in **section 4.2.3** above, 50 µL of TEOS added, for post coating, and the particles were stirred for 30 minutes. 50 µL of trimethoxysilyldiethylenetriamine (DETA) were added to attach amine groups. The mixture was left to stir for 24 hours before the particles were released from the microemulsion and washed (Chen *et al*., 2012). The particles were then washed 2 times with acetone and once with ethanol. The amine-functionalized SiNPs ($NH_2$-SiNPs) were resuspended in 10 mL of deionized water (**Scheme 9**).

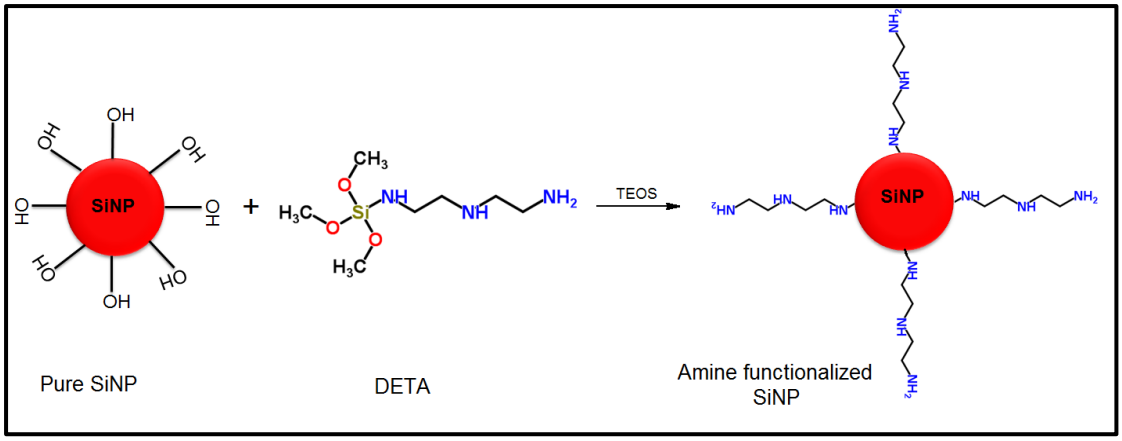


Scheme 9: Schematic diagram of surface modification of SiNPs with amine groups.

### 4.2.3.2. Carboxyl surface functionalization

#### i. Indirect attachment of carboxyl groups onto amine functionalized SiNPs:

The indirect attachment of carboxyl groups is described in **Figure 10**.

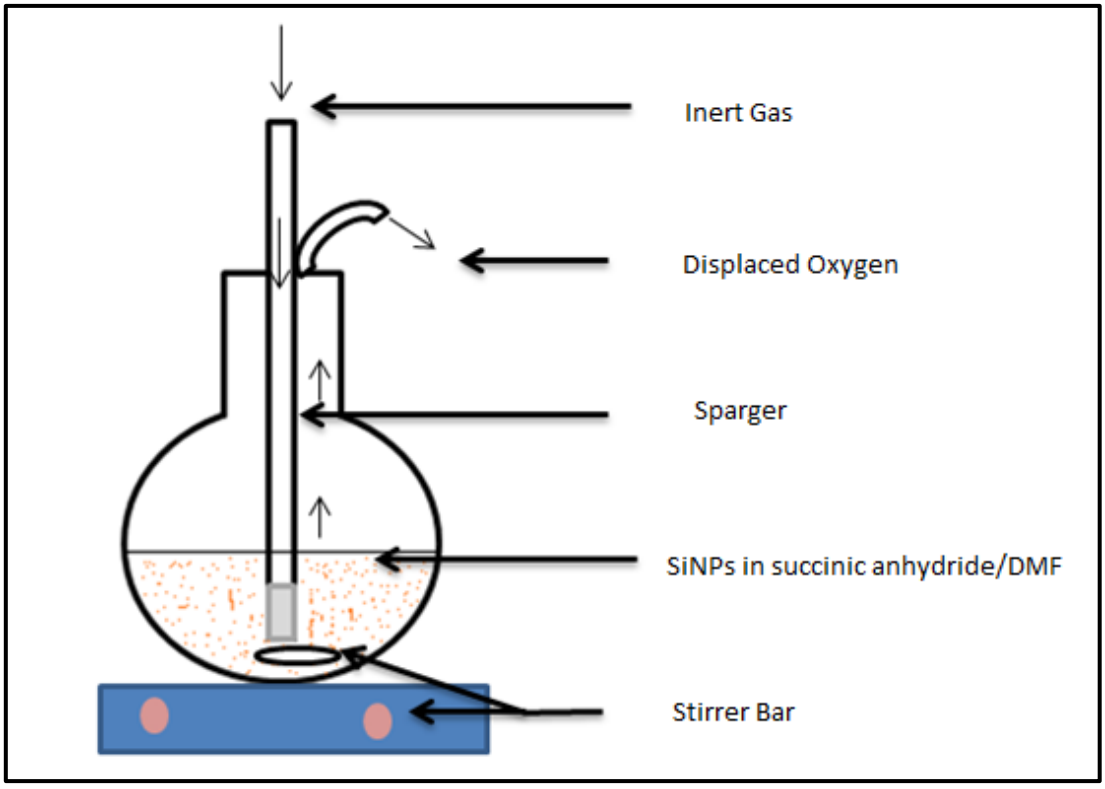


Figure 10: Carboxyl surface functionalization of SiNPs using succinic anhydride under inert conditions.

The dye-doped $NH_2$-SiNPs, as described in section **4.2.3.1**, were sonicated for 30 minutes and poured into a 25 mL volumetric flask. 15 mL of 10% succinic anhydride in dimethylformamide (DMF) were added and the suspension was purged with nitrogen for 18 hours at room temperature, while stirring at 200 rpm. The particles were washed with deionized water. The particles were resuspended in 10 mL of deionized water (**Figure 10**).

This method provided a very low particle yield. The method was, therefore, adjusted such that 10 mL of the dye-doped $NH_2$-SiNPs were centrifuged and 15 mL of succinic anhydride were purged with argon gas for 30 minutes. The particles were then resuspended in the succinic anhydride and purged for 30 minutes while stirring. They were left to stir for 18 hours, with continuous stirring without purging (**Scheme 10**).

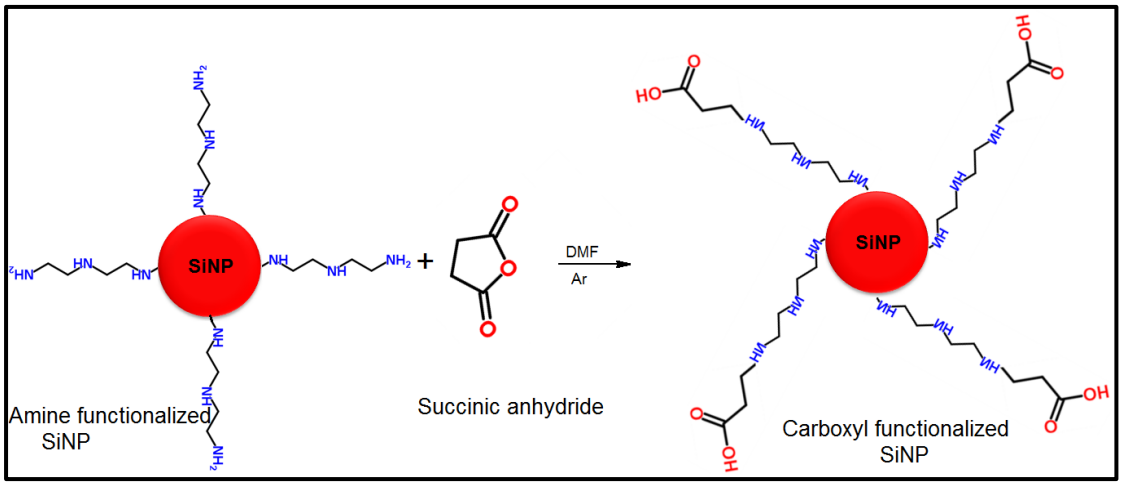


Scheme 10: Schematic diagram of the indirect attachment of carboxyl groups onto SiNPs.

### ii. Direct attachment of carboxyl groups onto SiNPs:

Another method of directly attaching the carboxyl groups was discovered by Cai *et al*. During the surface functionalization process, the particles were post coated as described in **section 4.2.3.1**, which involved adding 50 µL of TEOS to the SiNPs before the washing step, and for 30 minutes. 50µL of CETS were added to attach carboxyl groups (**Scheme 11**). The mixture was left to stir for

24 hours before the particles were released from the microemulsion and washed. The particles were stored in 0.05% tween 20 solution, at room temperature, until use (Cai *et al*., 2013).

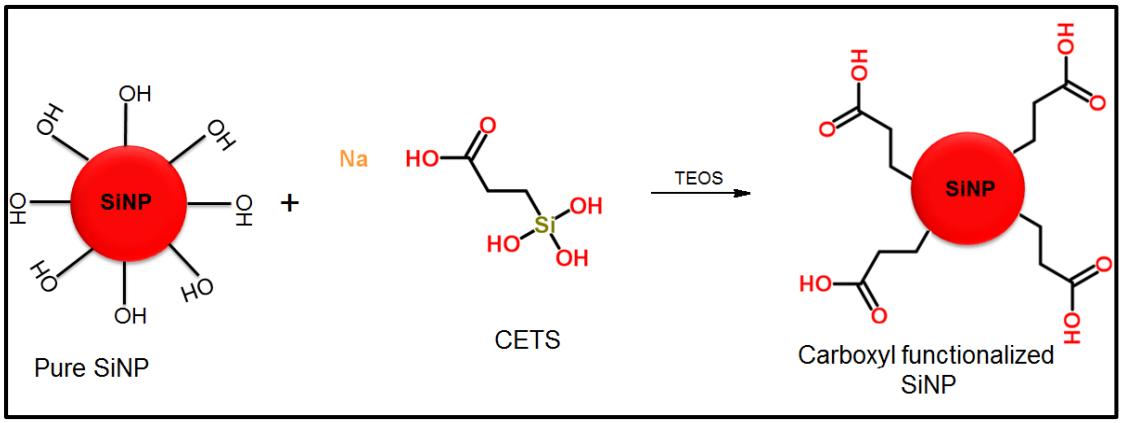


Scheme 11: Schematic diagram of the direct attachment of carboxyl groups onto SiNPs.

### 4.2.4. Immobilization of avidin to SiNPs

A mass of 1 mg of nanoparticles was centrifuged at 17000 rpm and 20 ºC, for 10 minutes to remove the suspension medium. The pellet was resuspended in 1 mL of 0.1 MES buffer, pH 5.5. The carboxyl groups were activated by adding 500 µL of 10 mM Sulfo-NHS and 40 mM EDC, dissolved in MES buffer, to the particle solution. The nanoparticles were incubated for 15 minutes at room temperature, in a shaker at 400 rpm. The nanoparticles were washed twice in 10 mM PBS buffer, pH 7.4, with 0.05% tween 20 and then resuspended in 1.5 mL PBS-tween solution. 50 µL of 4 mg/mL avidin solution were added to the particles and the mixture was incubated at room temperature, for 2 hours in a shaker at 400 rpm. The avidin modified particles were washed twice in 10 mM PBS-tween solution and resuspended in 40 mM tris-HCl with 0.05% BSA solution, for an hour, to block free carboxyl groups. The particles were washed twice with PBS-tween and resuspended in 10 mM PBS-tween solution (Chen *et al*., 2012) (**Scheme 12**).

### 4.2.5. Attachment of biotinylated-antibodies to avidin-functionalized SiNPs

13.3 µL of 4 mg/mL biotin-labelled antibodies were added to a particle suspension of 1.5 mL PBS-tween and incubated for an hour. The bioconjugated SiNPs were washed once with PBS-tween and resuspended in 1.5 mL 10 mM PBS-tween with 10 mg/mL BSA (**Scheme 12**).

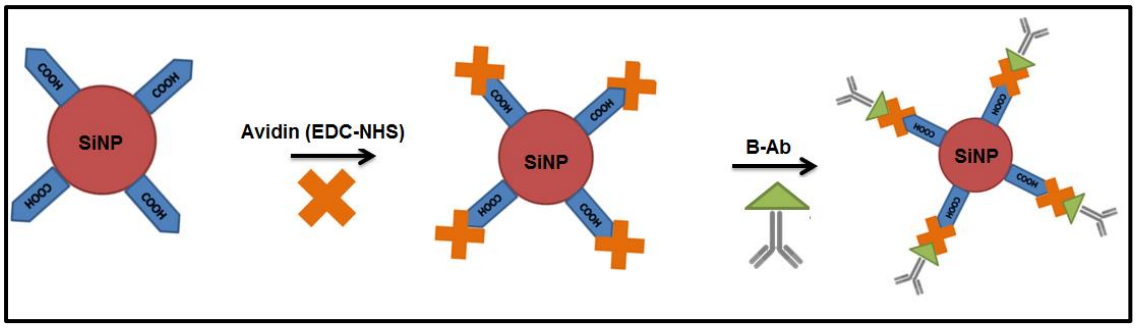


Scheme 12: A schematic diagram illustrating the immobilization of avidin onto SiNPs and the attachment of biotinylated antibodies.

### 4.2.6. Culture of *E. coli*

*E*. *coli* K12, a non-pathogenic strain, was plated on Luria Bertani (LB) agar plates for 48 hours. Some of the *E*. *coli* was scraped from the agar plates and resuspended in 14 mL of autoclaved, deionised water. The UV-vis was used to measure the bacteria concentration by measuring the optical density (OD) at 600 nm. An OD of 1 corresponds to a bacterial cell count of 8 x $10^8$ cells/mL (Agilent Technologies, 2013).

### 4.2.7. Avidin Quantification

The avidin immobilized onto SiNPs was quantified using the biotin (5-fluorescein) conjugate assay following the protocol given by Chen *et al*., 2012. All the data points in the assay were prepared in 1.5 mL volumes. Avidin concentrations ranging from 0 µg/mL to 2.2 µg/mL were used in the assay. A set amount of 52.5 µL, 1 µg/mL biotin (5-fluorescein) was added to each data

point. **Table 5** gives the composition of each data point used to plot the calibration graph.

Table 5: Composition of data points used for the avidin-biotin (5-fluorescein) standard curve.

| ***Avidin concentration (µg/mL)*** | ***Avidin solution (µL)*** | ***Biotin (5-fluorescein) (µL)*** | ***1xPBS (µL)*** |
|---|---|---|---|
| 0 | 0 | 52.5 | 1447.5 |
| 0.2 | 30 | 52.5 | 1417.5 |
| 0.4 | 60 | 52.5 | 1387.5 |
| 0.6 | 90 | 52.5 | 1357.5 |
| 0.8 | 120 | 52.5 | 1327.5 |
| 1 | 150 | 52.5 | 1297.5 |
| 1.2 | 180 | 52.5 | 1267.5 |
| 1.4 | 210 | 52.5 | 1237.5 |
| 1.6 | 240 | 52.5 | 1207.5 |
| 1.8 | 270 | 52.5 | 1177.5 |
| 2 | 300 | 52.5 | 1147.5 |
| 2.2 | 330 | 52.5 | 1117.5 |

In order to determine the concentration of avidin in the sample supernatant, a biotin (5-fluorescein) conjugate titration was done whereby the supernatant volumes were increased while the biotin (5-fluorescein) conjugate was kept constant. The samples were adjusted to a fixed volume of 1.5 mL using 1X PBS. **Table 6** gives the composition for each data point in the supernatant titration assay.

A volume of 300 µL of each data point was placed into a 96-well black plate and analyzed with the $FL_x800$ fluorescent plate reader. The biotin (5-fluorescein) conjugate excites at a wavelength of 490 nm and emits fluorescence at 524 nm. The appropriate filters were used in order to excite and detect at the aforementioned wavelengths.

Table 6: Composition data points used to determine the avidin concentration present in the supernatant of SiNPs after avidin conjugation

| ***Supernatant concentration (%)*** | ***Supernatant volume (µL)*** | ***Biotin (5-fluorescein) (µL)*** | ***1x PBS (µL)*** |
|---|---|---|---|
| 0.25 | 3.75 | 52.5 | 1443.75 |
| 0.5 | 7.5 | 52.5 | 1440 |
| 1 | 15 | 52.5 | 1432.5 |
| 1.67 | 24.98 | 52.5 | 1422.53 |
| 5 | 75 | 52.5 | 1372.5 |
| 7.5 | 112.5 | 52.5 | 1335 |
| 10 | 150 | 52.5 | 1297.5 |
| 12.5 | 187.5 | 52.5 | 1260 |
| 15 | 225 | 52.5 | 1222.5 |
| 17.5 | 262.5 | 52.5 | 1185 |
| 20 | 300 | 52.5 | 1147.5 |
| 22.5 | 337.5 | 52.5 | 1110 |

The avidin calibration curve was constructed using the sample compositions given in **Table 5**. The calibration curve was normalized according to the first data point that did not contain avidin. The normalized calibration curve shows the quenching of the biotin (5-fluorescein) conjugate associated with the avidin concentration. The linear portion of the calibration curve was fit with a linear curve. The equation generated by the linear curve was then used to calculate the amount of fluorescence quenching of the biotin (5-fluorescein) conjugate in the sample supernatant. The Bio-Tek Instruments Inc Fluorescence Plate Reader (FLx800) was used to determine the fluorescence intensity emmited by the biotin (5-fluorescein) conjugate. The 96-well plates were read off at excitation and emission wavelengths of 490 nm and 524 nm respectively, given that the appropriate filters were used.

### 4.2.8. Dye-loading of Ru(Bpy) dye in SiNPs

A serial dilution was conducted by preparing a stock solution of the dye with a concentration of 74.86 mg/mL (0.1 M). A two-times serial dilution was prepared from the stock solution. The UV-vis was used to collect the data points for the calibration curve. The absorbance of each dilution was read off at 450 nm and used in the construction of the curve. The same procedure was used, in conjunction with the spectrofluorometer, to determine the luminescence properties of the Ru(Bpy) dye and the dye-doped SiNPs. The PerkinElmer Lamda 35 UV Vis Spectrophotometer and the Jobin Yvon Nanolog FL3-22 Spectrofluorometer were used to quantify the dye loading and to determine the photoluminescence properties of the Ru(Bpy) dye and dye-doped SiNPs. The particle solutions were analyzed in 3mL quartz cuvettes, at room temperature.

### *4.2.9.* SiNPs-labelled *E. coli* fixing for TEM analysis

Biological samples that were viewed under TEM were fixed in order to keep the structure of the *E. coli* cells intact. 1 mL of a 2.5% glutaraldehyde solution (in 0.075 M PBS buffer at a pH of 7.4) was added to *E. coli* cells that were labelled with antibody-functionalized SiNPs and fixed for an hour for sectioning and imaging via TEM. The *E. coli*-SiNPs conjugates were rinsed three times for 5 minutes with 0.075 M phosphate buffer. Approximately 50 µL of an aqueous 0.5 % osmium tetroxide solution was added to the *E. coli*-SiNPs conjugates and allowed to infiltrate the conjugates for 30 minutes, followed by three washing cycles using distilled water. The pellet was subsequently dehydrated for 10 minutes with 30%, 50%, 70% and 90% ethanol respectively. Thereafter, the conjugates were dehydrated for 10 minutes, three times with 100% ethanol and stored in 100% ethanol for 20 hours. The conjugates were then infiltrated with 50% Quetol in 100% ethanol for 30 minutes and 100% Quetol for 3 hours. After removing Quetol, the conjugates were embedded in TAAB 812 embedding resin for 39 hours at 60°C. The polymerized conjugates were sectioned and stained for 3 minutes in lead acetate and 2 minutes in lead citrate, with 3 wash cycles in between.

### *4.2.10.* *E. coli* detection through fluorescence microscopy

Fluorescence microscopy was used to view the SiNPs-labelled *E. coli* cells. Samples were prepared by incubating 23 mg (120 µL) of SiNPs with 500 µL of $1x10^8$ *E. coli* concentrations for an hour followed by separation and washing by centrifuging at 16000 rpm at 30 s. The samples were concentrated to 20 µL in order to view the whole sample on a single glass slide. Controls of *E. coli* cells only and SiNPs only were also included. An Olympus BX41 fluorescence microscope (Olympus Microscopy, Essex, UK.), equipped with a 490 nm band-pass filter with a 510 nm cut-off filter was used to determine the level of agglomeration of the SiNPs, as well as to confirm the binding of the *E. coli* cells to antibody-functionalized SiNPs.

### 4.2.11. Application of SiNPs for *E. coli* detection

The initial experiment was performed on a bacteria concentration of $1x10^4$ CFU/mL. The particle concentration was varied, whereby particle masses between and inclusive of 0.3 mg and 0.75 mg were contacted with 500 µL *E. coli* in PBS. The controls were the lowest and highest particle concentrations without any bacteria. The controls were added to 500 µL of PBS without *E. coli*. The *E.coli* cells were contacted with SiNPs at ambient temperatures for an hour. The *E. coli* and SiNPs were spun down at 16000 rpm for 30 s. The supernatants were collected for analysis. Positive controls were included, which were centrifuged at 10000 rpms for 10 minutes. The positive controls were included in order to see the maximum fluorescence intensity that can be expected in relation to the particle masses introduced in the tests. After washing, all the samples were resuspended in PBS-tween. Triplicates of 300 µL of each sample were added to a black 96 well plate, and were read using the Bio-Tek Instruments Inc Fluorescence Plate Reader (FLx800). The 96-well plates were read off at excitation and emission wavelengths of 485 ± 20 and 645 ± 20 nm respectively.

## 4.3. Material characterisation

The dye-doped SiNPs and surface-functionalized dye-doped SiNPs were characterized with respect to size and morphology using a JEOL JEM 2100 High Resolution Transmission Electron Microscopy (HR-TEM) and JEOL 7500Field Emission Scanning Electron Microscopy (FE-SEM). Pure SiNPs were used as the control. The samples for the TEM analysis were prepared by dispersing the SiNPs in ethanol. The suspension was then vortexed and sonicated for 3 minutes each. A drop of particle solution was placed onto the carbon coated grid and the excess water was removed. The average particle size was determined by measuring 100 particles per sample from the TEM analysis. The samples for the SEM analysis were oven dried overnight and placed on the grid. They were then carbon coated 6 times for full coverage.

The surface charge and the degree of agglomeration were measured using the Malvern Zetasizer (Malvern, UK). 50 µL of the SiNP suspension were dispersed in 1 mL of deionized water. The resulting suspension was sonicated for 30 minutes before the analysis for size and 30 minutes before the analysis for surface charge.

The Perkin Elmer Spectrum 100 Attenuated Total Reflection Fourier Transform Infrared (ATR-FTIR), at a resolution of 4 $cm^{-1}$ was used to confirm the functional groups present on the nanoparticles surface, as well as the presence of the dye within the particles. The SiNPs were dried for 3 days using the freeze drier and scanned 16 times per run.

## 4.4. Results and Discussions

### 4.4.1. Synthesis of dye-doped SiNPs

The single-phase microemulsion system is isotropic and thermodynamically stable. The differences between microemulsions and emulsions are that microemulsions form droplets that are one magnitude smaller than emulsions (10 - 100 nm); microemulsions are usually transparent as compared to the cloudy emulsions; microemulsions do not require vigorous stirring in order for

them to form. Lastly, microemulsions are thermodynamically stable whereas emulsions are kinetically stable and eventually end up separating into the oil and water phase (Paul & Moulik, 2001). The oil phase consists of cyclohexane, hexanol and triton X-100. The water phase consists of water, TEOS and Ru(Bpy) dye. The water pool (nanodroplets) that forms in the bulk oil phase is regarded as the nanoreactor in the microemulsion system (**Scheme 13**). The nanodroplets are stabilized by the surfactant molecules whereby hexanol is a co-surfactant to triton X 100. The dye molecules are polar and water soluble, therefore they are readily encapsulated in the silica matrix. The ammonium hydroxide acts as a catalyst ($NH_3$) for the hydrolysis of TEOS as well as a reactant ($H_2O$) and this is how the SiNPs are formed. The SiNPs are precipitated out using acetone because acetone to destabilizes the emulsion by dissolving the surfactant. (Wang *et al*., 2008b; Santra *et al*., 2001b; Zhao *et al*., 2004b).

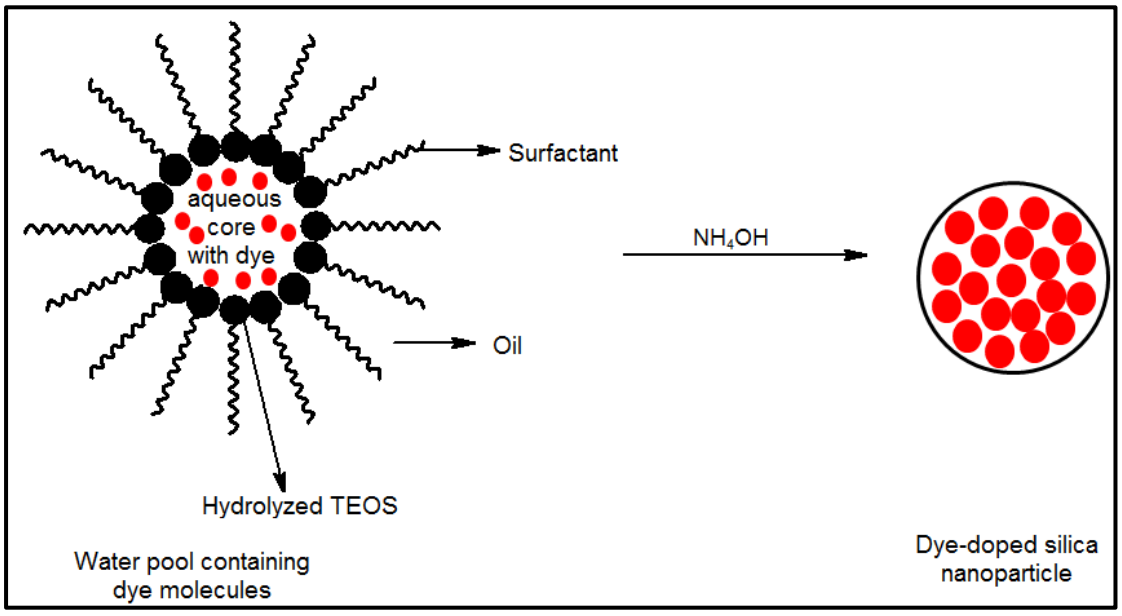


Scheme 13: Schematic diagram illustrating the way in which SiNPs form in a microemulsion (Santra *et al*., 2001).

Initially, pure and dye-doped SiNPs were synthesized following an experimental procedure from Bagwe *et al*. [2006]. The method followed for the preliminary synthesis of the SiNPs did not take into consideration the post coating of the nanoparticles. Post coating the nanoparticles before they were

surface functionalized introduced the new functional groups on the outside of the silica surface, whereas if they were not post coated, the functional groups would be attached in the interior of the silica shell. The method was adopted from Chen *et al*'s work (Chen *et al*., 2012).

It was discovered that the decomposition of ammonum hydroxide from $NH_4OH$ to $NH_3$ and $H_2O$, was detrimental to the synthesis of the SiNPs. This could be because ammonium hydroxide is a catalyst in the microemulsion. Therefore, should it decompose, then the hydrolysis of the TEOS cannot occur successfully. **Figure 13** shows the deformed SiNPs which were synthesized using ammonium hydroxide that had decomposed. Crystals were also observed, which could have been the dye that was not properly encapsulated, therefore being attached on the outer surface of the SiNPs.

#### 4.4.1.1. TEM Analysis

The TEM images in **Figure 11** show the morphology of the particles synthesized by the Chen *et al* method. This method seemed to work much better than the method used in the preliminary studies. The SiNPs looked more dispersed and more spherical. The pure SiNPs and the pure dye-doped SiNPs are displayed in **Figure 11 A** and **B** respectively. It was seen that encapsulating the dye in the nanoparticles increased the size significantly. The amine functionalized SiNPs (**Figure 11 C**) appeared to have an increased surface roughness when compared to the dye-doped SiNPs. This may be indicative of the surface been successfully functionalized with amine groups.

The introduction of carboxyl groups onto the SiNPs surface was to reduce agglomeration due to their negative charge. Therefore, carboxylated SiNPs (COOH-SiNPs) were synthesised in order to reduce agglomeration througho steric hindrance and still be to bind the avidin for the attachment of biotinylated antibodies.

The TEM image in **Figure 11 D** demonstrates the morphology of the COOH-SiNPs. A rough surface was observed, which is possibly indicative of the attachment of carboxyl groups onto the SiNPs. The particles still had a spherical morphology and were uniform in size; therefore the attachment of the carboxyl groups did not have an effect on the shape of the particles when compared to the dye-doped particles without surface modification. The particles appear agglomerated in this image; however other techniques were used to prove the reduction of agglomeration following carboxylation.

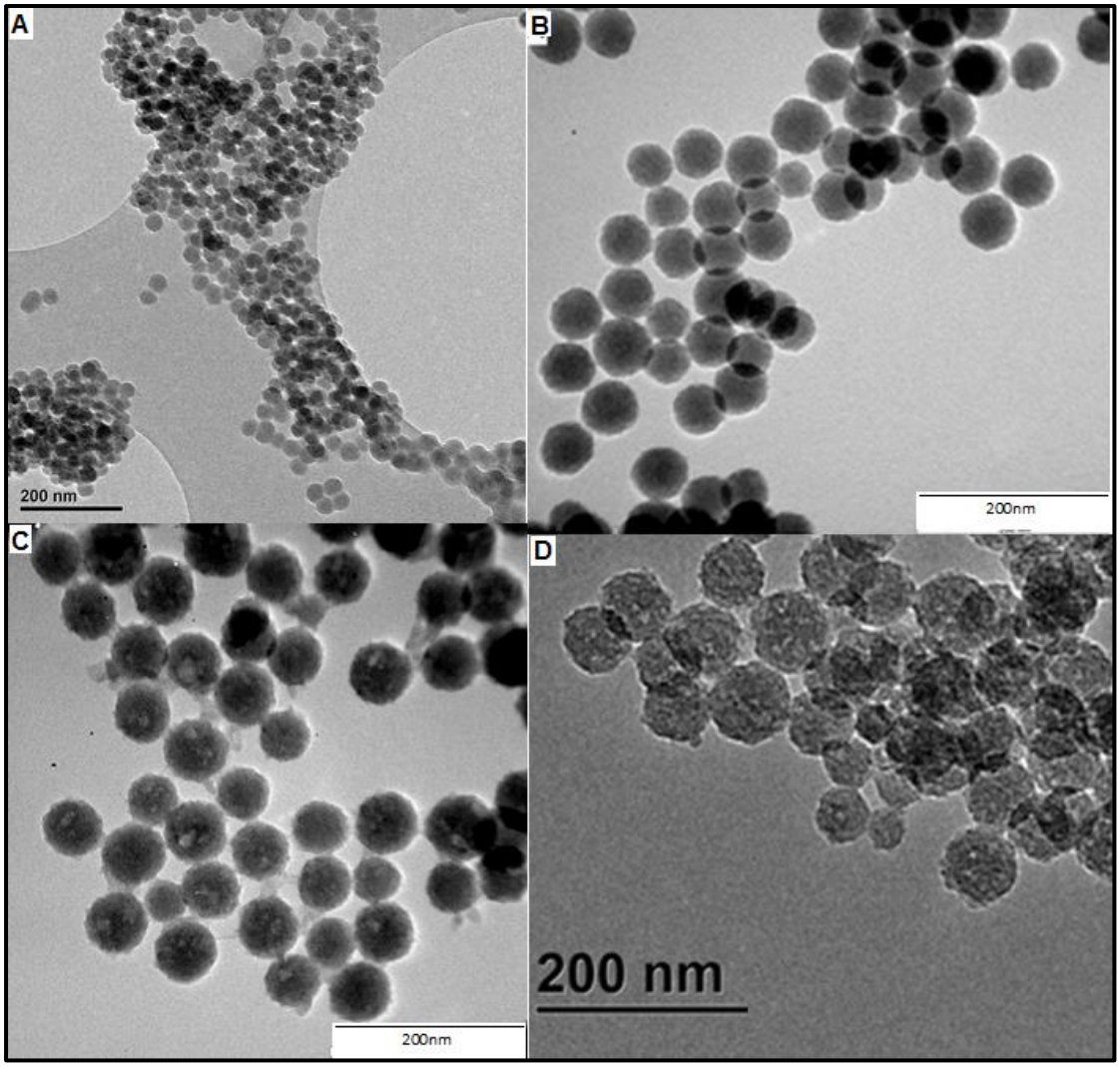


Figure 11: TEM Images of A) Pure SiNPs, B) Dye-doped SiNPs, C) amine functionalized dye-doped SiNPs and D) carboxyl functionalized SiNPs

**Table** 7 gives the overall comparison of size of the pure and surface modified SiNPs.

Table 7: Comparison of the size of the different particles that were synthesized.

| | ***Average particles size (nm) from TEM (n=100)*** |
|---|---|
| **Pure SiNPs** | 21.20 ± 3.10 |
| **Dye-doped SiNPs** | 53.32 ± 5.59 |
| **Dye-doped $NH_2$-SiNPs** | 60.86 ± 6.68 |
| **Dye-doped COOH-SiNPs (indirect attachment)** | 68.02 ± 7.29 |
| **Dye-doped COOH-SiNPs (direct attachment)** | 75.06 ± 4.50 |

According to literature, the size of our SiNPs was <100 nm, and thus far the particle size was satisfactory (Chen *et al*., 2012; Cai *et al*., 2013; Bagwe *et al*., 2004). The particle size for the pure SiNPs was found to be 21.20 ± 3.10 nm. It was observed that the particle size almost doubled to 53.32 ± 5.59 nm when the Ru(Bpy) dye was encapsulated. Following that the SiNPs were washed to remove the residual dye on the surface of the SiNPs, this result may prove that the dye was successfully encapsulated in the silica matrix. The particle size increased even further, to 60.86 ± 6.68 nm, when the amine groups were attached onto the silica surface. The increase in size was due to the longer chain lengths from the amine functional group introduced through DETA. The addition of carboxyl groups had the same effect on the size of the SiNPs, which was also expected. The size of the SiNPs that were functionalized with COOH groups using the indirect method had a size of 68.02 ± 7.29 nm. On the other hand the size of the SiNPs functionalized with COOH groups using the direct attachment method yielded particles with a size of 75.06 ± 4.5 nm. The difference in size could be attributed to the difference in chain lengths of

the succinic anhydride and the CETS. Since the carboxyl groups were introduced to introduce steric hindrance, the chains were even longer than those of the amine groups; hence the increase in size.

### 4.4.2. Mass yield

A mass yield study was conducted on the dye-doped amine-functionalized SiNPs in order to see how much of the TEOS was converted into product. An experiment, done in triplicates, was dedicated to this study, whereby the end product was dried and weighed. The average mass yield from 1.39 g of TEOS was found to be 46.7 ± 3.54%. The yield is not that high, but this could be due to the TEOS not being the limiting agent in the reaction that takes place when the experiment is conducted. The reaction kinetics might be in such a way that the TEOS does not go through 100 % conversion; hence it is not the limiting reagent. Further studies regarding the reaction kinetics could aid in justifying why the TEOS is not completely converted into product.

#### 4.4.2.1. SEM analysis

A SEM analysis was done on the dye-doped SiNPs and the dye-doped $NH_2$-SiNPs (**Figure 12**).

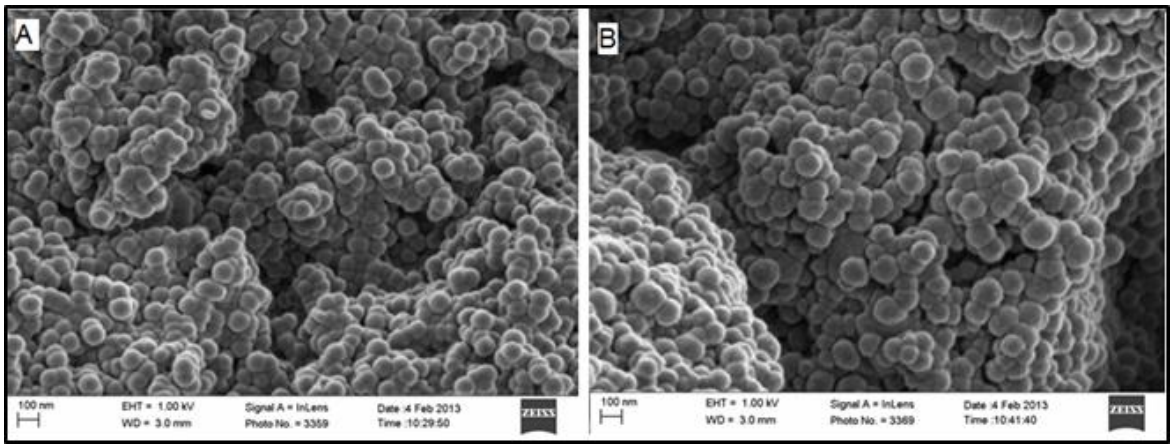


Figure 12: SEM images of A) Dye-doped SiNs and B) Dye-doped $NH_2$-SiNPs.

The SiNPs were freeze-dried prior to the analysis. The SiNPs appeared agglomerated but uniform in size. The agglomeration of the particles could be attributed to the drying of the particles before analysis. It was seen that the morphology of the SiNPs was not altered following surface modification. The $NH_2$-SiNPs (**Figure 12 A)** were rougher on the surface when compared to the dye-doped SiNPs (**Figure 12 B**), which may indicate that amine groups were attached onto the surface. There were no crystalline structures observed on the SiNPs, therefore showing that the Ru(Bpy) dye was encapsulated in the silica matrix rather than attached to the surface of the SiNPs.

The stability of ammonium hydroxide was found to be crucial as the degradation thereof lead to an alteration of the SiNPs during synthesis (**section 4.4.1**). The SiNPs were no longer spherical and the were crystal structures which may have been from the TEOS which was probably crystalized (**Figure 13**).

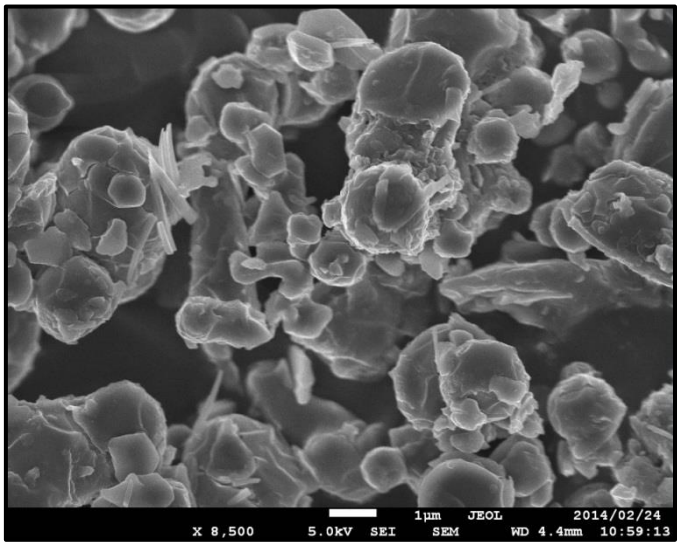


Figure 13: SEM image of deformed SiNPs after being synthesized with ammonium hydroxide that had degraded.

### 4.4.3. Surface charge

The particle size was determined using the ZetaSizer. Samples were analyzed in triplicates, along with three measurement cycles. The preliminary

results showed that dye-doped SiNPs had a particle size of 3981± 632 nm. It was discovered that the particles were agglomerating because the measurements were not corresponding with the sizes on the TEM images.

In the attempt to eliminate particle agglomeration, dialysis was used as an alternative washing mechanism, as it was thought that separation by centrifugation was the main cause of agglomeration. Three samples were washed for 24 hours with the water being changed every 2 hours. $NH_2$-SiNPs were used for these experiments.

Washing the particles through dialysis was not aiding the reduction of agglomeration because the oil phase would interfere with the process. The first wash was then done by centrifuging the emulsion to get rid of the oil phase. The average particle size, as determined by the ZetaSizer, was 611.7 ± 65.5 nm, with an average surface charge of -15 ± 12.9 mV. The particle size was too big, which showed that the particles were still forming agglomerates. The surface charge on the other hand, was not representative because of the very high deviation between samples. It was then decided that dialysis will not be used for the purpose of this study because centrifugation was still introduced prior to dialysis. This defeated the purposes of determining the efficacy of the study.

Since the use of dialysis was futile, it was decided to introduce surfactants as dispersing agents. Surfactants have the ability to prevent particles in solution to aggregate, thus preventing agglomeration. In the presence of a surfactant, the interfacial energy between the solid particles and liquid interfaces is reduced. This leads to the formation of new surfaces between the solid phase and the solutions instead of forming aggregates. Another advantage is that the electrostatic repulsive forces between the particles increase as the surfactant adsorbs to the particle surface; hence the reduction in agglomeration (Pilemand, 2002).

The surfactants of choice were Polyvinyl Alcohol (PVA) and tween 20. Surfactant concentrations of 0.5, 1 and 1.5 %, in combination with sonication times of 10 and 15 minutes, were studied. The effect of the surfactants and sonication times were visualized under the fluorescence microscope a 100x magnification. Dye-doped, $NH_2$-SiNPs were used for this study.

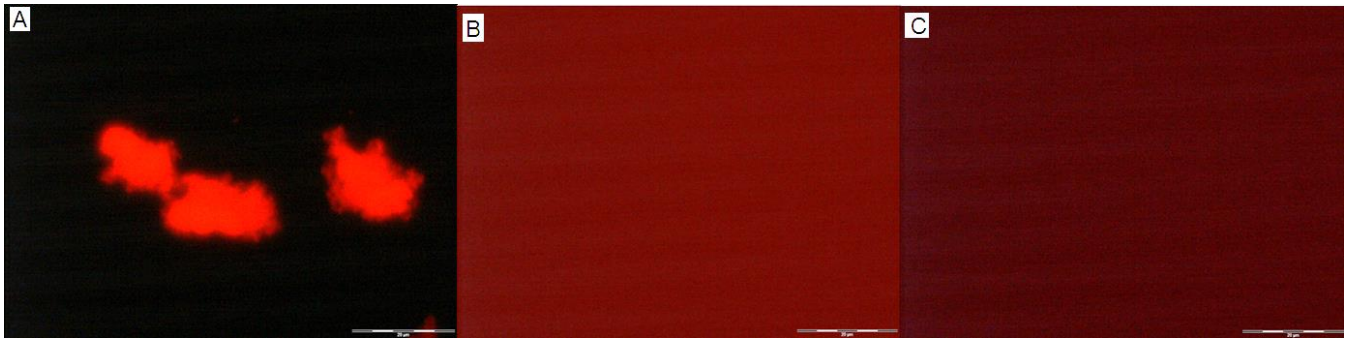


Figure 14: Fluorescent images of dye-doped SiNPs in A) water (no surfactant), B) 0.5% Tween 20 and C) 0.5 % PVA solutions.

The addition of surfactants was meant to reduce agglomeration of the particles by increasing the stability of the particle suspension. The bright signal observed in **Figure 14 A**, indicated that the particles were agglomerating in water. After the addition of surfactant, a red haze was observed in **Figure 14 B** and **Figure 14 C**. It was, therefore, evident that the addition of surfactants to the particle suspensions aided the reduction of particle agglomeration. The use of higher surfactant concentrations resulted in the same observation as that of the 0.5%. It was then decided that the particle suspensions would, in future, be stabilized using Tween 20. Tween 20 was the main choice of surfactant because of its common use in biotechnology; i.e. it is commonly used as a washing agent in Western blots, while preventing non-specific binding of antibodies (Wu *et al*., 2002) and reduces protein aggregation (Chou *et al*., 2005). Tween 20 was also used to stabilize gold nanoparticles in a high-ionic strength solution (Cheng-Yan *et al*., 2010).

After eventually seeing that the ZetaSizer was not giving accurate readings regarding the particle size, it was decided that the particle size would be

determined using the TEM images of the particles. **Table 8** gives the overall comparison of the pure and surface modified SiNPs. The surface charge was measured using the ZetaSizer.

Table 8: Comparison of the zeta potential of the different particles that were synthesized.

| | ***Zeta Potential (mV)*** |
|---|---|
| **Pure SiNPs** | -19.4 ±0.40 |
| **Dye-doped SiNPs** | -14 ± 1.0 |
| **Dye-doped $NH_2$-SiNPs** | +18.0 ± 0.51 |
| **Dye-doped COOH-SiNPs (indirect attachment)** | -23.3 ± 4.12 |
| **Dye-doped COOH-SiNPs (direct attachement)** | - 31.9 ± 1.1 |

The surface charge or zeta potential is attributed to the overall surface charge of the particles.The zeta potential aids in predicting the colloidal stability of the nanoparticle solution that results from the repulsive forces. A sample is considered to be well dispersed if the surface charge is close to 30 mV and above (Tansub *et al*., 2012). If all the nanoparticles possess a large negative or positive charge above 30 mV, they will be stable in solution because of the high repulsion forces amongst them (Heurtault *et al*., 2003; Müller *et al*., 2001; Müller & Jacobs, 2002). This will prevent agglomeration. A low surface charge results in flocculation or coagulation of nanoparticles. Surface modification is usually performed in order to increase surface charge thus improving the long-term stability of the nanoparticles (Wang *et al*., 2008b).

The zeta potential of the pure SiNPs was -19.4 ± 0.4 mV. The negative charge was expected and has been reported previously because the surface of the silica has a negative charge (Bagwe *et al*., 2004). The Zeta Potential of

the dye-doped SiNPs was -14 ± 1.0mV. The decrease in surface charge was due to the dye molecules which possess a positive charge. The Ru(Bpy) dye has a positive charge (**Figure 16)** and so there is an electrostatic attraction between the dye and the negatively charged silica matrix (Bagwe *et al*. , 2004); therefore these weak molecular interactions that facilitate the entrapment of the dye decrease the surface charge of the particles. There is also a possibility that some dye molecules were also on the surface of the SiNPs, leading to the decrease in surface charge. The +18.0 ± 0.51 mV surface charge of the amine-functionalized SiNPs was due to the addition of primary amines seeing that primary amines have a positive charge at a neutral pH.

The zeta potential of the amine functionalized SiNPs was positive but was also lower than 30mV. The particles agglomerated due to the inconsistency of surface charge, therefore attracting negatively charged particles. The charge was not strong enough to create strong repulsion forces between the particles.

Bagwe *et. al* stated that the high sensitivity provided by the fluorescence signal enhancement, selectivity and reproducibility of nanoparticle-based bioassays can be inhibited by the tendency of the silica nanoparticles to agglomerate irreversibly and cause non-specific binding. This phenomenon explains why it is vital to have SiNPs that are well dispersed. Bagwe *et al* continues on to say, “Excess functional groups that follow after surface modification are capable of binding to or interacting with various chemical and biological species, which could also lead to false positive or negative signals” (Bagwe *et al*., 2006).

The introduction of carboxyl groups to the surface of the SiNPs was intended to eliminate agglomeration. Carboxyl groups possess a negative charge. The surface charge of the carboxyl-modified SiNPs was measured to be - 31.9 ± 1.1 mV. The charge is high enough to keep the particles apart and therefore keeping the particles stable in suspension. A high surface charge and the addition of surfactant ensure that the suspension remains stable at all times.

The SiNPs reported in this study were found to be in the same range as those reported by other researchers (
**Table** 9).

Table 9: Surface charge of fluorescent dye-doped SiNPs-COOH in other studies synthesized using the same experimental procedure.

| Researchers | Direct/Indirect attachment | Zeta Potential (mV) |
|---|---|---|
| (Cai *et al*., 2011) | Direct | -20.3 |
| (Chen *et al* , 2012a) | Indirect | -43.8 |
| (Auger *et al*., 2011) | Direct | -45.9 |

The variation of the surface charge may be attributed to the different techniques and lab equipment/glassware dimensions that were used during synthesis, like microemulsion preparations; however the reported SiNPs have an acceptable charge.

The direct carboxylation method has proved to be superior to that of the indirect carboxyl attachment. Therefore, SiNPs that are directly carboxylated will be used in further tests and applications.

The versatility of the SiNPs was tested by the attempt to encapsulate different dyes in the silica matrix. The different dyes that were tried were: Rhodamine 6G and B and methylene blue. The attempt to encapsulate these dyes failed because all these dyes were negatively charged. The SiNPs also have a negative charge. Therefore, instead of the dye being encapsulated, the Silica and the dye repelled each other. This prevented the dyes from being encapsulated in the silica matrix. Positively charged dyes were not tested due to financial and time constraints and these can be investigated in the future.

### 4.4.4. Attenuated Total Reflection Fourier Transform Infrared (ATR-FTIR) analysis

FTIR analyses were performed on the pure, dye-doped and amine functionalized silica nanoparticles. The Ru(Bpy) dye powder was also analyzed for control purposes.

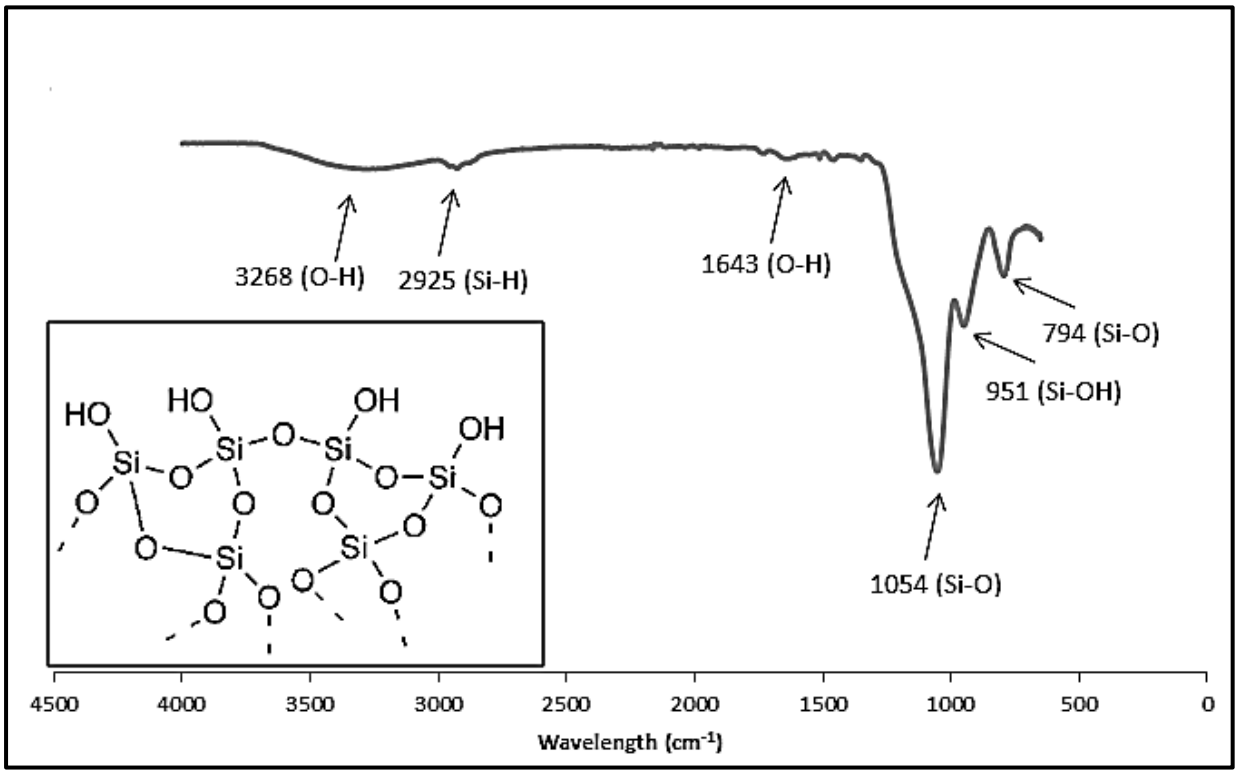


Figure 15: FTIR spectrum of pure SiNPs that are not surface functionalized. The structure of the silica matrix is given in the bottom left.

The FTIR spectrum in **Figure 15** shows the absorption bands that are characteristic bands of pure SiNPs. The absorption bands at 3268 $cm^{-1}$ and 1643 $cm^{-1}$ are attributed to the O-H vibrations; the band at 2925 $cm^{-1}$ from the Si-H vibration. There's a symmetric vibration of the Si-O band at 1054 $cm^{-1}$, an asymmetric vibration of the Si-OH band at 951 $cm^{-1}$ and a symmetric vibration of the Si-O band at 794 $cm^{-1}$ (Beganskiene *et al*., 2004; Knipping *et al*., 2004; Perez Leon *et al*., 2006).

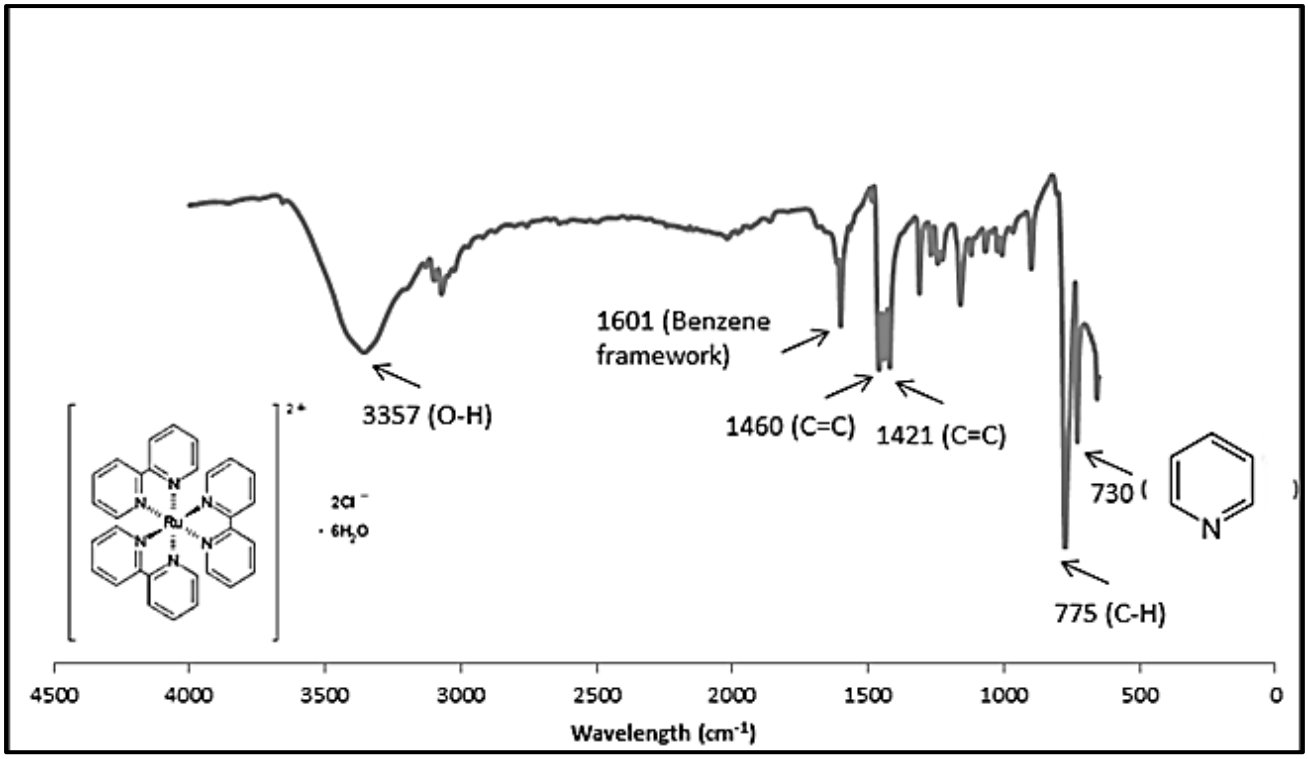


Figure 16: FTIR spectra and chemical structure of the Ru(Bpy) dye (Bagwe *et al*., 2004).

The FTIR spectrum of the Ru(Bpy) dye is shown in **Figure 16**. An absorption band representing an O-H stretch at 3357 $cm^{-1}$was observed for the Ru(bpy) dye. The characteristic peaks of the Ru(Bpy) dye are as follows: 1601 $cm^{-1}$ attributes to weak benzene groups; 1460 $cm^{-1}$and 1421 $cm^{-1}$ attributed by the C=C bipyridine stretch; 775 $cm^{-1}$ represents the C-H vibrations; and 730 $cm^{-1}$ is attributed to the monosubstituted benzene rings (Perez Leon *et al*., 2006).

**Figure 17** shows the FTIR spectra of the Ru(Bpy) dye, pure and dye-doped SiNPs. The three spectra were compared to see if the dye was present in the dye-doped particles.

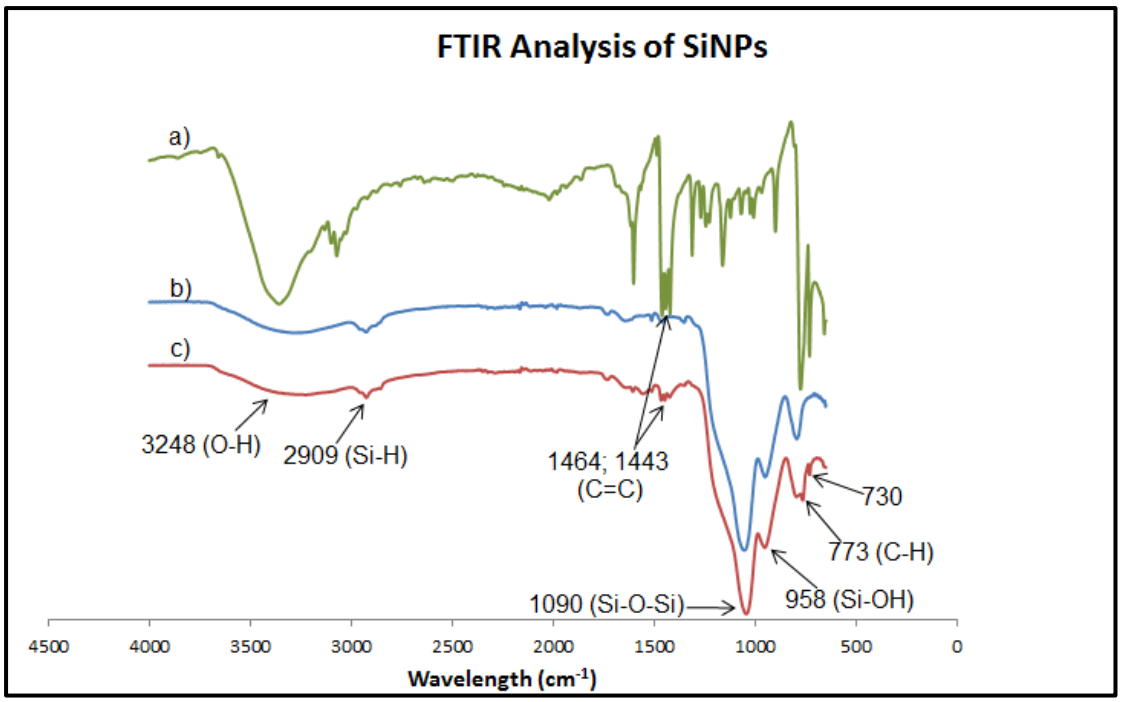


Figure 17: FTIR spectra of a) Ru(Bpy) dye, b) pure SiNPs and c) dye-doped SiNPs (Bagwe *et al*., 2004).

The dye-doped silica nanoparticles have the characteristic peaks of the Ru(Bpy) dye as well as those of silica. The characteristic bands of the dye shifted from 1460 $cm^{-1}$and 1421 $cm^{-1}$ to 1464 $cm^{-1}$ and 1443 $cm^{-1}$ respectively. The shift in these peaks is indicative that the dye is present in the SiNPs matrix. This is also true because the residual dye was washed off after synthesis. The peak at 1054 $cm^{-1}$ shifted to 1090 $cm^{-1}$ and this is due to the addition of Ru(Bpy) dye. The presence of the band at 1090 $cm^{-1}$,730 $cm^{-1}$ and 773 $cm^{-1}$ makes it evident that the silica nanoparticles have not degraded after the addition of the dye, because it is characteristic of the silica (Bagwe *et al*., 2004). The characteristic peaks of the Ru(Bpy) dye are not that strong and therefore other characteristic tools were used to further prove the presence of the Ru(Bpy) dye in the silica matrix (**Section 4.4.5** and **Section 4.4.6**).

The spectra of the amine functionalized SiNPs and the carboxyl functionalized SiNPs are shown in **Figure 18** . The carboxyl modified SiNPs represented in **Figure 18** are those that are attached through the conversion of amine groups.

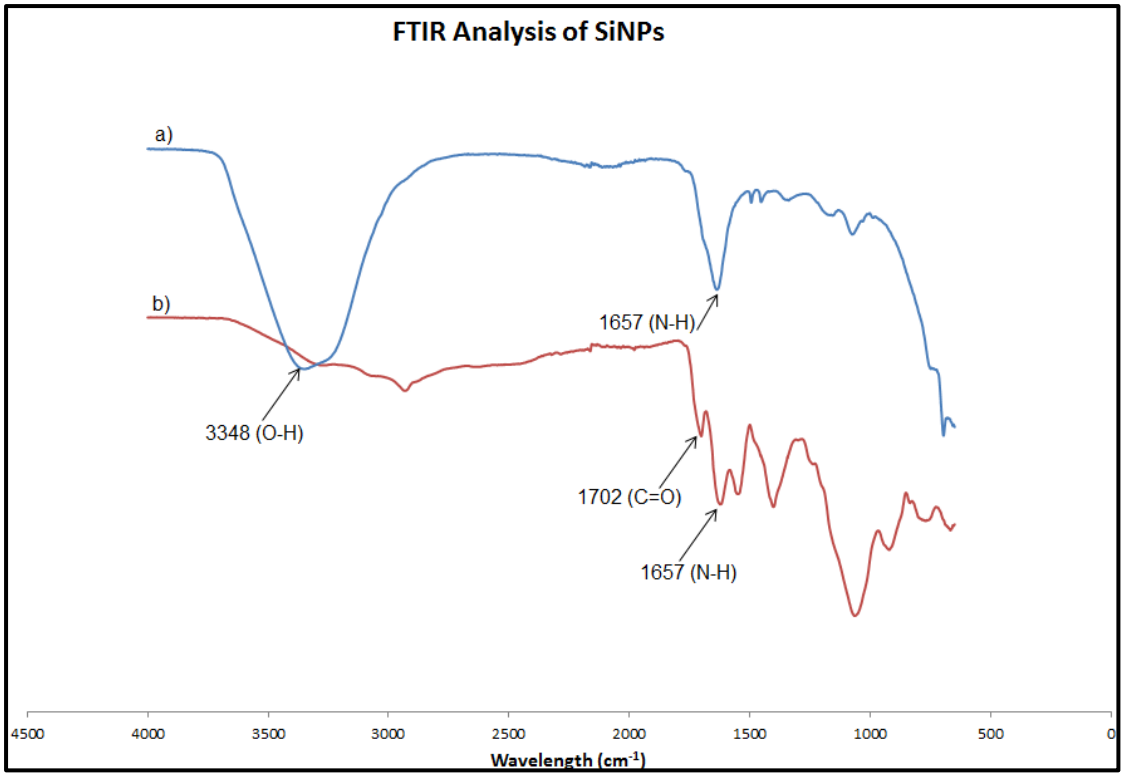


Figure 18 : FTIR spectra of a) amine functionalized SiNPs with an amine peak at 1657 $cm^{-1}$ and b) carboxyl functionalized SiNPs with a carboxyl peak at 1702 $cm^{-1}$. The carboxyl groups were attached through the conversion of amine groups using succinic anhydride.

The adsorption band at 1657 $cm^{-1}$ is attributed to the amide I stretch, which confirms that there are amine groups on the surface of the SiNPs (Ma *et al*., 2004). It was observed that the Si-O-Si band was reduced, which could be due to the high moisture content that is seen at 3348 $cm^{-1}$.

For the spectrum representing the COOH-SiNPs, the absorption band at 1702 $cm^{-1}$ is attributed to the C=O stretch, which confirms the attachment of carboxyl groups. The two spectra are superimposed to indicate that the peak at 1657 $cm^{-1}$ is still observed on the COOH-SiNPs spectrum. This means there are still some amine groups present on the carboxyl modified SiNPs, whereas only the carboxyl groups were expected. Therefore, not all the amine groups were converted to carboxyl groups. The amount of succinic anhydride used may have not been sufficient to facilitate complete conversion of the amine groups to carboxyl groups. Purging for 18 hours may have been too

much such that the DMF ended up evaporating while the experiment was running.

The COOH-SiNPs were attached directly through the use of the CETS. **Figure 19** shows the FTIR spectra of COOH-SiNPs in comparison to that of pure SiNPs.

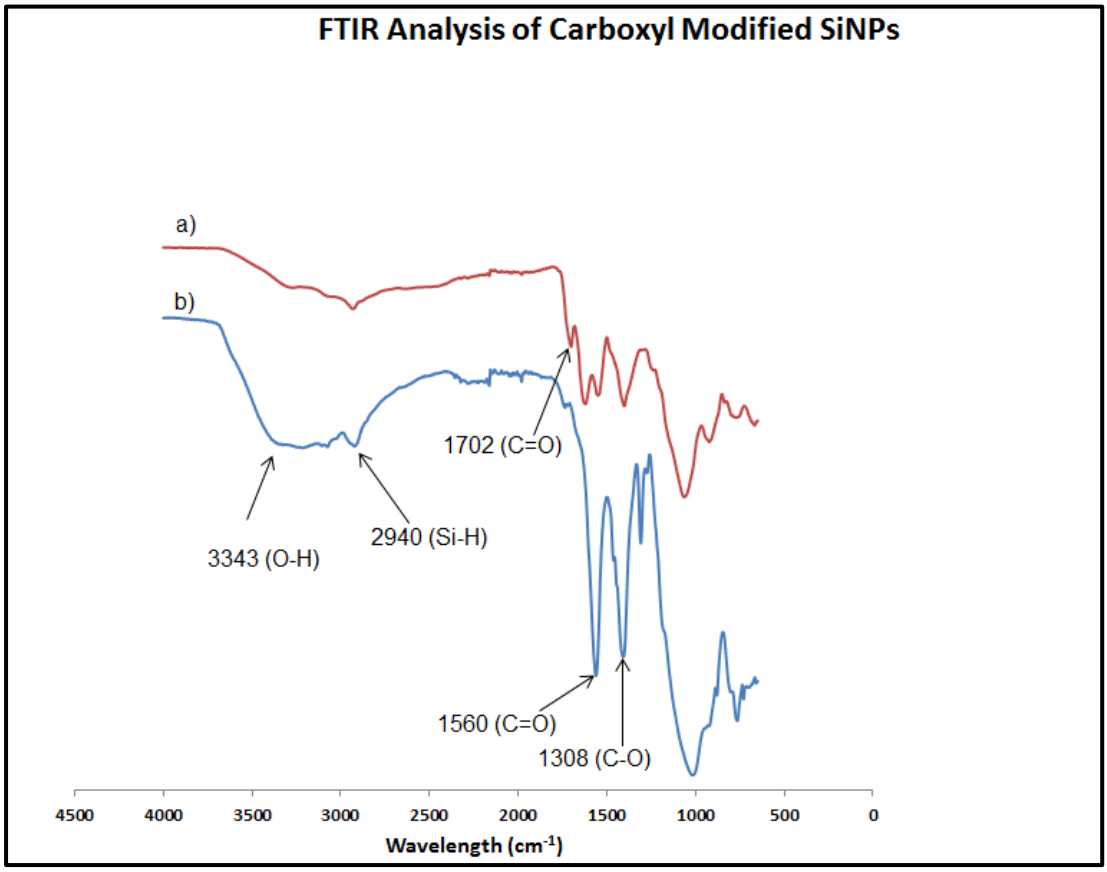


Figure 19: A comparison between a) the direct and b) indirect attachment of carboxyl groups onto SiNPs. The direct method entails introducing an organosilane with carboxyl groups during the particle synthesis. The indirect method entails making use of succinic anhydride to convert the amine groups to carboxyl groups.

The peak at 1560 $cm^{-1}$ indicates that the carboxyl groups were successfully attached onto the silica surface (**Figure 19**). The peak is indicative of the C=O stretch vibration, which concludes that there are carboxyl groups on the silica surface (Cai *et al*., 2013). It was also observed that the C=O peak at 1702 $cm^{-}$

[1] was less intense than that in **Figure 19**. The direct attachment of carboxyl groups yields more carboxyl groups than the indirect method. The diffused O-H bond was also indicative of the carboxyl groups. The silica matrix was still intact and this was seen with the sharp Si-O-Si vibration at 1034 $cm^{-1}$ and the Si-H vibration at 2920 $cm^{-1}$.

The attachment of antibodies was determined using the FTIR. In this study the antibodies were passively adsorbed onto the SiNPs without the use of avidn and biotinylated antibodies.

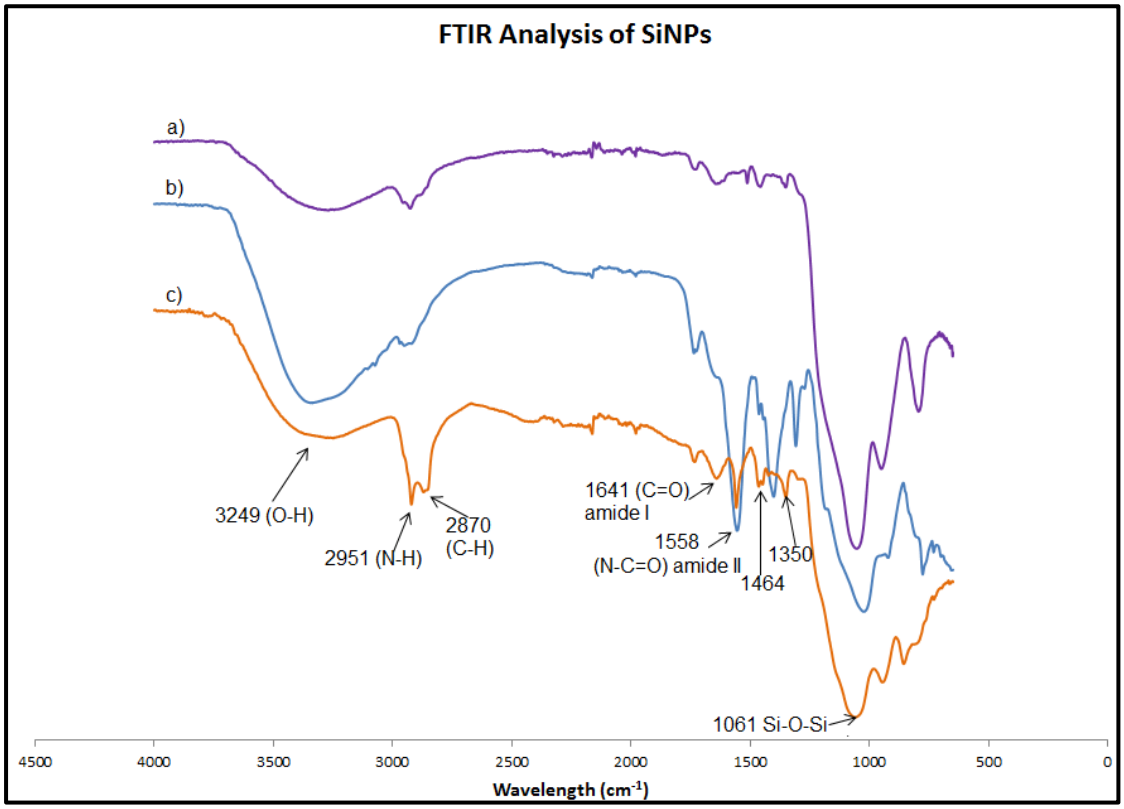


Figure 20: FTIR spectra of pure SiNPs (a), carboxyl functionalized SiNPs (b) and antibody-functionalized SiNPs (c).

The peaks at 1641 $cm^{-1}$ and 1558 $cm^{-1}$ are attributed to amide I and amide II stretches respectively. Peaks at 2951 $cm^{-1}$ and 2870 $cm^{-1}$ are attributed to the N-H and C-H stretches respectively and the peaks at 1350 and 1464 $cm^{-1}$ are characteristic of carboxyl stretches found in amino acids. These peaks

confirm the successful attachment of antibodies on the Si surface (**Figure 20**). The Silica matrix is still intact as seen by the Si-O-Si peak at 1061 $cm^{-1}$.

### 4.4.5. Absorbance studies using Ultraviolet-Visible Adsorption Spectroscopy

Following the results observed on FTIR, UV-vis adsorption spectroscopy was conducted to determine if the Ru(Bpy) dye was present in the silica matrix.

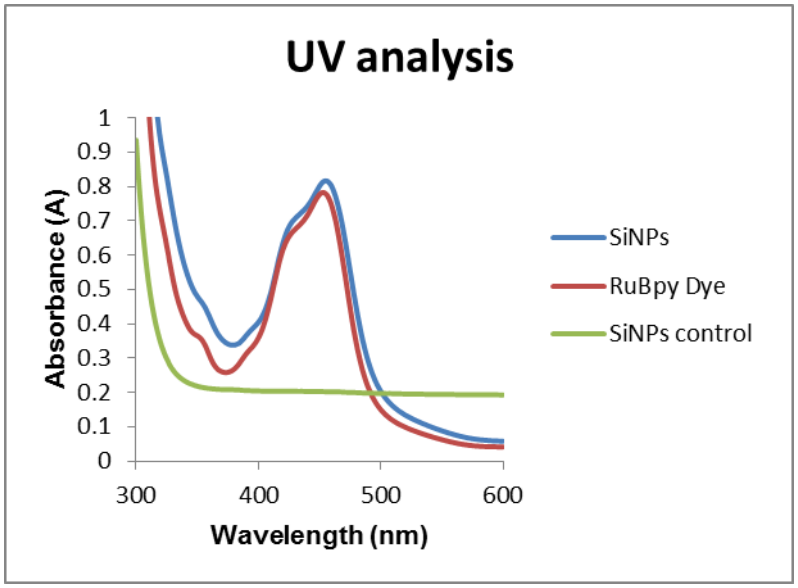


Figure 21: UV analysis of 0.27 mg/mL Ru(Bpy) dye, 0.27 mg/mL dye in dye-doped SiNPs and pure SiNPs.

One distinctive peak occurred at a wavelength of 450 nm for the Ru(Bpy) dye and the dye-doped SiNPs spectra ((Zhao *et al*., 2004a; Bagwe *et al*., 2004; Tan *et al*., 2004). There was no peak on the UV spectrum of the pure SiNPs (**Figure 21**)**.** These observations assume that the dye was encapsulated in the silica matrix. Following these observations, the dye was quantified.

In order to be able to quantify the dye loading in the silica matrix, a calibration curve was plotted (**Figure 22**).

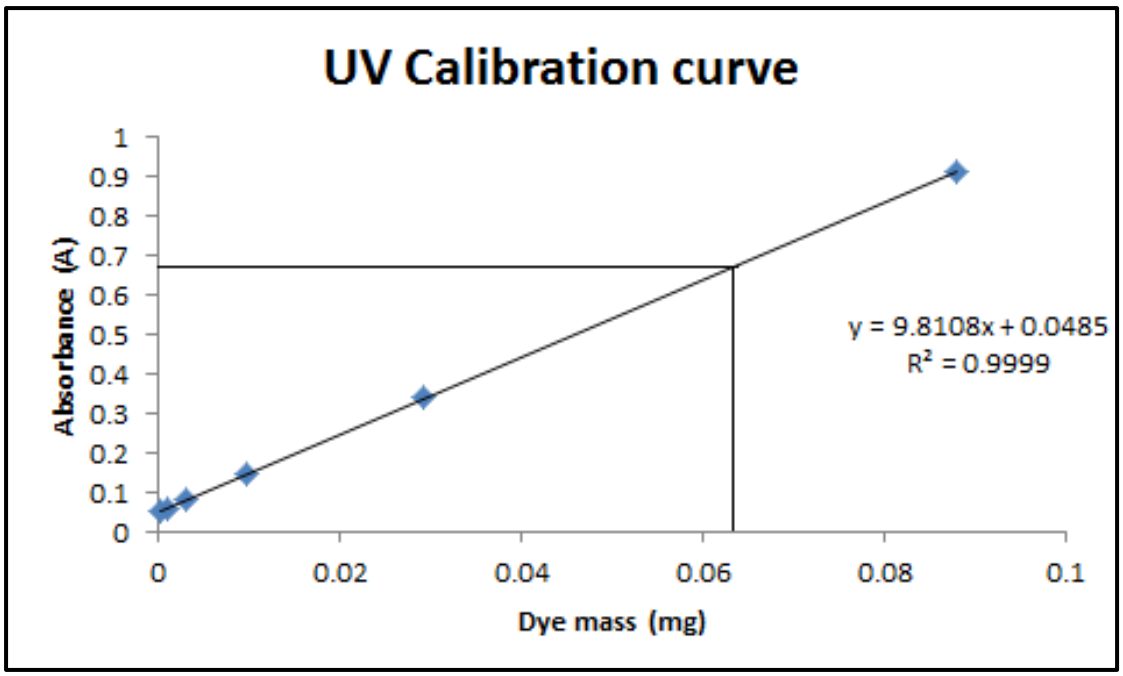


Figure 22: The calibration graph of the Ru(Bpy) dye obtained from the absorption spectra of the UV Vis at 450 nm by serial dilution of a stock solution of 6.5 mg/mL.

The concentration of the dye in the dye-doped SiNPs was calculated using the calibration equation that was developed from the calibration curve, where y = 9.8108+0.0485 with an $R^2$ value of 0.9999. The stock solution was diluted 10 times with deionized water and analyzed with the UV-vis. The diluted stock solution gave an absorbance intensity of 0.687 absorbance units. At this absorbance, the mass of dye in the dye-doped SiNPs was calculated taking into account the dilution factor of 10. The dye content in the dye-doped SiNPs was calculated to be 0.695 mg per 65 mg of SiNPs.

### 4.4.6. Fluorescence properties of the Ru(Bpy) dye and dye-doped SiNPs

The optical properties of the RuBpy dye and the SiNPs were also characterized by determining the excitation and emission spectra of both substances using fluorescence spectroscopy. The substances were in aqueous medium when they were characterized using the UV-vis spectrometer and the spectrofluorometer.

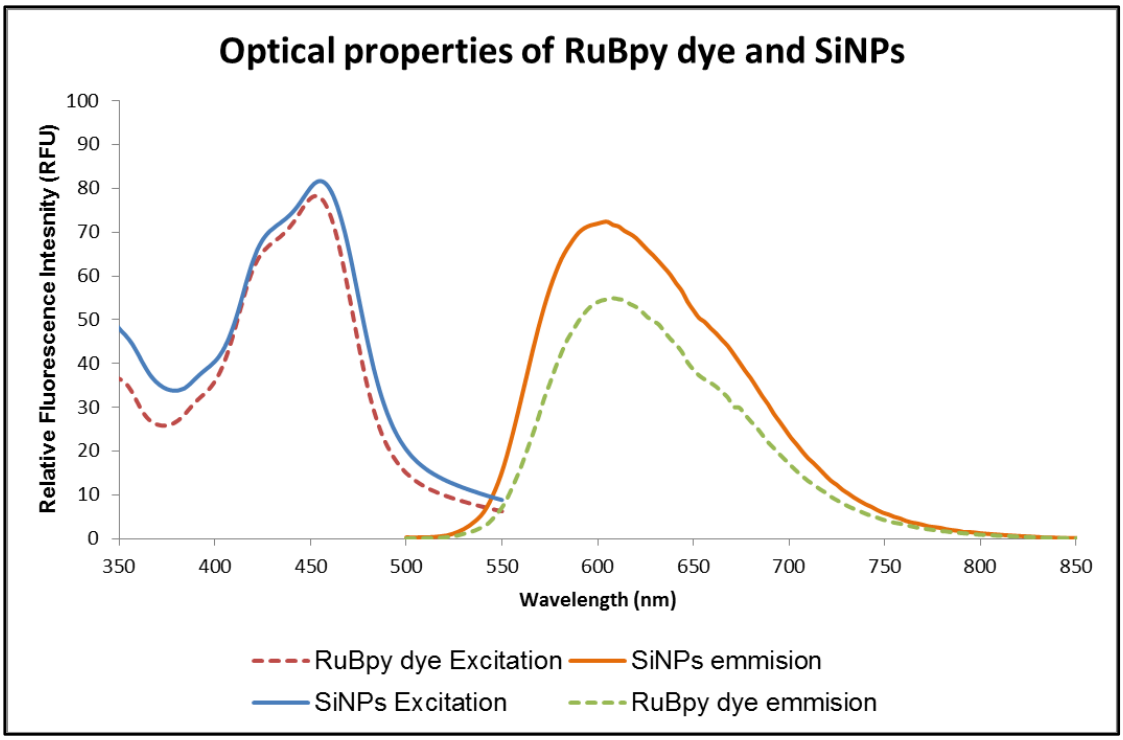


Figure 23: Fluorescence excitation obtained using UV-vis and emission spectra obtained using spectrofluorometer of SiNPs (blue and purple dashed lines) and RuBpy dye (red and green solid lines).

**Figure 23** shows the excitation and emission spectra of the RuBpy dye and the SiNPs. It was found that the RuBpy dye and dye-doped SiNPs exhibited an emission at 608 and 605 nm respectively when excited at 451 nm. The excitation spectrum of the dye-doped SiNPs is not significantly different to that of the Ru(Bpy) dye. There is a 3 nm shift in the emission spectra of the dye-doped SiNPs. This is due to the weak interactions between the silica matrix and the RuBpy dye (Santra *et al*., 2001b).The spectra of the dye and dye-doped SiNPs did not display large difference, which meant that encapsulating the dye did not affect the spectral properties of the dye. In fact, encapsulating the dye enhanced the dye's optical properties. This was seen when the relationship between absorbance and concentration/mass of the pure dye and the dye-doped SiNPs was investigated. It was found that at a dye mass of 0.812 mg, the maximum fluorescence intensities for the SiNPs and the RuBpy dye were 2.19 $x10^7$ RFU and 7.42 x $10^6$ RFU respectively. These results suggest that the encapsulated dye was 3 fold brighter than the free dye.

Therefore, encapsulating the RuBpy dye in the silica matrix enhances the dye's optical properties.

### 4.4.7. Fluorescamine assay to determine primary amine groups on SiNPs

The fluorescamine assay is a method used to determine the presence of primary amine groups on peptides and proteins (Üdenfriend, 1999). The fluorescamine reagent reacts with primary amines to form a highly fluorescent moiety (**Scheme 14**). In this instance, the fluorescamine assay was used to confirm the attachment of amine groups on the SiNPs surfaces.

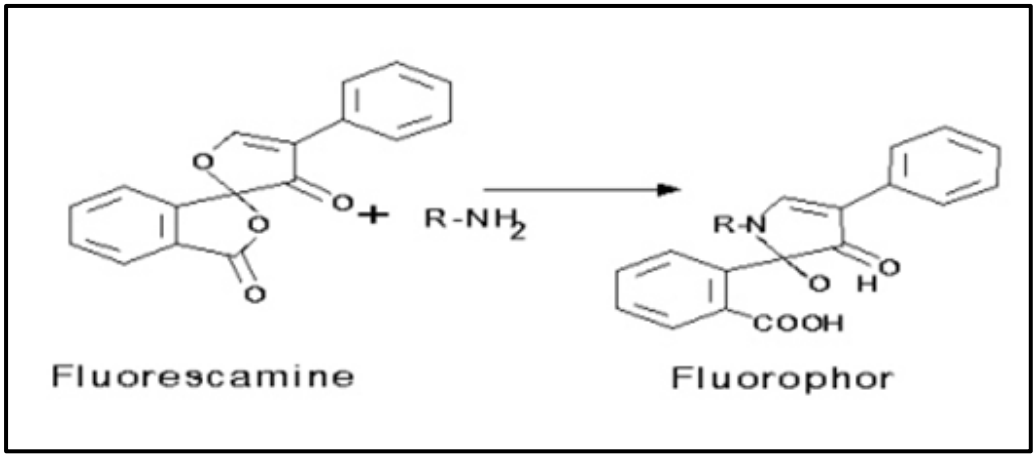


Scheme 14: A schematic diagram of the fluorescamine reacting with primary amines to form a fluorescent product.

Fluorescamine is a reagent that reacts with primary amines in the picomole range. Its reaction with amines is almost instantaneous at room temperature in aqueous media. The products are highly fluorescent, whereas the reagent and its degradation products do not fluoresce. The resulting fluorescence is directly proportional to the concentration of the amine groups (Üdenfriend *et al*., 1972).

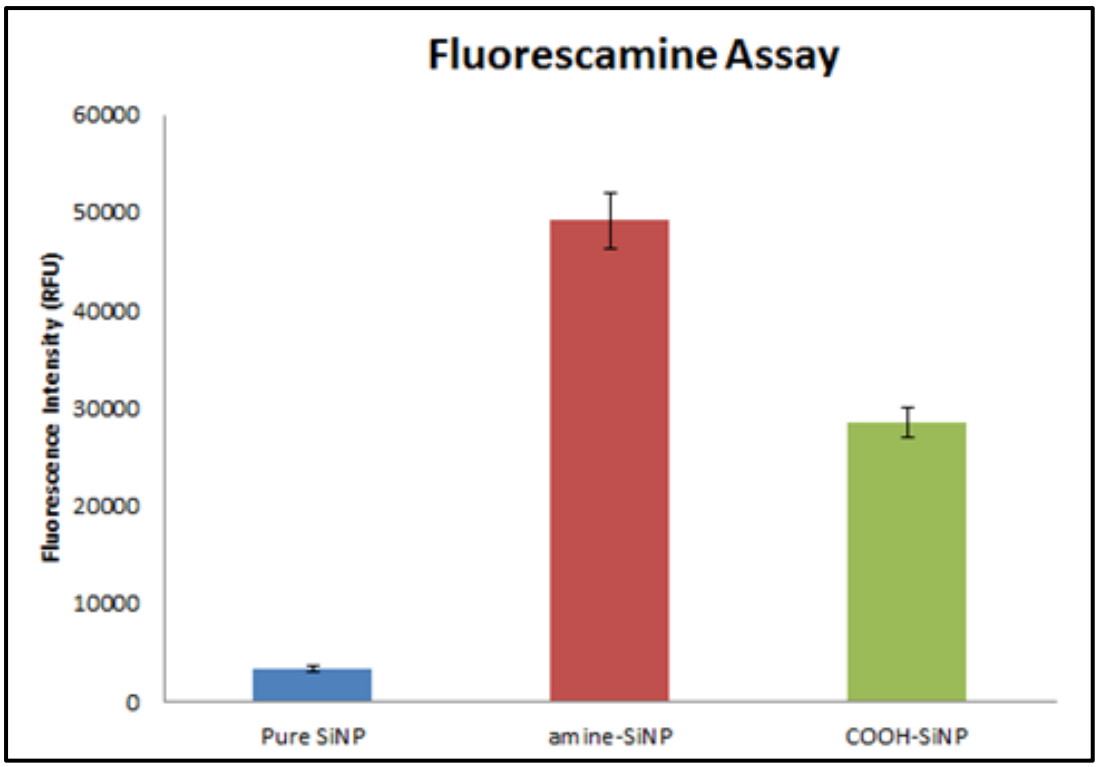


Figure 24: A graph showing the results of a fluorescamine assay performed on pure, amine – and carboxyl surface functionalized SiNPs (n=3).

The assay indicated that there was a significantly higher concentration of amine groups attached on the $NH_2$-SiNPs as compared to the pure SiNPs and COOH-SiNPs (**Figure 24**). The fluorescence intensity recorded for the $NH_2$-SiNPs was 44297.67 ± 9124 RFU. There was a very low signal from the pure SiNPs (3398.67 ± 310 RFU) that were not modified with any amine groups. An unexpected result was observed with the COOH-SiNPs, whereby a signal intensity of 28525.33 ± 1622 RFU was registered. Assuming that the fluorescence intensity was directly proportional to the amount of amine groups, it could be said that there was ~64% conversion of the amine groups to carboxyl groups. This meant that COOH-SiNPs still contained a large number of unreacted amine groups, and hence the method used to modify the silica surface with carboxyl groups was not efficient; however, there was a significant difference between the $NH_2$-SiNPs and the COOH-SiNPs. This result was also observed in the FTIR analysis in **Figure 18**. Had all the amine groups been converted to carboxyl groups, the fluorescence intensity would have been similar to that of the pure SiNPs that had no amine groups on the

surface. This method is only qualitative; therefore the exact amount of amine groups could not be determined.

The fluorescamine assay was repeated with SiNPs that were synthesized using the direct carboxylation method (**Figure 25**). The fluorescence intensities of the pure SiNPs and COOH-SiNPs were 54.33 ± 2.5 RFU and 318.00 ± 54 RFU respectively. The $NH_2$-SiNPs gave a fluorescence intensity of 34854.33 ± 4921 RFU. These results show that there was no presence of any primary amine groups in the COOH-SiNPs sample, therefore proving that the direct carboxylation method was superior to that of converting the amine groups to carboxyl groups.

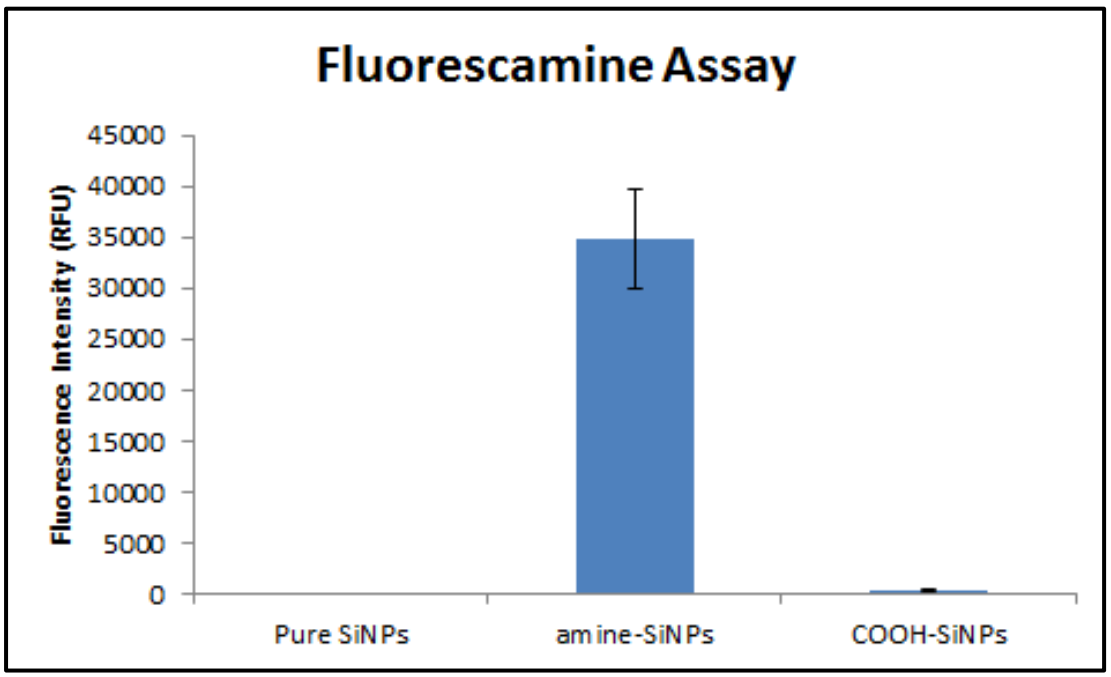


Figure 25: A graph showing results for a fluorescamine assay performed on SiNPs synthesized using the direct carboxylation method (n=3).

### 4.4.8. Quantitation of avidin immobilized on SiNPs

The attachment of antibodies onto the SiNPs is dependent on the amount of avidin available on the surface of the SiNPs. Therefore, it is crucial to attach as much avidin as possible onto the SiNP surface. The binding of avidin to the COOH-SiNPs was evaluated by the use of a fluorescent label, biotin (5-

fluorescein) conjugate. The amount of residual avidin in the supernatant was determined following the method given by (Chen *et al*., 2012). The reaction of biotin (5-flourescein) with avidin, due to the affinity binding, leads to the quenching of the conjugate's fluorescence activity. The chemical structure of biotin (5-fluorescein) conjugate is shown in **Figure 26**.

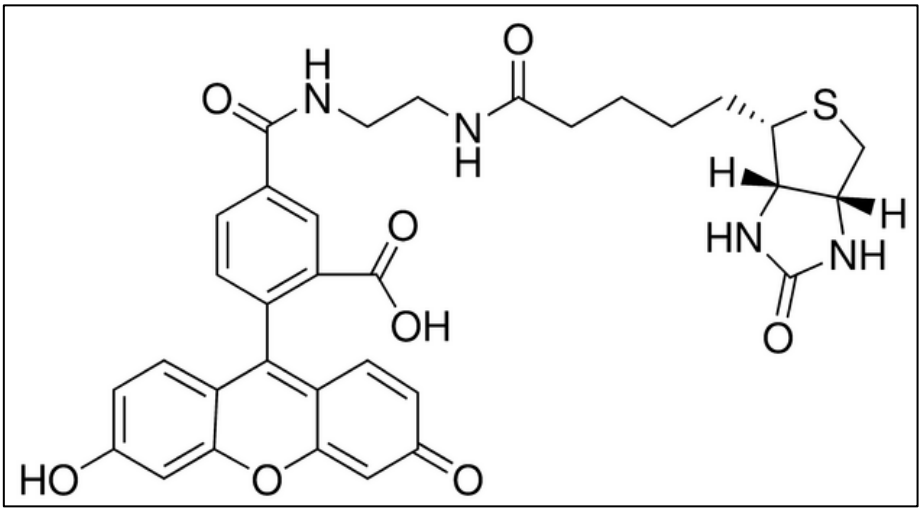


Figure 26: Chemical structure of biotin (5-florescein) conjugate.

The supernatant separated from the conjugated NPs after avidin attachment was analyzed to determine the amount of residual avidin in solution, thus indirectly determining the amount of avidin immobilized on the SiNPs surface. A calibration curve was constructed by plotting the data points representing the difference in fluorescence intensity of the maximum biotin (5-fluorescein) conjugate and each data point. The equation "y = 20192 + 797.58" with an R value of 0.9878, was used to determine the avidin concentration (**Figure 27**).

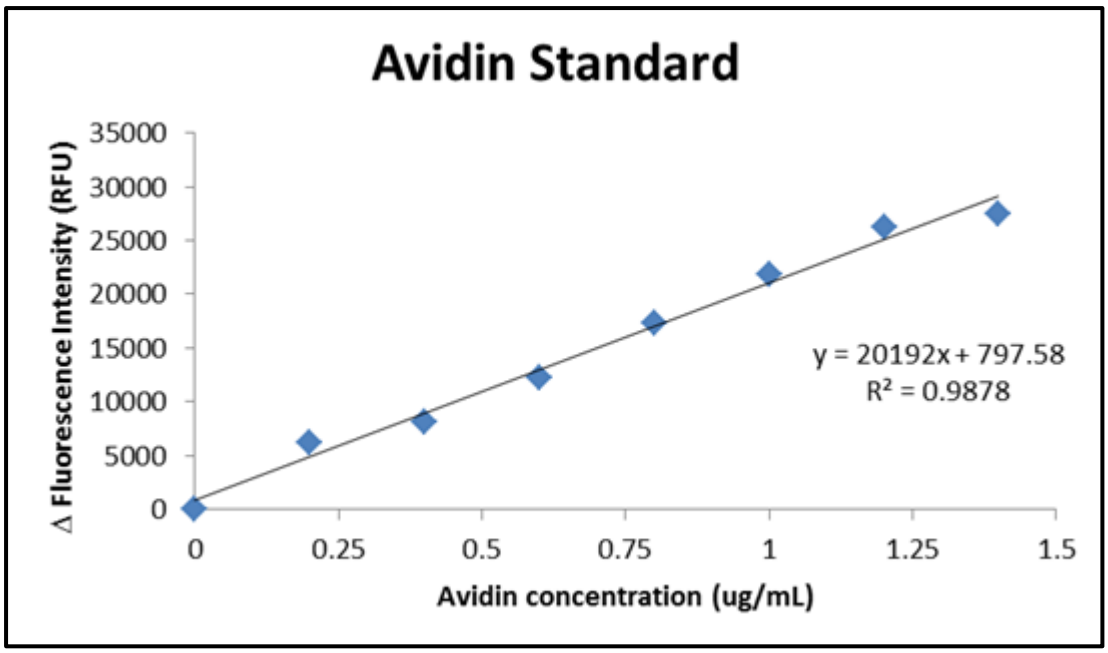


Figure 27: Calibration curve indicating the difference in fluorescence intensity of biotin (5-fluorescein) and avidin concentrations present in the supernatant.

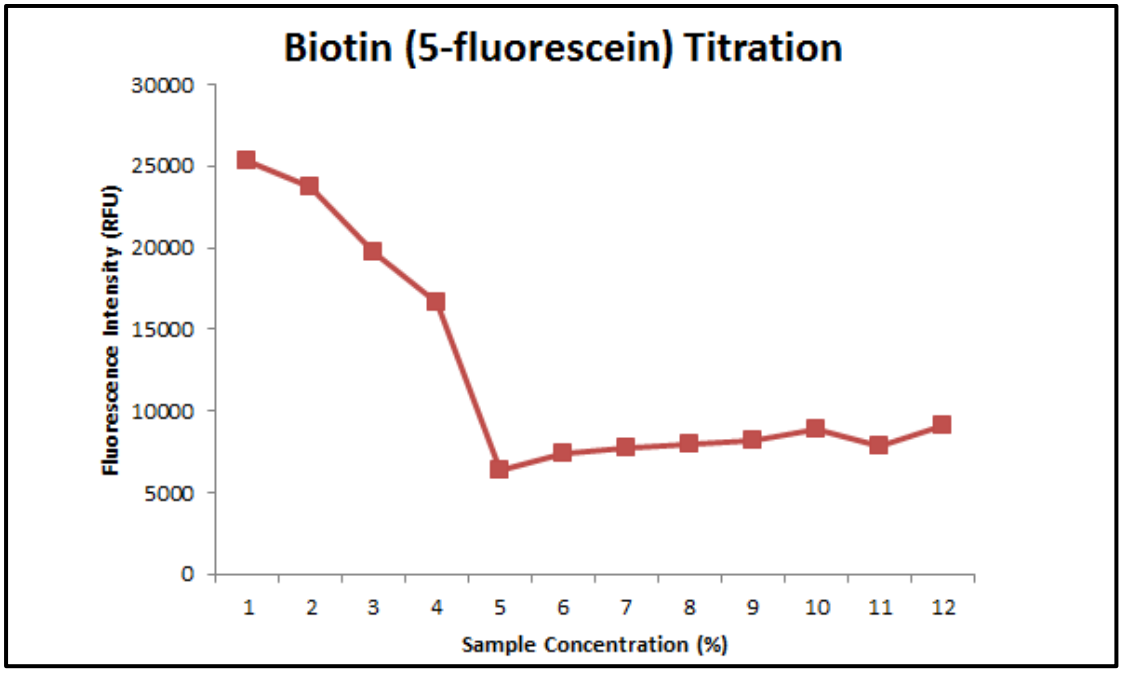


Figure 28: Titration of biotin (5-fluorescein) conjugate in the presence of avidin in the supernatant of the SiNPs samples (n=3).

The fluorescence of the biotin (5-fluorescein) conjugate was decreasing because it was being quenched by the avidin present in the supernatant. The fluorescence of the biotin (5-fluorescein) conjugate was completely quenched at 5 nM (**Figure 28**). The increase in the fluorescence signal after 5% is indicative of the saturation of avidin in the supernatant. This meant that at the mimina of 5%, there was enough avidin in the supernatant to completely quench the biotin (5-fluorescein) conjugate. The presence of avidin in the supernatant was indicative that there was a sufficient amount immobilized on the SiNPs surface. The fluorescence intensity at that data point was then substituted back into the calibration curve equation. It was found that 95% of initial avidin used for bioconjugation was immobilized on the SiNPs surface. The biotin (5-fluorescein) study indicated that all the sites on the Si surface were saturated with avidin.

### 4.4.9. Application of SiNPs for *E. coli* detection

The attachment of antibodies to the SiNPs and the binding efficiency of the antibodies were tested using a centrifuge based method. In this experiment, an *E. coli* concentration of $1x10^4$ CFU/mL was used.

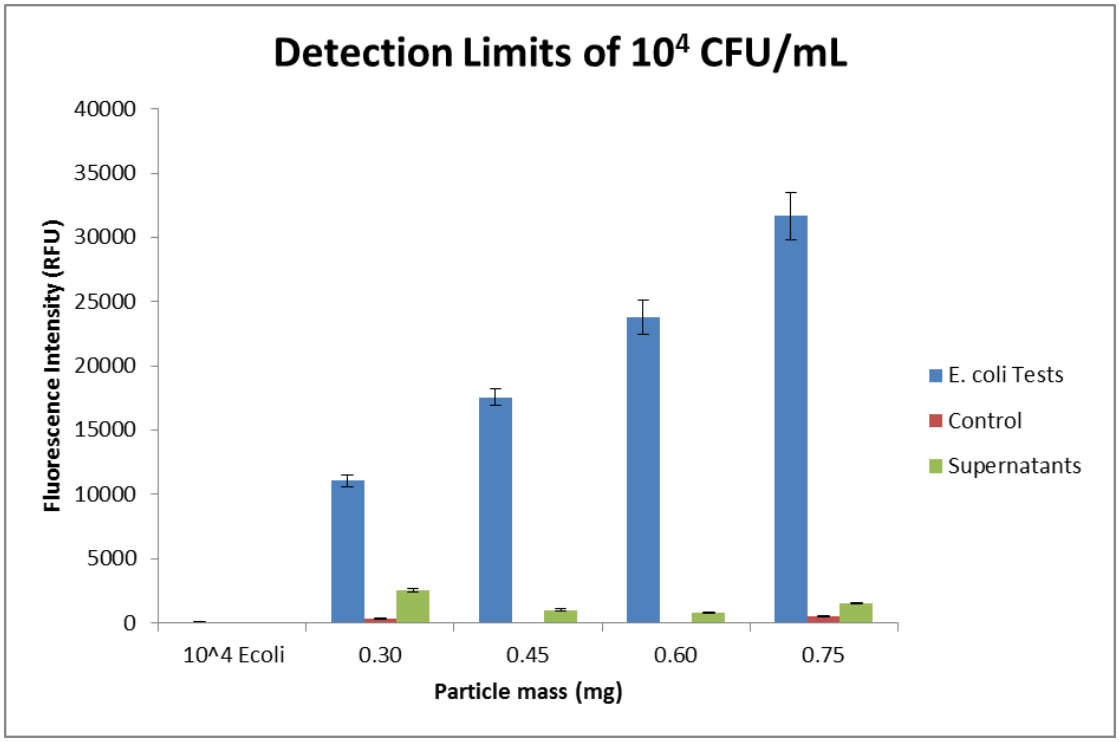


Figure 29: Fluorescence intensity of the detection of *E. coli* using bioconjugated, dye-doped SiNPs as a function of particle mass (n=3).

In this experiment, an *E. coli* concentration of $1x10^4$ CFU/mL was used. It was observed that the fluorescence intensity increased with the increase in particle concentration. The increase fluorescence intensity with an increase in particle mass could mean that the maximum binding capacity of the particles was not reached. The control signals were significantly low (P-value = $2.09x10^{-6}$ for 0.30 mg SiNPs and $8.11x10^{-6}$ for 0.75 mg SiNPs), meaning there was minimal non-specific binding. The supernatants gave very low signals compared to those of the bound tests, meaning that most of the particles were bound to the bacteria ( **Figure 29**).

The same experiment was repeated and the results are shown in **Figure 30**. Positive controls were included, which were centrifuged at 10000 rpms for 10 minutes. The positive controls were included in order to see the maximum fluorescence intensity that can be expected in relation to the particle masses introduced in the tests.

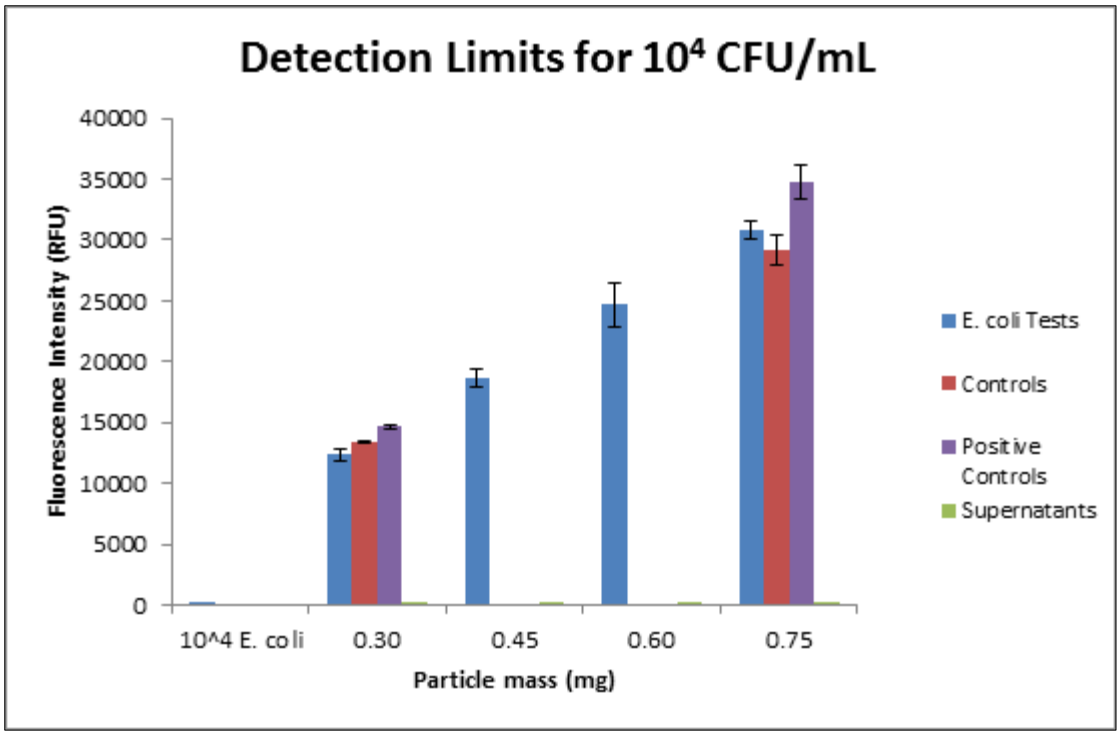


Figure 30: Fluorescence intensity of the detection of *E. coli* using bioconjugated, dye-doped SiNPs as a function of particle mass with positive controls (particles that are retained in order to obtain maximum fluorescence intensity) (n=3).

The trend in **Figure 29** was observed in **Figure 30** as well. The increase in particle concentration led to a significant increase in the fluorescence intensity (P-value = 1.57 x $10^{-7}$). However, a concern arose when the controls without *E. coli* gave similar fluorescence intensities as the tests. The controls emitted a high fluorescent signal possibly due to the high density of the SiNPs. The nanoparticles may have been retained during centrifugation making it difficult to separate. Although there was a significant difference between the control and test at lower concentrations of 0.30 mg/mL SiNPs (P-value 0.022), the statistics revealed that there was no significant difference between the test and control at 0.75 mg/mL (p-value of 0.12). The control and test signals were similar possibly because of the particles being retained during the centrifugation step. These results are therefore, inconclusive. The positive control signals were higher than all the other signals as expected. The supernatant signals were also low as seen in the previous experiment. The

signal from the *E. coli* was very low, which means that the bacteria do not fluoresce when irradiated.

The increase in the controls signal led to another experiment whereby the *E. coli* concentration was varied and the particle concentration was kept constant. The concentration of choice was 0.45 mg/480 µL. The concentration was chosen on a basis that the particle concentration was still giving a significant signal compared to the controls without *E. coli* (**Figure 31**). *E. coli* concentrations of $10^2$, $10^3$ and $10^4$ CFU/mL were investigated.

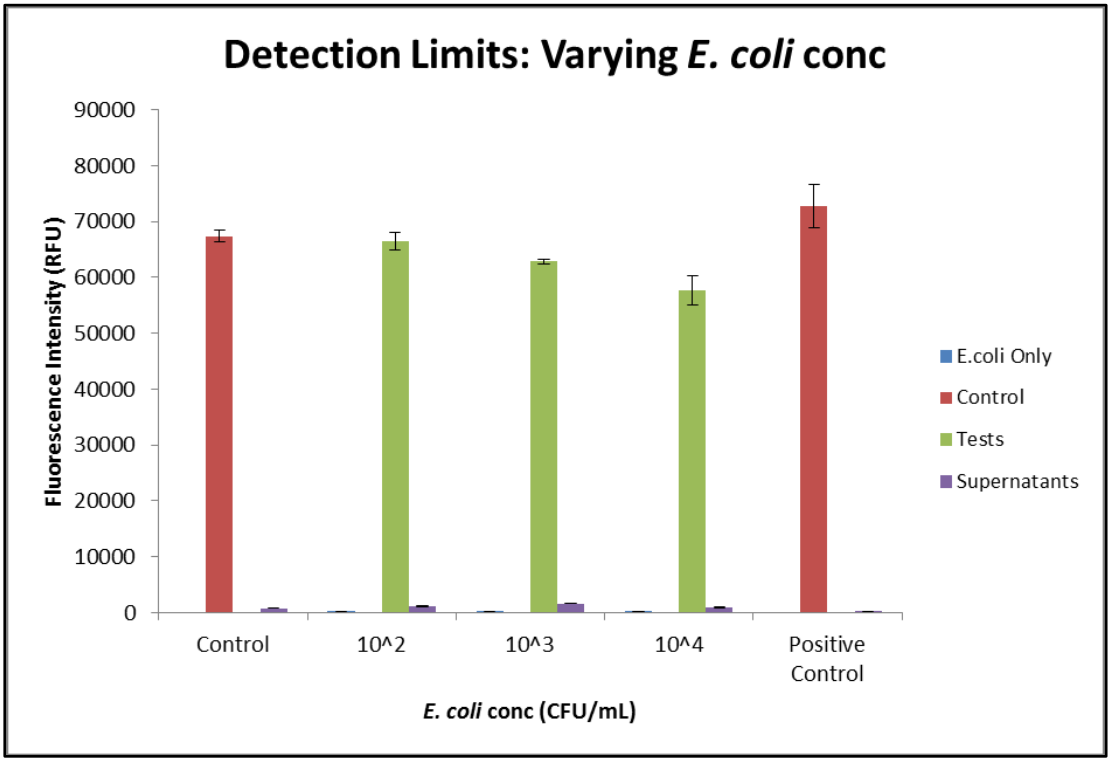


Figure 31: Fluorescence intensity of the detection of *E. coli* using bioconjugated, dye-doped SiNPs as a function of E. coli concentration with positive controls (n=3).

In **Figure 31**, it was observed that the fluorescence signal was increasing significantly with the decrease in *E. coli* concentration (p-value = 0.0027). This could mean that the amount of SiNPs was more sufficient for lower *E. coli* concentrations. The increase in *E. coli* cells, while keeping the particle mass

constant, reduced the fluorescence intensity because the *E. coli* cells were, to some extent, hindering the light from reaching the dye-doped SiNPs. However, the control (no bacteria, only nanoparticles) was giving a higher signal than that of the test signals. The positive control was not significantly higher than that of the test control (p-value = 0.077). The supernatants seemed to have the least amount of particles as seen in the graph. This was a good observation except that it was expected that the control supernatants would have a higher fluorescent signal, indicating that the SiNPs were not binding to the *E. coli* cells.

### 4.4.10. Microscopic detection of *E. coli*

The successful attachment of antibodies to the SiNPs and the SiNPs to *E. coli* was confirmed using TEM. An *E. coli* concentration of $10^4$ CFU/mL was contacted with 23 mg (120 µL) of antibody-labelled SiNPs in 500 µL PBS-tween, pH 7.4 for an hour; thereafter the SiNPs-labelled *E.coli* cells were prepared for TEM analysis.

**Figure 32 A** and **B** shows that the bioconjugation of the SiNPs was successful because there were spherical SiNPs around the surface of the *E. coli* cells, which have an ellipsoidal shape. **Figure 32 C** shows the control *E. coli*, which was not contacted with antibody-conjugated SiNPs. There was a distinct difference between the cell membranes of the *E. coli* cell membranes in the control image and that of the SiNPs bound to the *E. coli* cells

The successful attachment of antibodies to the SiNPs was also confirmed through fluorescence microscopy. The particle and *E. coli* concentrations that were used for the fluorescence microscopy study were the same as those used for the TEM analysis. The results that were obtained through electronic microscopy were correlated by fluorescence (**Figure 33**).

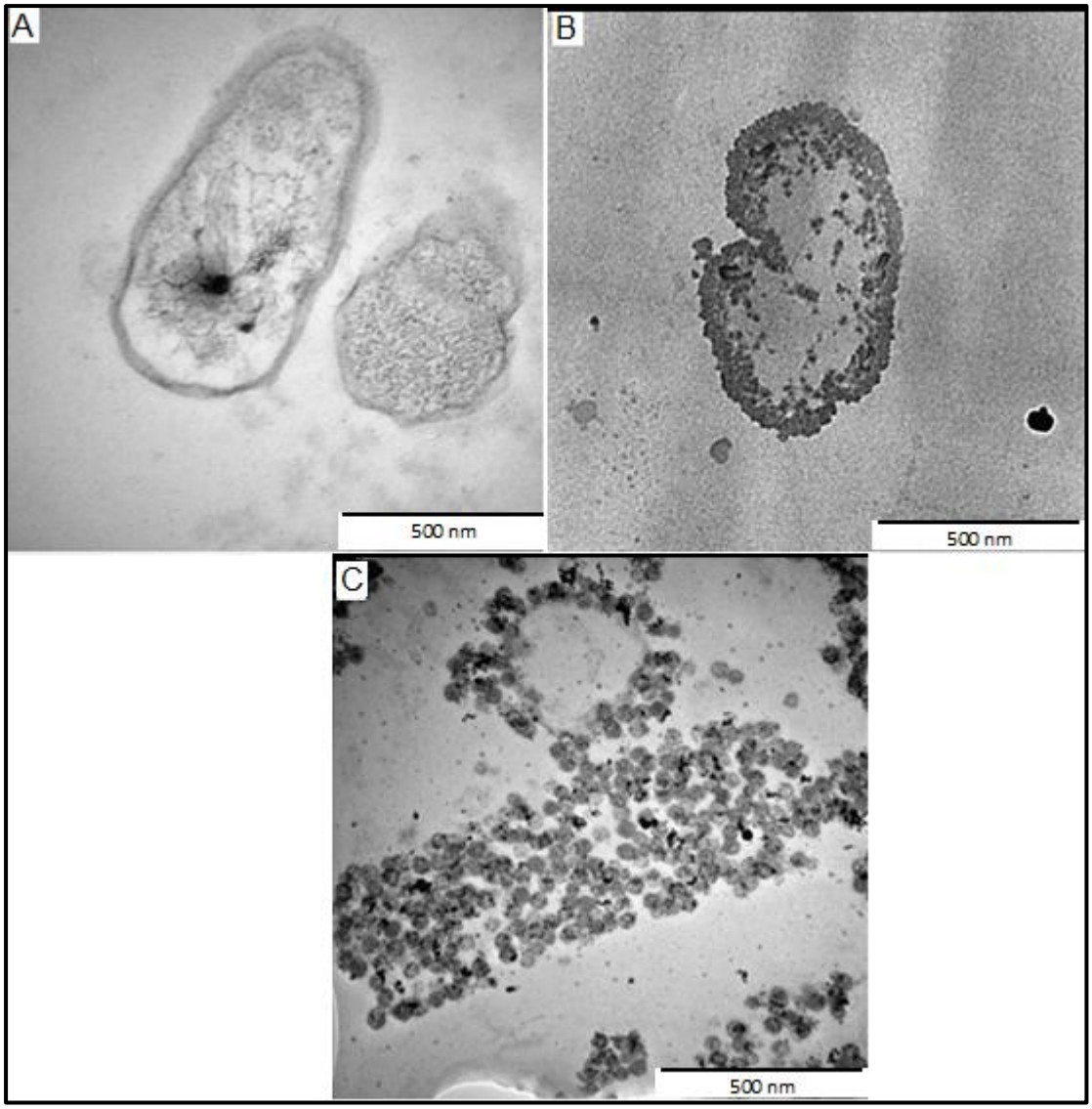


Figure 32: TEM images of A) Cross-sectional image of *E. coli* that was not contacted with SiNPs and B) & C) Cross-sectional images of antibody-conjugated SiNPs bound to *E.coli* cells.

A red haze was observed in **Figure 33 A**, which indicated that the SiNPs were not agglomerating in the absence of *E. coli* cells. This also meant that there was no contamination of the SiNPs, because there were no bright signals observed. Localized signal intensities were observed in **Figure 33 B** & **C**. The signals were in the approximate shape and size of E. coli cells. It was therefore evident that the SiNPs were binding to the *E. coli* cells and that the SiNPs were performing as markers through antibody-antigen recognition.

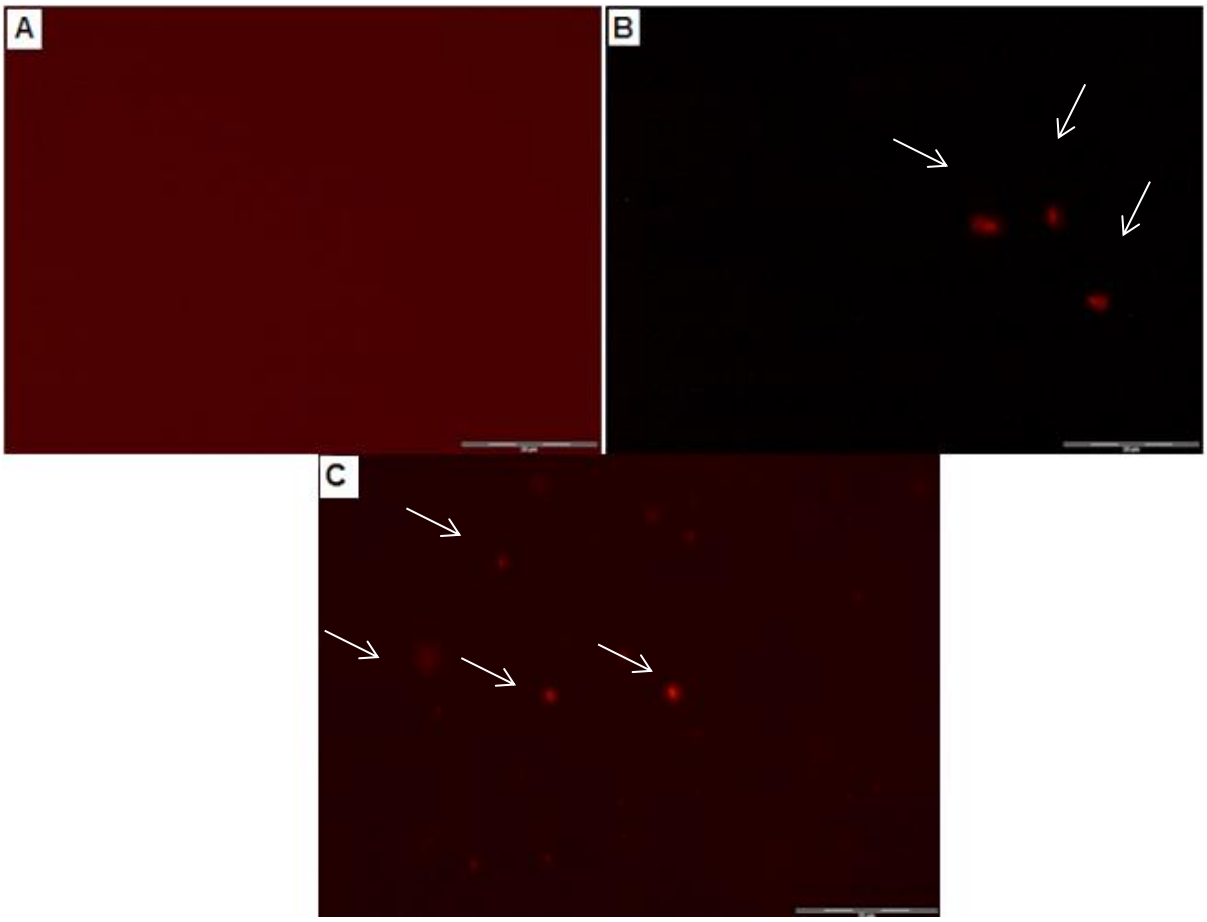


Figure 33: Fluorescent field images of A) dye-doped SiNPs and B & C) *E. coli* cells (the cells are in the direction arrows) incubated with dye-doped antibody-labelled SiNPs.

## 4.5. Conclusions

The experimental results have shown that the SiNPs are easy to prepare and functionalize. The SiNPs were uniform in size as seen on the TEM images but, the particles tend to form agglomerates or appear in clusters rather than as individual particles due to freeze drying. It was also seen using fluorescence microscopy that introducing surfactants increased the stability of the SiNPs in suspension considerably.

The SiNPs were successfully impregnated with the Ru(Bpy) dye and these results were confirmed by the FTIR, the UV-Vis and fluorimetry. The dye was quantified using the calibration curve that was developed and it was found that the dye loading was 0.065mg per 65 mg of dye-doped SiNPs. Amine and carboxyl groups were successfully attached onto the silica surface as seen on the FTIR spectra.

The amine groups were successfully attached to the SiNPs surfaces as seen with the fluorescamine assay. However, not all amine groups were converted to carboxyl groups.

It was established that low surface charge was one of the factors that caused agglomeration as there was not enough charge to cause repulsion between the particles. The negative charge was increased with the addition of carboxyl groups that are negatively charged.

The method that employs the direct attachment of carboxyl groups has shown to work well as a distinct –COOH peak was observed on the FTIR spectrum. The SiNPs functionalized using the direct attachment method gave a better surface charge (-32 mV) rather than the indirect method (-23 mV). The SiNPs whereby carboxyl groups were attached directly were used for all the studies which were conducted.

It was found that the optical properties of the free RuBPy dye were enhanced when the dye was encapsulated in the silica matrix. The dye-doped SiNPs were 22 times brighter than the pure Ru(Bpy) dye.

The biotin (5-fluorescein) assay indicated that 95% of the initial avidin added during bioconjugation was attached onto the SiNPs. There was residual avidin in the supernatant, which could mean that the amount of avidin used for bioconjugation was sufficient.

The detection limits study through the use of a fluorescence plate reader was inconclusive due to the high control signals that were observed. In future studies, the centrifugation step can be eliminated by performing ELISAs without the enzymatic reactions. However, the TEM and fluorescent microscopy results prove that the SiNPs are binding to the *E. coli* cells.

# Chapter 5: Synthesis and characterization of magnetic nanocomposites for *E. coli* preconcentration

## 5.1. Introduction

In recent years, magnetic nanoparticles (MNPs) have been the focus in biotechnology and pathogen detection (Cheng *et al*., 2009). Magnetic nanoparticles are biocompatible, exhibit low toxicity and they possess magnetic properties making them ideal for separations, diagnostics and magnetic imaging for detection. MNPs are functionalized with biorecognition molecules such as antibodies and aptamers in order to be used in specified targeting and recognition applications (Cheng *et al*., 2009; Wei *et al*., 2009; Huang *et al*., 2010). This study demonstrates the use of poly (1(2-carboxyethyl)pyrrole)) magnetic nanocomposites (PPy-COOH/ $Fe_3O_4$ MNCs) in the form of immunomagnetic separators.

PPy was chosen as the conducting polymer of choice because it can be synthesized with carboxyl groups. The presence of carboxyl groups makes it possible to attach avidin on the polymer surface, therefore making it possible to dictate the orientation of the antibodies on the polymer surface. Unlike with polyaniline, antibodies would have to be passively adsorbed onto the polyaniline surface, meaning that the orientation of antibodies would be heterogeneous (**Section 2.3**).

## 5.2. Experimental

### 5.2.1. Materials

Table 10: Materials used to synthesize magnetic nanocomposites.

| | |
|---|---|
| N-1(2-Cyanoethyl)pyrrole | Sigma Aldrich, USA |
| Diethyl ether | Sigma Aldrich, USA |
| Hydrochloric acid | Sigma Aldrich, USA |
| Potassium hydroxide | Merck, USA |

| | |
|---|---|
| Iron (III) chloride ($FeCl_3$) | Sigma Aldrich, USA |
| Iron oxide ($Fe_3O_4$) | Sigma Aldrich, USA |

### 5.2.2. Synthesis of magnetic carboxyl-functionalized polypyrrole monomer

The carboxyethylpyrrole monomer were synthesized according to procedures in literature (Wolowacz *et al*., 1992; Chen *et al*., 2012) by hydrolyzing 12.5g of 1-(2-cynoethyl)pyrrole with 60 mL of 6.7 (M) potassium hydroxide (KOH). The mixture was refluxed under argon atmosphere until there was no $NH_3$ (g) gas evolving. The reddish solution was acidified to a pH of 5 using 8 M hydrochloric acid (HCl). The product was extracted five times, using ~500 mL diethyl ether. The diethyl ether was evaporated and the crude product was recrystallized twice using boiling cyclohexane to form a white crystalline product (Azioune *et al*., 2004). The experimental setup shares the same concept as that in figure 2.2 (**Scheme 15**).

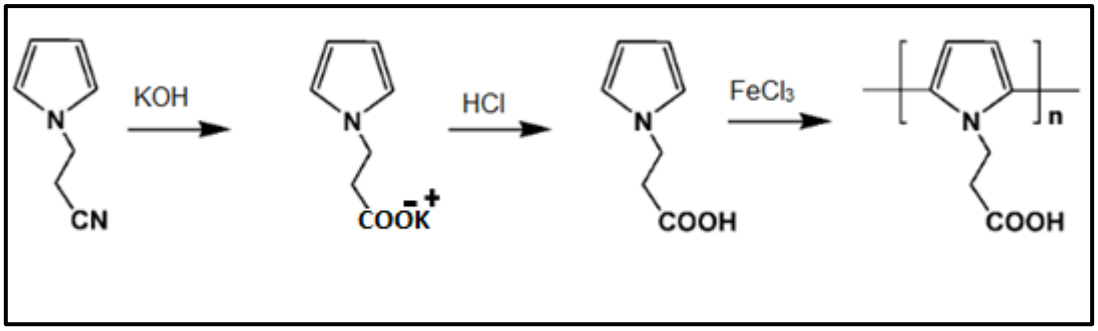


Scheme 15: A schematic diagram of the formation of Poly (1(2-carboxyethyl)pyrrole)) homopolymer (Lee *et al*., 2006).

### 5.2.3. Preparation of the carboxyl-functionalized polypyrrole magnetic nanocomposites (MNCs) by *in-situ* polymerization

0.025 g of $Fe_3O_4$ was dispersed in 20 mL of water and ultrasonicated for 30 minutes in order to get better dispersion of the $Fe_3O_4$. 0.2 g of carboxyethylpyrrole monomer (prepared above) was dissolved in the $Fe_3O_4$ dispersed suspension. 1.5 g of $FeCl_3$, the oxidizing agent, was added to the

solution and left to polymerize for 6 hours under constant shaking, at room temperature (Azioune *et al*., 2004). The black precipitate was filtered and washed with deionized water until there was no colour observed in the filtrate and finally washed with acetone. The MNCs were dried at 60°C for 3 days under vacuum. As a control, carboxyethylpyrrole homopolymer was also synthesized as above, except in the absence of $Fe_3O_4$.

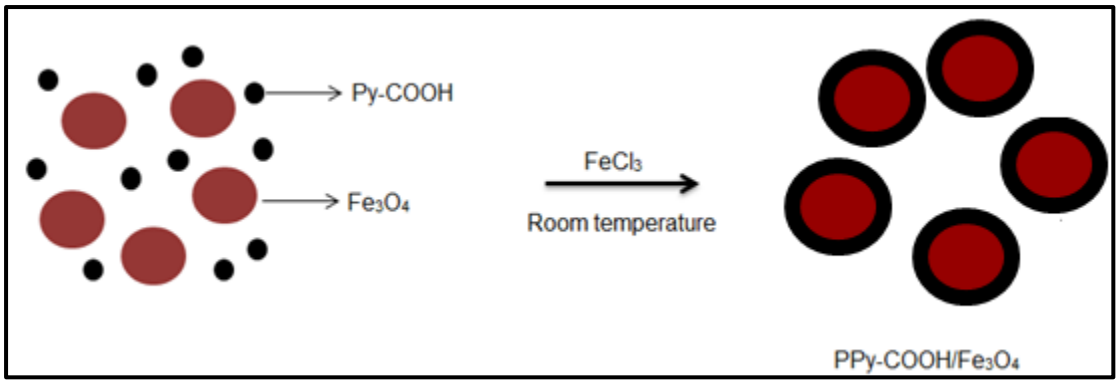


Scheme 16: A schematic diagram of the synthesis of MNCs.

### 5.2.4. Bioconjugation of MNCs

Biotinylated antibodies were attached to MNCs to enable them to bind to the *E. coli* during IMS. 1 mg of MNCs was centrifuged at 17000 rpm and 20 ºC, for 10 minutes to remove the suspension medium. The pellet was resuspended in 1 mL of 0.1 MES buffer, pH 5.5. The carboxyl groups were activated by adding 500 µL of 10 mM Sulfo-NHS and 40 mM EDC, dissolved in MES buffer, to the MNCs suspension. The MNCs were incubated in a shaker at 400 rpm, for 15 minutes at room temperature. The nanoparticles were washed twice in 10 mM PBS buffer, pH 7.4, with 0.05% Tween 20 and then resuspended in 1.5 mL PBS-Tween solution. 50 µL of 4 mg/mL avidin solution was added to the MNCS and the mixture was incubated at room temperature, for 2 hours in a shaker at 400 rpm. The avidin modified particles were washed twice in 10 mM PBS-tween solution and resuspended in 40 mM Tris-HCl with 0.05% BSA solution, for an hour, to block free carboxylates. The particles were washed twice with PBS-Tween and resuspended in 10 mM PBS-Tween solution with 10 mg/mL BSA for storage at 4°C (Chen *et al*., 2012).

### 5.2.5. Attachment of biotinylated-antibodies to avidin-functionalized MNCPs

13.3 µL of 4 mg/mL biotin-labelled antibodies were added to a particle suspension of 1.5 mL PBS-tween and incubated for an hour. The bioconjugated SiNPs were washed once with PBS-tween and resuspended in 1.5 mL 10 mM PBS-tween with 10 mg/mL BSA (**Scheme 17**).

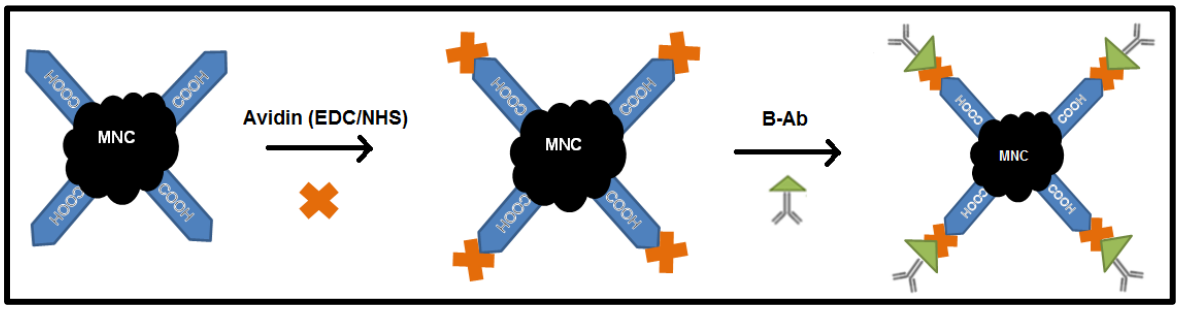


Scheme 17: A schematic diagram illustrating the immobilization of avidin onto SiNPs and the attachment of biotinylated antibodies.

### 5.2.6. Culture of *E. coli*

*E. coli* K12, a non-pathogenic strain, were plated on Luria Bertani (LB) agar plates for 48 hours. Some of the *E. coli* will be scraped from the agar plates and resuspended in 14 mL of autoclaved, deionised water. The UV-vis was used to measure the bacteria concentration by measuring the optical density (OD) at 600 nm. An OD of 1 corresponds to a bacterial cell count of 8 x $10^8$ cells/mL (Agilent Technologies, 2013).

### 5.2.7. Magnetism testing and preconcentration

The magnetism of the MNCs was tested using a magnetic separator (Dynal® Invitrogen Bead Separator). The magnetic separator has two permanent magnets on either side. The magnet generates a large spatial variation in its magnetic field, which is how the separation occurs. 2 mg of MNCs were suspended in 5 mL of 10 mM PBS solution in 15 mL tubes and ultrasonicated till the suspension was homogenous. The tubes were then inserted into the

magnetic separator. It is ideal to characterize the MNCs using a Vibrating Shaking Magnetometer (VSM), however the availability was very limited, which is why the magnetism of the MNCs was determined by visual inspection. This method was also appropriate to determine if the $Fe_3O_4$ was leaching out of the polymer shell.

Preconcentration of different *E. coli* concentrations, in 10 mL of water, were carried out in a magnetic separator. The *E. coli* cells were contacted with MNCs for an hour and preconcentrated. The supernatant was collected and plated on LB agar for 24 hours. The colonies that grew on the plates were counted in order to determine the percentage of *E. coli* cells captured by the MNCs.

### 5.2.8. Material Characterization

The pure and surface-functionalized dye-doped SiNPs were characterized with respect to size and morphology using a JEOL JEM 2100 High Resolution Transmission Electron Microscopy (HR-TEM) and JEOL 7500 Field Emission Scanning Electron Microscopy (FE-SEM).

TEM was used to visualize attachment of the MNC's to the surface of the *E.coli* cells. Biological samples that were viewed under TEM were fixed in order to keep the structure of the *E. coli* cells intact.

An *E. coli* concentration of $10^4$ CFU/mL was contacted with 23 mg of antibody-labelled MNCs in 500 µL PBS, pH 7.4 for an hour. The samples were washed once with PBS-tween and prepared as described in **section 4.3**.

The fixing process was as follows: 1 mL of a 2.5% glutaraldehyde solution (in 0.075 M PBS buffer at a pH of 7.4) was added to *E. coli* cells that were labelled with antibody-functionalized MNCs and fixed for an hour for sectioning and imaging via TEM. The *E. coli*-MNCs conjugates were rinsed three times for 5 minutes with 0.075 M phosphate buffer. Approximately 50 µL

of an aqueous 0.5 % osmium tetroxide solution was added to the *E. coli*-MNCs conjugates and allowed to infiltrate the conjugates for 30 minutes, followed by three washing cycles using distilled water. The pellet was subsequently dehydrated for 10 minutes with 30%, 50%, 70% and 90% ethanol respectively. Thereafter, the conjugates were dehydrated for 10 minutes, three times with 100% ethanol and stored in 100% ethanol for 20 hours. The conjugates were then infiltrated with 50% Quetol in 100% ethanol for 30 minutes and 100% Quetol for 3 hours. After removing Quetol, the conjugates were embedded in TAAB 812 embedding resin for 39 hours at 60°C. The polymerized conjugates were sectioned and stained for 3 minutes in lead acetate and 2 minutes in lead citrate, with 3 wash cycles in between.

The Perkin Elmer Spectrum 100 Attenuated Total Reflection Fourier Transform Infrared (ATR-FTIR), at a resolution of 4 $cm^{-1}$ was used to confirm the functional groups present on the nanoparticles surface. The sample was scanned 16 times per run.

X-ray diffraction patterns were measured on a PANalytical X'Pert PRO-diffractometer using Cu Kα radiation at a wavelength (λ) of 1.5406 Å while the variable slits were set at 45 kV/40 mA. The MNCs were analyzed in the form of a dry powder.

## 5.3. Results and discussions

### 5.3.1. Synthesis of MNCs

The PPy-COOH/$Fe_3O_4$ MNCs were synthesized as described in the experimental section. They appeared as a fine black powder. The final weight of the MNCs was 0.101 g from 0.225g of starting material. The yield of PPy-COOH contained in the nanocomposites was 49%. The morphology of the MNCs was investigated using SEM and the images are represented in **Figure 34**.

$Fe_3O_4$ MNCs appear as aggregates of the MNCs powders whereby A) represents PPy-COOH nanocomposites without magnetite and B) represents PPy-COOH nanocomposites with magnetite. The morphology of both the magnetite-free NCs and the MNCs is the same. However, the MNCs show to be bigger in size because of the magnetite that is encapsulated in the PPy shell. The scale bar is at 100 nm for both images.

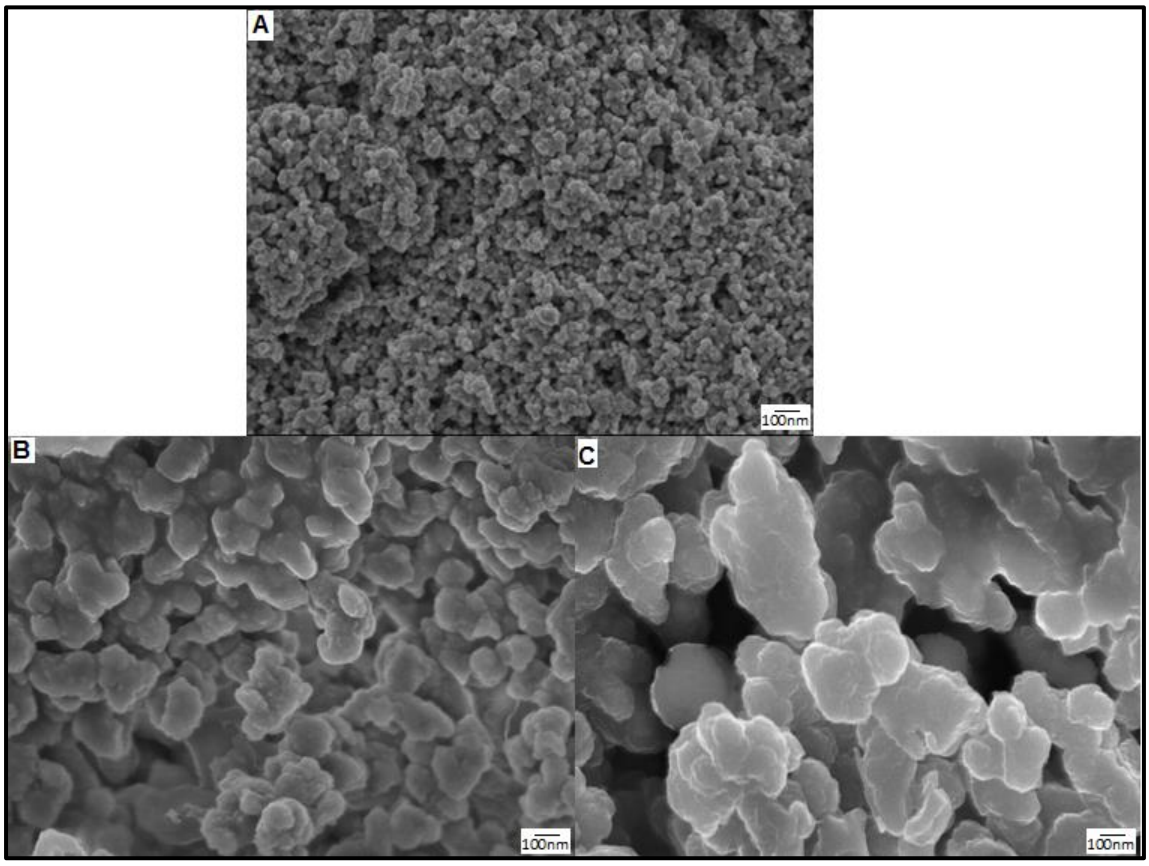


Figure 34: SEM images of A) $Fe_3O_4$ nanoparticles, B) PPy-COOH homopolymer and C) PPy-COOH MNCs with a magnetite core.

### 5.3.2. ATR-FTIR analysis of MNCs

The composition of the carboxyethylpolypryrrole nanocomposites was confirmed with the ATR-FTIR (**Figure 35**).

The presence of carboxyl groups was confirmed when a peak at 1703 $cm^{-1}$ was observed for both the PPy-COOH homopolymer (**Figure 35 b**) and the MNCs (**Figure 35 c**), of which it was not observed in (**Figure 35 a**). The peak

at 1399 $cm^{-1}$ is also an indicative of the carboxylate ion (Maeda *et al*., 1995) however, it is also indicative of the conjugated C-N stretching, which means that the peaks are overlapping. The peak at 1551 $cm^{-1}$ (**Figure 35 a**) shifted to 1590 $cm^{-1}$ (**Figure 35 b & c**), which emphasizes the alteration of the polymer backbone.

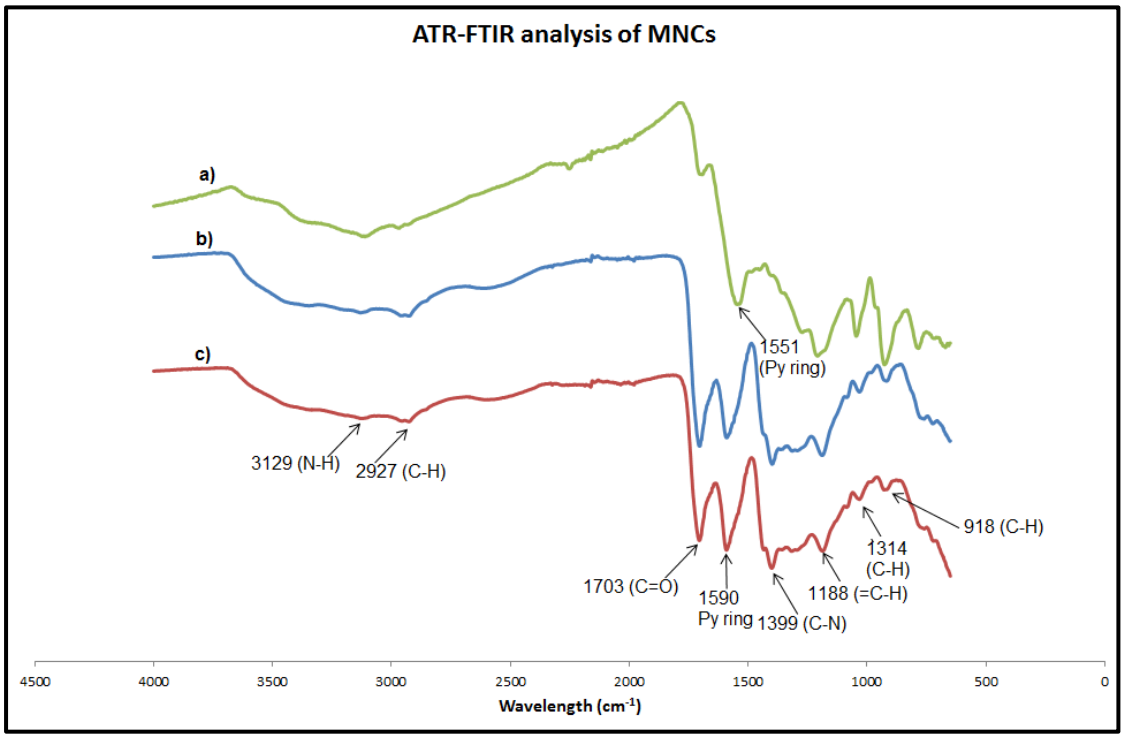


Figure 35: FTIR spectra of a) pyrrolecyanide monomer, b) PPy-COOH homopolymer and c) PPy-COOH/ $Fe_3O_4$

The broad band at 3129 $cm^{-1}$ was due to the N-H stretching vibration. Characteristic bands of doped polypyrrole were observed at 1590 $cm^{-1}$ (asymmetric ring stretch), and 1314 $cm^{-1}$ and 918 $cm^{-1}$ were due to the C-H deformation. The peak at 2927 $cm^{-1}$ was attributed to the C-H stretching vibrations. Peaks at 1188 $cm^{-1}$ and 918 $cm^{-1}$ were indicative of the conductive state of the PPy-COOH (Jiang et al. , 2012; Maeda et al. , 1995; Yu et al. , 2005). The peaks at 928 $cm^{-1}$ and 1317 $cm^{-1}$ in the PPy-COOH spectrum shifted to the right (918 $cm^{-1}$ and 1314 $cm^{-1}$) in the PPy-COOH/$Fe_3O_4$ spectrum. This could mean that the Fe from the magnetite was interacting with the N in the PPy-COOH (Deng *et al*., 2003). There were no major

structural differences, meaning that the functionality of PPy-COOH/$Fe_3O_4$ was not altered.

### 5.3.3. X-ray diffraction (XRD) study

The XRD was used to determine crystalline phases in the MNCs. The amorphous pattern of the homopolymer was observed (**Figure 36 a**). The resultant pattern of $Fe_3O_4$ is shown in **Figure 36 b**. Peaks were observed at $2\theta$= 30.013°, 35.475°, 43.038°, 57.904° and 62.498° were indicative of nanocrystalline structure of $Fe_3O_4$. The same peaks were observed on the MNCs pattern (**Figure 36 c**), which proves the interaction of the homopolymer with $Fe_3O_4$. The peaks are attributable to the cubic structure of the $Fe_3O_4$ (Karaoğlu *et al*., 2011; Bhaumik *et al*., 2011).

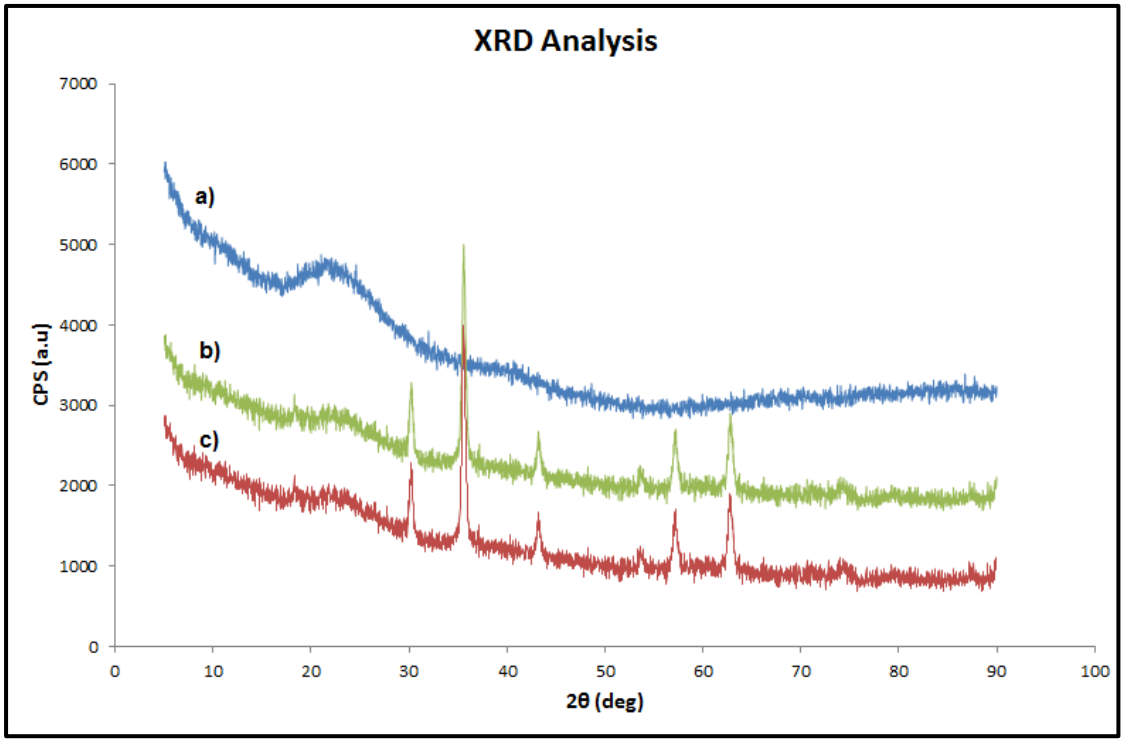


Figure 36: XRD powder pattern of a) PPy-COOH, b) $Fe_3O_4$ and c) MNCs.

The magnetism of the MNCs was tested using a magnetic separator (Dynal® Invitrogen Bead Separator). It was observed that as the MNCs got exposed to a magnetic field, they moved towards the source of the magnetic force

**(Figure 37)**. This indicated that the MNCs had magnetic properties. Following the separation, the solution was clear, which indicated that the $Fe_3O_4$ was not leaching out of the polymer matrix.

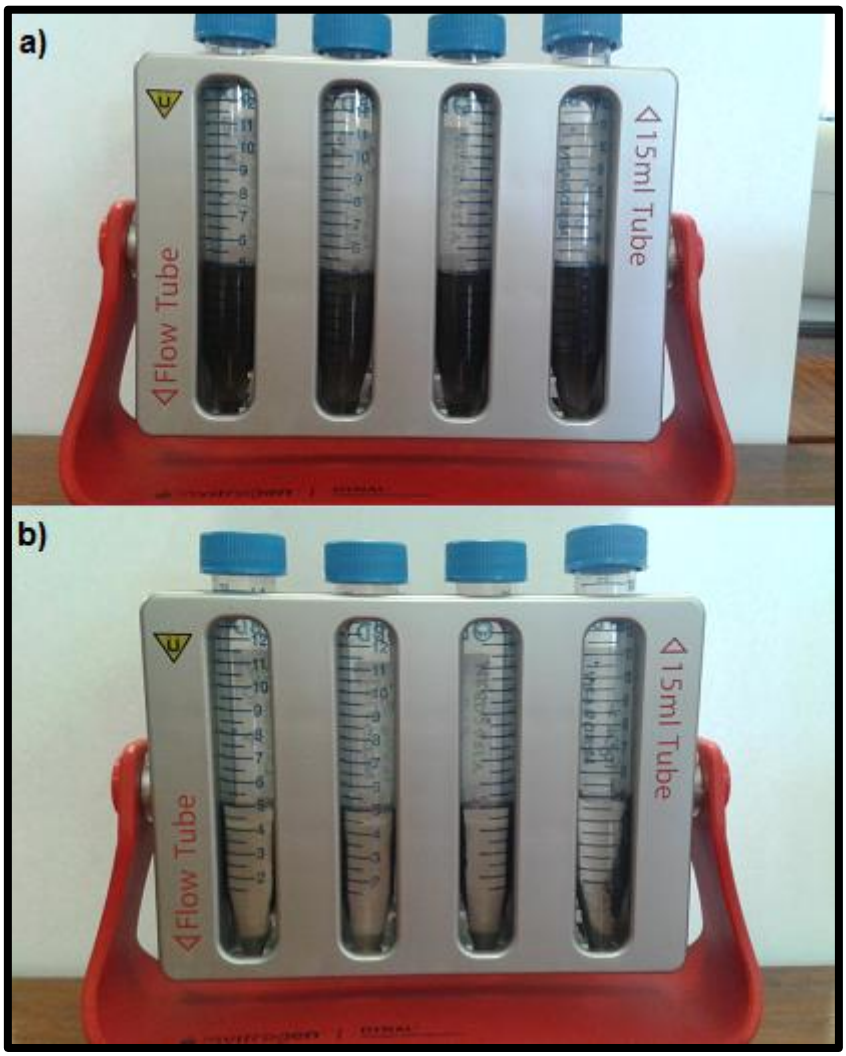


Figure 37: Images of a) MNCs in suspension before magnetic separation and b) MNCs that have been separated by a magnetic force.

### *5.3.4.* Application of MNCs for preconcentration of *E. coli*

TEM was used to confirm the successful binding of MNCs to *E. coli* cells therefore, confirming the successful attachment of antibodies to the MNCs.

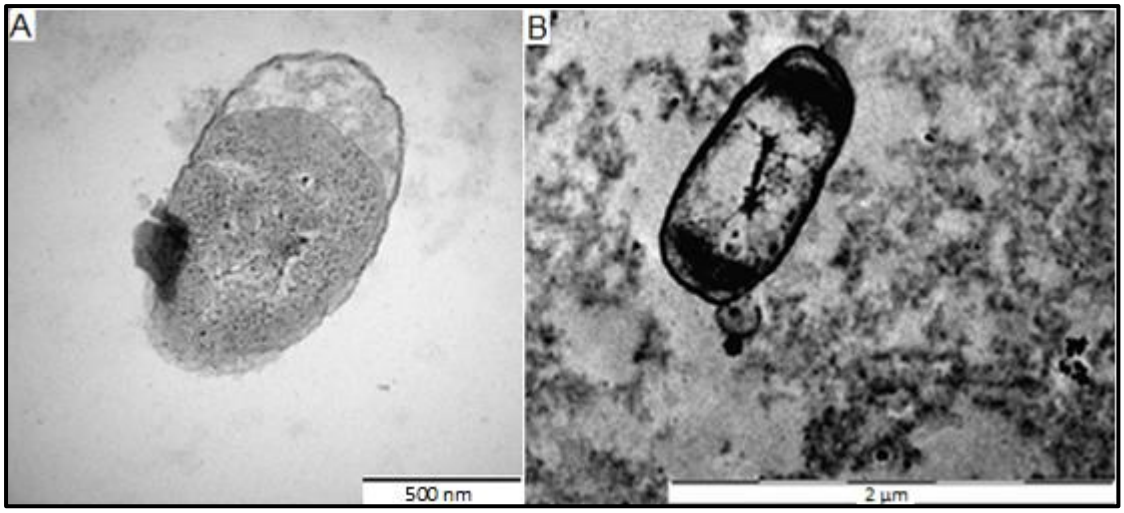


Figure 38: TEM images of A) an *E. coli* cell without MNCs. and B) an *E. coli* cell labelled with MNCs

It was seen that the attachment of MNCs to the *E. coli* surface was successful. There is a notable difference in the cell wall of the E. coli cell in **Figure 38 A**, which is the MNCs-labelled cell, compared to that in **Figure 38 B**, which is the control cell.

Following the confirmed binding of the MNCs to the *E.coli* cells, the MNCs were tested on a larger scale. Synthetic water was prepared in volumes of 10mL and in *E.coli* concentrations of $1x10^9$, $1x10^8$ and $1x10^6$ CFU/mL in autoclaved deionised water. 2, 4, 10, and 15 mg of antibody-labelled MNCs were added to the spiked water and left to contact for an hour, at room temperature. The *E. coli* cells that were captured were separated from the solution with the aid of a magnetic separator. The capture efficiency was determined by plating of the unbound cells in the supernatant onto designated agar plates. The capture efficiency was calculated by dividing the number of the cells in that were bound which is the difference between the total number of the cells and supernatant over the total number of cells. The capture efficiency results are presented in **Table 11**.

Table 11: Capture efficiency of MNCs to *E. coli* cells.

| ***E. coli sample (CFU/mL)*** | ***MNC mass (mg)*** | ***Relative Capture Efficiency (%)*** |
|---|---|---|
| $1x10^6$ | 2 | 70 |
| $1x10^6$ | 4 | 80 |
| $1x10^6$ | 10 | 100 |
| $1x10^6$ | 15 | 100 |
| $1x10^8$ | 2 | 30.4 |
| $1x10^8$ | 4 | 50 |
| $1x10^9$ | 10 | 76 |
| $1x10^9$ | 15 | 89.9 |

It was decided that 2 and 4 mg would not be sufficient for $1x10^9$ CFU/mL. Hence the staring mass was 10 mg. The results in **Table 11** show a general trend that as the MNCs mass increased, so did the capture efficiency. It was also seen that the capture efficiency increased with the decrease in *E. coli* concentrations whilst the mass of the MNCs was kept constant. This was attributed to the increased availability of the MNCs active sites/surface area. It was seen that it was possible to capture ~100% *E. coli* cells with a MNCs concentration of 1 mg/mL and above for E. coli concentrations of $1x10^6$ CFU/mL. Due to financial contraints and the high cost of the material, the study was ended at the concentration of $1X10^6$ CFU/mL. These results form a good basis for up scaling the process to preconcentrating 100 mL of water samples, as required by the SANS 241 standards.

## 5.4. Conclusions

The MNCs were successfully synthesized using the *in situ* polymerization technique. The presence of carboxyl groups was seen on the FTIR spectrum. There were no significant differences in the structure of the PPy-COOH and PPy-COOH/$Fe_3O_4$. The FTIR and XRD results showed that there was, however, an interaction between the $Fe_3O_4$ and the polymer matrix.

The SEM results showed that the $Fe_3O_4$ was encapsulated in the polymer shell. These results were also confirmed by XRD. It was also seen that the carboxyethyl pyrrole homopolymer is amorphous and the addition of $Fe_3O_4$ introduces crystallinity. It was proven that the MNCs had magnetic behavior with the aid of the magnetic separator.

It was seen through TEM that the antibody-labelled MNCs were successfully binding to the *E. coli* cells, meaning that the antibodies were also successfully attached on the MNCs. It was found that the capture efficiency increased with the decrease in *E. coli* concentration while keeping the MNCs concentration constant. It could be said that the MNCs were suitable to use as immunomagnetic separators. However, further studies should be conducted in order to preconcentrate the *E. coli* at 100 mL volumes, as per the requirements of SANS 241 standards.

# Chapter 6: Conclusions and Recommendations

Literature suggested that there is a need for a point of use device for the detection of pathogens in the water and food industries. It was found that among various possible solutions, the use of nanomaterials was better suited to deliver on the development of a point-of-use device. Literature is also in agreement that signal intensities of dye molecules are increased through encapsulation, as they are protected from external environments. Literature suggested that use of fluorescent lables/nanoparticles is becoming prominent in most tests such as lateral flow tests. Thus synthesis of SiNPs and MNCs would be complimentary in a point-of-use device.

The aims of this study, to synthesize dye-doped and surface functionalized SiNPs as well as carboxyethlypyrrole MNCs, for signal amplification and preconcentration of *E. coli* cells in water, were achieved.

## 6.1. Conclusions

### 6.1.1. SiNPs

Uniformly-sized dye-doped and surface functionalized SiNPs were successfully synthesized using the microemulsion method. SiNPs were successfully functionalized with amine and carboxyl groups as well as avidin as determined by HR-TEM, FE-SEM, ATR-FTIR, Zeta Sizer and UV and fluorescence spectroscopy. However, it was found that the direct attachment of carboxyl groups onto the Si surface yielded better attachment of carboxyl groups thus resulting in higher particle suspension stability.

The centrifugal method of detection is not suitable for the detection of *E. coli* using SiNPs due to the dense nature of the nanoparticles. This led to specificity tests not being done because the SiNPs will be retained regardless, meaning that there will be false positives for other strains of bacteria.

SiNPs have, however, proved to amplify the signal of captured *E. coli* cells through fluorescence imaging. It was also shown that the particles bind to the *E. coli* cells using HR-TEM. Thus, there is potential that these nanoparticles can be incorporated in a point of use device.

### 6.1.2. MNCs

MNCs were synthesized and successfully functionalized with carboxyl groups as determined by FE-SEM, XRD and FTIR.

MNCs were found to be functional as they captured the *E. coli* cells; therefore proof of concept was shown that the MNCs could preconcentrate *E. coli*.

The MNCs were synthesized and characterized with the TEM and FTIR. There was a successful conversion of the cyanide group to the carboxyl group through oxidative hydrolysis. The structure of the MNCs was confirmed using SEM. There were no significant differences in the structure of the PPy-COOH and PPy-COOH/$Fe_3O_4$.

The SEM results indicated that the size of the MNCs was larger than that of the homopolymer. Thus, $Fe_3O_4$ was successfully encapsulated in the polymer matrix. . It was proven that the MNCs had magnetic behavior with the aid of the magnetic separator. The $Fe_3O_4$ pattern was observed in the MNCs, further indicating the successful encapsulation of $Fe_3O_4$ in the polymer matrix.

It was seen through TEM that the antibody-labelled MNCs were successfully binding to the *E. coli* cells, meaning that the antibodies were also successfully attached on the MNCs. It was found that the capture efficiency increased with the decrease in *E. coli* concentration while keeping the MNCs concentration constant. It could be said that the MNCs were suitable to use as immunomagnetic separators. However, further studies should be conducted in order to preconcentrate the *E. coli* at 100 mL volumes, as per the requirements of SANS 241 standards.

## 6.2. Recommendations

Positively charged dyes should be investigated.

Detection limits have not yet been determined; therefore studies concerning that should be undertaken.

Release studies should be conducted in order to determine the degree of reusability of the MNCs.

The preconcentration process should be scaled up to the desired volume of 100 mL, as depicted in the SANS 241 standards.

Specificity studies should be conducted in order to see if the nanoparticles/antibodies are cross-reacting with other bacteria strains.

## References


AGILENT TECHNOLOGIES, 2013-last update, *E. coli* cell culture concentration from $OD_{600}$ calculator. Available: http://www.genomics.agilent.com/bioCalcs.jsp# [2014].

AIRENNE, K.J., MARJOMÄKI, V.S. and KULOMAA, M.S., 1999. Recombinant avidin and avidin–fusion proteins. *Biomolecular engineering,* **16**(1–4), pp. 87-92.

AUGER, A., SAMUEL, J., PONCELET, O. and RACCURT, O., 2011. A comparative study of non-covalent encapsulation methods for organic dyes into silica nanoparticles. *Nanoscale research letters,* **6**(1), pp. 1-12.

AZIOUNE, A., SLIMANE, A., B., HAMOU, L., A., PLEUVY, A., CHEHIMI, M., M., PERRUCHOT, C. and ARMES, S., P., 2004. Synthesis and characterization of active ester-functionalized polypyrrole-silica nanoparticles: application to the covalent attachment of proteins. *Langmuir : the ACS journal of surfaces and colloids,* **20**(8), pp. 3350-3356.

AZO Network, 1 January 2015, 2015-last update, attenuated total reflection (ATR) mode – advantages for FT-IR spectroscopy [Homepage of AZO Network], [Online]. Available: http://www.azom.com/article.aspx?ArticleID=5958 [March, 2015].

BAGWE, R.P., HILLIARD, L.R. and TAN, W., 2006. Surface Modification of Silica Nanoparticles to Reduce Aggregation and Nonspecific Binding. *Langmuir,* **22**, pp. 4357-4362.

BAGWE, R.P., YANG, C., HILLIARD, L.R. and TAN, W., 2004. Optimization of Dye-Doped Silica Nanoparticles Prepared Using a Reverse Microemulsion Method. *Langmuir,* **20**, pp. 8336-8342.

BAI, Y., SONG, M., CUI, Y., SHI, C., WANG, D., PAOLI, G.C. and SHI, X., 2013. A rapid method for the detection of foodborne pathogens by extraction of a trace amount of DNA from raw milk based on amino-modified silica-coated magnetic nanoparticles and polymerase chain reaction. *Analytica Chimica Acta*, **787**, pp. 93-101.

BALASUBRAMANIAN, A.K., SONI, K.A., BESKOK, A. and PILLAI, S.D., 2007. A microfluidic device for continuous capture and concentration of microorganisms from potable water. *Lab on a Chip,* **7**(10), pp. 1315-1321.

BAMRUNGSAP, S., APIWAT, C., CHANTIMA, W., DHARAKUL, T. and WIRIYACHAIPORN, N., 2014. Rapid and sensitive lateral flow immunoassay for influenza antigen using fluorescently-doped silica nanoparticles. *Microchimica Acta,* **181**(1-2), pp. 223-230.

BASHIR, R., GOMEZ, R., SARIKAYA, A., LADISCH, M.R., STURGIS, J. and ROBINSON, J.P., 2001. Adsorption of avidin on microfabricated surfaces for protein biochip applications. *Biotechnology and bioengineering,* **73**(4), pp. 324-328.

BEGANSKIENE, A., SIRUTKAITIS, V., KURTINAITIENE, M., JUSKENAS, R. and KAREIVA, A., 2004. FTIR, TEM and NMR Investigations of Stober Silica Nanoparticles. *material science,* **10**, pp. 287-290.

BHAUMIK, M., LESWIFI, T.Y., MAITY, A., SRINIVASU, V.V. and ONYANGO, M.S., 2011. Removal of fluoride from aqueous solution by polypyrrole/Fe3O4 magnetic nanocomposite. *Journal of hazardous materials,* **186**(1), pp. 150-159.

BROOKS, B.W., DEVENISH, J., LUTZE-WALLACE, C.L., MILNES, D., ROBERTSON, R.H. and BERLIE-SURUJBALLI, G., 2004. Evaluation of a monoclonal antibody-based enzyme-linked immunosorbent assay for detection of *Campylobacter fetus* in bovine preputial washing and vaginal mucus samples. *Vet. Microbiol.,* **103**, pp. 77-84.

CAI, J., YAO, C., XIA, J., WANG, J., CHEN, M., HUANG, J., CHANG, K., LIU, C., PAN, H. and FU, W., 2011. Rapid parallelized and quantitative analysis of five pathogenic bacteria by ITS hybridization using QCM biosensor. *Sensors and Actuators B: Chemical,* **155**(2), pp. 500-504.

CAI, L., CHEN, Z., CHEN, M., TANG, H. and PANG, D., 2013. MUC-1 aptamer-conjugated dye-doped silica nanoparticles for MCF-7 cells detection. *Biomaterials,* **34**(2), pp. 371-381.

CAKMAK, G., KÜÇÜKYAVUZ, Z., AND KÜÇÜKYAVUZ, S, 2005. Conductive copolymers of polyaniline, polypyrrole and poly (dimethylsiloxane). *Synthetic metals*, **151**(1), pp. 10-18.

Chemical Engineering Methods and Technology: Fourier Transform Infrared Spectroscopy: Developments, Techniques and Applications. 2010. New York, NY, USA: Nova Science Publishers, Inc.

CHEN, X. and TONG, A., 2012. Modification of silica nanoparticles with fluorescein hydrozide for Cu(II) sensing. *Dyes and Pigments,* **1**, pp. 1-8.

CHEN, Z., CAI, L., DONG, X., TANG, H. and PANG, D., 2012a. Covalent conjugation of avidin with dye-doped silica nanopaticles and preparation of high density avidin nanoparticles as photostable bioprobes. *Biosensors and Bioelectronics,* **37**(1), pp. 75-81.

CHENG, Y., LIU, Y., HUANG, J., LI, K., ZHANG, W., XIAN, Y. and JIN, L., 2009. Combining biofunctional magnetic nanoparticles and ATP bioluminescence for rapid detection of Escherichia coli. *Talanta,* **77**(4), pp. 1332-1336.

CHENG-YAN, L., CHENG-JU, Y., YEN-HSIU, L. and AND WEI-LUNG, T., 2010. Colorimetric Sensing of Silver(I) and Mercury(II) Ions Based on an Assembly of Tween 20-Stabilized Gold Nanoparticles. *Anal. Chem.,* **82**, pp. 6830-6837.

CHIH-HUNG WANG, CHIA-JUNG CHANG, JIUNN-JONG WU and GWO-BIN LEE, 2013a. A new pathogen detection system by utilizing nanogold modified specific probe and vancomycin coated magnetic beads on an integrated microfluidic device, *Micro Electro Mechanical Systems (MEMS), 2013 IEEE 26th International Conference on,* 2013a, pp. 94-97.

CHOU, D.K., KRISHNAMURTHY, R., RANDOLPH, T.W., CARPENTER, J.F. and MANNING, M.C., 2005. Effects of Tween 20® and Tween 80® on the stability of Albutropin during agitation. *Journal of pharmaceutical sciences,* **94**(6), pp. 1368-1381.

CONNELLY, J.T. and BAEUMNER, A.J., 2012. Biosensors for the detection of waterborne pathogens. *Analytical and bioanalytical chemistry,* **402**(1), pp. 117-127.

DE DIOS, A.S. and DÍAZ-GARCÍA, M.E., 2010. Multifunctional nanoparticles: Analytical prospects. *Analytica Chimica Acta,* **666**(1–2), pp. 1-22.

DENG, J., PENG, Y., HE, C., LONG, X., LI, P. and CHAN, A.S., 2003. Magnetic and conducting Fe3O4–polypyrrole nanoparticles with core-shell structure. *Polymer International,* **52**(7), pp. 1182-1187.

DIAMANDIS, E.P. and CHRISTOPOULOS, T.K., 1991. The Biotin-(Strept) Avidin System: Principles and Applications in Biotechnology. *Clin. Chem.,* **37**, pp. 625-636.

DUDAK, F.C., BOYACI, İ.H., JURKEVICA, A., HOSSAIN, M., AQUILAR, Z., HALSALL, B.H. and SELISKAR, J.C., 2009. Determination of viable Escherichia coli using antibody-coated paramagnetic beads with fluorescence detection. *Anal Bioanal Chem,* **393**, pp. 949-956.

DUTROW, B., L. and CLARK, C., M., 14 December 2013, 2013-last update, X-ray powder diffraction (XRD) [Homepage of Carleton College], [Online]. Available: http://serc.carleton.edu/research_education/geochemsheets/techniques/XRD.html [April, 2015].

FRATAMICO, P.M., 2003. Comparison of culture, polymerase chain reaction (PCR), TaqMan *Salmonella*, and Transia Card *Salmonella* assays for detection of *Salmonella* spp. in naturally-contaminated ground chicken, ground turkey, and ground beef. *Molecular and cellular probes,* **17**(5), pp. 215-221.

FREDJ, H.B., HELALI, S., ESSEGHAIER, C., VONNA, L., VIDAL, L. and ABDELGHANI, A., 2008. Labeled magnetic nanoparticles assembly on polypyrrole film for biosensor applications. *Talanta,* **75**(3), pp. 740-747.

FRISKEN, B.J., 2001. Revisiting the method of cumulants for the analysis of dynamic light-scattering data. *Applied Optics,* **40**(24), pp. 4087-4091.

FU, X., HUANG, K. and LIU, S., 2010. A rapid and universal bacteria-counting approach using CdSe/ZnS/SiO2 composite nanoparticles as fluorescence probe. *Analytical and Bioanalytical chemistry,* **396**(4), pp. 1397-1404.

FU, Z., ROGELJ, S. and KIEFT, T.L., 2005. Rapid detection of Escherichia coli O157:H7 by immunomagnetic separation and real-time PCR. *International journal of food microbiology,* **99**(1), pp. 47-57.

GUNASEKERA, T.S., ATTFIELD, P.V. and VEAL, D.A., 2000a. A flow cytometry method for rapid detection and enumeration of total bacteria in milk. *Applied and Environmental Microbiology,* **66**(3), pp. 1228-1232.

GUVEN, B., BASARAN-AKGUL, N., TEMUR, E., TAMER, U. and BOYAC, I.H., 2011. SERS-based sandwich immunoassay using antibody coated magnetic nanoparticles for Escherichia coli enumeration. *The Royal Society of Chemistry,* **136**, pp. 740-748.

HAHN, M.A., TABB, J.S. and KRAUSS, T.D., 2005. Detection of single bacterial pathogens with semiconductor quantum dots. *Analytical Chemistry,* **77**(15), pp. 4861-4869.

HE, X., WANG, K., TAN, W., XIAO, D., LI, J. and YANG, X., 2001. A novel fluorescent label based on biological fluorescent nanoparticles and its application in cell recognition. *Chin.Sci.Bull,* **46**, pp. 1962-1965.

HEREDIA, K.L. and MAYNARD, H.D., 2006. Synthesis of protein–polymer conjugates. *Org.Biomol.Chem.,* **5**(1), pp. 45-53.

HERMANSON, G.T., 2013. Bioconjugate techniques. Academic press.

HERR, J.K., SMITH, J.E., MEDLEY, C.D., SHANGGUAN, D. and TAN, W., 2006. Aptamer-conjugated nanoparticles for selective collection and detection of cancer cells. *Analytical Chemistry,* **78**(9), pp. 2918-2924.

HEURTAULT, B., SAULNIER, P., PECH, B., PROUST, J. and BENOIT, J., 2003. Physico-chemical stability of colloidal lipid particles. *Biomaterials,* **24**(23), pp. 4283-4300.

HOLMLIN, R.E., SCHIAVONI, M., CHEN, C.Y., SMITH, S.P., PRENTISS, M.G. and WHITESIDES, G.M., 2000. Light-driven microfabrication: Assembly of multicomponent, three-dimensional structures by using optical tweezers. *Angewandte Chemie,* **39**(19), pp. 3503-3506.

HUANG, X., AGUILAR, Z.P., LI, H., LAI, W., WEI, H., XU, H. and XIONG, Y., 2013. Fluorescent Ru (phen) 32 -Doped Silica Nanoparticles-Based ICTS Sensor for Quantitative Detection of Enrofloxacin Residues in Chicken Meat. *Analytical Chemistry,* **85**(10), pp. 5120-5128.

HUANG, Y., WANG, Y. and YAN, X., 2010. Amine-Functionalized Magnetic Nanoparticles for Rapid Capture and Removal of Bacterial Pathogens. *Environ. Sci. Technol.,* **44**, pp. 7908-7913.

IDEEX and LABORATORIES, January, 2013-last update, colilert [Homepage of IDEEX Laboratories], [Online]. Available: http://www.idexx.com/view/xhtml/en_us/water/products/colilert.jsf [June, 2013].

IQBAL, Z., LAI, E., P.C. and AVIS, T., J., 2012. Development of polymer-modified magnetic nanoparticles and quantum dots for *Escherichia coli* binding test. *Microchim Acta,* **176**, pp. 193-200.

JANEWAY, C.A., TRAVERS, P., and WALPORT, M., eds, 2001. *Immunobiology: The Immune System in Health and Disease. 5th edition.*

JIANG, H., ZHANG, A., SUN, Y., RU, X., GE, D. and SHI, W., 2012. Poly(1-(2-carboxyethyl)pyrrole)/polypyrrole composite nanowires for glucose biosensor. *Electrochimica Acta,* **70**(0), pp. 278-285.

KARAOĞLU, E., BAYKAL, A., DELIGÖZ, H., ŞENEL, M., SÖZERI, H. and TOPRAK, M.S., 2011. Synthesis and characteristics of poly(3-pyrrol-1-ylpropanoic acid) (PPyAA)–Fe3O4 nanocomposite. *Journal of Alloys and Compounds,* **509**(33), pp. 8460-8468.

KATAYAMA, H., SHIMASAKI, A. and OHGAKI, S., 2002. Development of a virus concentration method and its application to detection of enterovirus and Norwalk virus from coastal seawater. *Applied and Environmental Microbiology,* **68**(3), pp. 1033-1039.

KELL, A.J., STEWART, G., RYAN, S., PEYTAVI, R., BOISSINOT, M., HULETSKY, A., BERGERON, M.G. and SIMARD, B., 2008a. Vancomycin-Modified Nanoparticles for Efficient Targeting and Preconcentration of Gram-Positive and Gram-Negative Bacteria. *American Chemical Society,* **2**, pp. 1777-1788.

KITTIGUL, L., EKCHALOEMKIET, S., UTRARACHKIJ, F., SIRIPANICHGON, K., SUJIRARAT, D., PUNGCHITTON, S. and BOONTHUM, A., 2005. An efficient virus concentration method and RT-nested PCR for detection of rotaviruses in environmental water samples. *Journal of virological methods,* **124**(1), pp. 117-122.

KITTIGUL, L., KHAMOUN, P., SUJIRARAT, D., UTRARACHKIJ, F., CHITPIROM, K., CHAICHANTANAKIT, N. and VATHANOPHAS, K., 2001. An

improved method for concentrating rotavirus from water samples. *Memorias do Instituto Oswaldo Cruz,* **96**(6), pp. 815-821.

KNIPPING, J., WIGGERS, H., RELLINGHAUS, B., ROTH, P., KONJHODZIC, D. and MEIER, C., 2004. Synthesis of High Purity Silicon Nanoparticles in a Low Pressure Microwave Reactor. *J. Nanosci. Nanotech,* **4**, pp. 1039-1044.

KNOPP, D., TANG, D. and NIESSNER, R., 2009. Review: Bioanalytical applications of biomolecule-functionalized nanometer-sized doped silica particles. *Analytica Chimica Acta,* **647**(1), pp. 14-30.

LAFFEY, B., D. 1995. *Monoclonal Antibodies to Bovine Serum Albumin: Affinity Purification and Physicochemical Characterization.*

LAKOWICZ, J.R., 2007. Principles of fluorescence spectroscopy. Springer Science & Business Media.

LAZCKA, O., CAMPO, F.J.D. and MUÑOZ, F.X., 2007. Pathogen detection: A perspective of traditional methods and biosensors. *Biosensors and Bioelectronics,* **22**(7), pp. 1205-1217.

LEE, J., SERNA, F., NICKELS, J. and SCHMIDT, C.E., 2006. Carboxylic acid-functionalized conductive polypyrrole as a bioactive platform for cell adhesion. *Biomacromolecules,* **7**(6), pp. 1692-1695.

LEE, J. and DEININGER, R.A., 2004. Detection of E. coli in beach water within 1 hour using immunomagnetic separation and ATP bioluminescence. *Luminescence,* **19**(1), pp. 31-36.

LIFE TECHNOLOGIES, 2014-last update, the molecular probes (R) handbook. Available: http://www.lifetechnologies.com/za/en/home/references/molecular-probes-the-handbook/introduction-to-fluorescence-techniques.html [Septmeber, 2014].

LIU, H., WANG, Y., LI, H., WANG, Z. and XU, D., 2013. Luminescent Rhodamine B doped core–shell silica nanoparticle labels for protein microarray detection. *Dyes and Pigments,* **98**(1), pp. 119-124.

MA, D., LI, M., PATIL, A. and MANN, S., 2004. Fabrication of Protein/Silica Core-Shell Nanoparticles by Microemulsion-Based Molecular Wrapping. *Adv Mater,* **16**, pp. 1838-1841.

MADONNA, A.J., BASILE, F., FURLONG, E. and VOORHEES, K.J., 2001. Detection of bacteria from biological mixtures using immunomagnetic separation combined with matrix-assisted laser desorption/ionization time-of-flight mass spectrometry. *Rapid Communications in Mass Spectrometry,* **15**(13), pp. 1068-1074.

MAEDA, S., CORRADI, R. and ARMES, S., P., 1995. Synthesis and Characterization of Carboxylic Acid-Functionalized Polypryrrole-Silica Microparticles. *Macromolecules,* **28**, pp. 2905-2911.

MECHERY, S.J., ZHAO, X.J., WANG, L., HILLIARD, L.R., MUNTEANU, A. and TAN, W., 2006. Using bioconjugated nanoparticles to monitor E. coli in a flow channel. *Chem Asian J.,* **1**, pp. 384-390.

MOUFFOUK, F., ROSA DA COSTA, ANA M, MARTINS, J., ZOUROB, M., ABU-SALAH, K.M. and ALROKAYAN, S.A., 2011. Development of a highly sensitive bacteria detection assay using fluorescent pH-responsive polymeric micelles. *Biosensors and Bioelectronics,* **26**(8), pp. 3517-3523.

MUKHOPADHYAY, B., MARTINS, M.B., KARAMANSKA, R., RUSSELL, D.A. and FIELD, R.A., 2009. Bacterial detection using carbohydrate-functionalised CdS quantum dots: a model study exploiting *E. coli* recognition of mannosides. *Tetrahedron letters,* **50**(8), pp. 886-889.

MÜLLER, R. and JACOBS, C., 2002. Buparvaquone mucoadhesive nanosuspension: preparation, optimisation and long-term stability. *International journal of pharmaceutics,* **237**(1), pp. 151-161.

MÜLLER, R., JACOBS, C. and KAYSER, O., 2001. Nanosuspensions as particulate drug formulations in therapy: rationale for development and what we can expect for the future. *Advanced Drug Delivery Reviews,* **47**(1), pp. 3-19.

MURCIA, M.J. and NAUMANN, C.A., 2005. Biofunctionalization of fluorescent nanoparticles. *Nanotechnologies for the life sciences,* .

MY Scope, Electron-matter interactions. Available: http://www.ammrf.org.au/myscope/sem/background/concepts/interactions.php .[April, 2015]

OW, H., LARSON, D.R., SRIVASTAVA, M., BAIRD, B.A., WEBB, W.W. and WIESNER, U., 2005. Bright and stable core-shell fluorescent silica nanoparticles. *Nano letters,* **5**(1), pp. 113-117.

OZALP, V.C., BAYRAMOGLU, G., KAVRUK, M., KESKIN, B.B., OKTEM, H.A. and ARICA, M.Y., 2014. Pathogen detection by core–shell type aptamer-magnetic preconcentration coupled to real-time PCR. *Analytical Biochemistry,* **447**(0), pp. 119-125.

PAUL, B.K. and MOULIK, S.P., 2001. Uses and applications of microemulsions. *CURRENT SCIENCE-BANGALORE-,* **80**(8), pp. 990-1001.

PEREZ LEON, C., KADOR, L., PENG, B. and THELAKKAT, M., 2006. Characterization of the Adsorption of Ru-bpy Dyes on Mesoporous $TiO_2$ Films with UV-Vis, Raman and FTIR Spectroscopies. *J. Phys. Chem,* **110**, pp. 8723-8730.

PILEMAND, C., 2002. *Surfactants: Their abilities and important physico-chemical properties.* 87-7904-108-6.

QI, C., FENG, J., WANG, Z., MENG, Y., YAN, X. and JIN, G., 2006. Application of Optical Protein-chip in Detecting Phage M13KO7. *Chinese journal of biotechnology,* **22**(5), pp. 856-860.

RAHMAN, M. A., KUMAR, P., PARK, D. S., and SHIM, Y. B. 2008. Electrochemical sensors based on organic conjugated polymers. *Sensors*, ***8***(1), pp. 118-141.

ROMPRE, A., SERVAIS, P., BAUDART, J., DE-ROUBIN, M. and LAUREN, P., 2002. Detection and enumeration of coliforms in drinking water: current methods and emerging approaches. *J Microbial Methods,* **49**, pp. 31-54.

ROUX, S., TILLEMENT, O., BILLOTEY, C., COLL, J., DUC, G., MARQUETTE, C. and PERRIAT, P., 2010. Multifunctional nanoparticles: from the detection of biomolecules to the therapy. *International Journal of Nanotechnology,* **7**(4), pp. 781-801.

*SANS 241-1:2011 Drinking Water Part 1: Microbiological, physical, aesthetic and chemical determinants.* . 2011

SANTRA, S., TAPEC, R., THEODOROPOULOU, N., DOBSON, J., HEBARD, A. and TAN, W., 2001a. Synthesis and Characterization of Silica-Coated Iron Oxide Nanoparticles in Microemulsion: The Effect of Nonionic Surfactants. *Langmuir,* **17**, pp. 2900-2960.

SANTRA, S., WANG, K., TAPEC, R. and TAN, W., 2001b. Development of novel dye-doped silica nanoparticles for biomarker application. *Journal of Biomedical Optics,* **6**, pp. 160-166.

SETTERINGTON, E.B. and ALOCILJA, E.C., 2011. Rapid electrochemical detection of polyaniline-labeled Escherichia coli O157:H7. *Biosensors and Bioelectronics,* **26**(5), pp. 2208-2214.

SKOOG, D., HOLLER, F.J. and NIEMAN, T., 1998. An introduction to infrared spectrometry. *Principles of Instrumental Analysis, 5th ed.Harcourt Brace and Company, Philadelphia, USA,* , pp. 380-428.

SKOTTRUP, P.D., NICOLAISEN, M. and JUSTESEN, A.F., 2008. Towards on-site pathogen detection using antibody-based sensors. *Biosensors and Bioelectronics,* **24**(3), pp. 339-348.

SMITH, J.E., WANG, L. and TAN, W., 2006. Bioconjugated silica-coated nanoparticles for bioseparation and bioanalysis. *TrAC Trends in Analytical Chemistry,* **25**(9), pp. 848-855.

TAGUCHI, T., ARAKAKI, A., TAKEYAMA, H., HARAGUCHI, S., YOSHINO, M., KANEKO, M., ISHIMORI, Y. and MATSUNAGA, T., 2007. Detection of

Cryptosporidium parvum oocysts using a microfluidic device equipped with the SUS micromesh and FITC-labeled antibody. *Biotechnology and bioengineering,* **96**(2), pp. 272-280.

TAN, W., WANG, K., HE, X., ZHAO, X.J., DRAKE, T., WANG, L. and BAGWE, R.P., 2004. Bionanotechnology based on silica nanoparticles. *Medicinal research reviews,* **24**(5), pp. 621-638.

TANSUB, W., TUITEMWONG, K., LIMSUWAN, P., THEPAROONRAT, S. and TUITEMWONG, P., 2012. Synthesis of Antibodies-Conjugated Fluorescent Dye-Doped Silica Nanoparticles for a Rapid Single Step Detection of *Campylobacter jejuni* in Live Poultry. *Journal of nanomaterials,* **1**, pp. 1-7.

TAYLOR, J.R., FANG, M.M. and NIE, S., 2000. Probing specific sequences on single DNA molecules with bioconjugated fluorescent nanoparticles. *Analytical Chemistry,* **72**(9), pp. 1979-1986.

THEPWIWATJIT, N., THATTIYAPHONG, A., LIMSUWAN, P., TUITEMWONG, K. and TUITEMWONG, P., 2013. Antibody-conjugated rubpy dye-doped silica nanoparticles as signal amplification for microscopic detection of vibrio cholerae O1. *Journal of Nanomaterials,* **2013**, pp. 92.

THOREK, D.L., ELIAS, D.R. and TSOURKAS, A., 2009. Comparative analysis of nanoparticle-antibody conjugations: carbodiimide versus click chemistry. *Molecular imaging,* **8**(4), pp. 221.

TISSUE, B., M., 9 December 2012, 1996-last update, ultraviolet and visible absorption spectroscopy (uv-vis) [Homepage of Science Hypermedia], [Online]. Available: https://www.uam.es/docencia/quimcursos/Scimedia/chem-ed/spec/uv-vis/uv-vis.htm [March, 2015].

TORUN, Ö., HAKKI BOYACI, İ., TEMÜR, E. and TAMER, U., 2012. Comparison of sensing strategies in SPR biosensor for rapid and sensitive enumeration of bacteria. *Biosensors and Bioelectronics,* **37**(1), pp. 53-60.

TRUDEAU, A., 13 February 2012, 2012-last update, using toads to understand animal behavior [Homepage of HHMI], [Online]. Available: http://www.unc.edu/depts/our/hhmi/hhmi-ft_learning_modules/animalbehaviormodule/analyze.html [December 6, 2013].

TURNEY, K., DRAKE, T.J., SMITH, J.E., TAN, W. and HARRISON, W., 2004. Functionalized nanoparticles for liquid atmospheric pressure matrix-assisted laser desorption/ionization peptide analysis. *Rapid communications in mass spectrometry,* **18**(20), pp. 2367-2374.

UDENFRIEND, S., STEIN, S., BOHLEN, P., DAIRMAN, W., LEIMGRUBER, W. and WEIGELE, M., 1972. Fluorescamine: A Reagent for Assay of Amino Acids, Peptides, Proteins, and Primary Amines in the Picomole Range. *American Association for the Advancement of Science,* **178**, pp. 871-872.

VERBARG, J., PLATH, W.D., SHRIVER-LAKE, L.C., HOWELL, P.B., ERICKSON, J.S., GOLDEN, J.P. and LIGLER, F.S., 2013. Catch and Release: Integrated System for Multiplexed Detection of Bacteria. *Anal. Chem.,* **85**, pp. 4944-4950.

VERMETTE, P., GENGENBACH, T., DIVISEKERA, U., KAMBOURIS, P.A., GRIESSER, H.J. and MEAGHER, L., 2003. Immobilization and surface characterization of NeutrAvidin biotin-binding protein on different hydrogel interlayers. *Journal of colloid and interface science,* **259**(1), pp. 13-26.

VOELKER, C., 1 January 2015, 2015-last update, dynamic light scattering,: measuring particle size and distribution [Homepage of Brunner Web], [Online]. Available: http://www.lsinstruments.ch/technology/dynamic_light_scattering_dls/ [March, 2015].

WANG, L., ESTEVEZ, M.-., O'DONOGHU, M. and TAN, W., 2008a. Fluorophore-Free Luminescent Organosilica Nanoparticles. *Langmuir,* **24**, pp. 1635-1639.

WANG, L., ZHAO, W. and TAN, W., 2008b. Bioconjugated silica nanoparticles: Development and applications. *Chemistry and Materials Science,* **1**, pp. 99-115.

WEI, H., CHENG, S., ZHANG, X. and ZHUO, R., 2009. Thermo-sensitive polymeric micelles based on poly(N-isopropylacrylamide) as drug carriers. *Progress in Polymer Science,* **34**(9), pp. 893-910.

WITTENBERG, N.J. and HAYNES, C.L., 2009. Using nanoparticles to push the limits of detection. *Wiley Interdisciplinary Reviews: Nanomedicine and Nanobiotechnology,* **1**(2), pp. 237-254.

WOLOWACZ, S.E., YON HIN, B. and LOWE, C.R., 1992. Covalent electropolymerization of glucose oxidase in polypyrrole. *Analytical Chemistry,* **64**(14), pp. 1541-1545.

WORLD HEALTH ORGANISATION, April 2013, 2011-last update, water and sanitation [Homepage of World Health Organisation], [Online]. Available: http://www.who.int/gho/mdg/environmental_sustainability/en/index.html [October, 2013].

WRIGHT, D., J., CHAPMAN, P., A. and SIDDONS, C., A., 1994. Immunomagnetic separation as a sensitive method for isolating *Escherichia coli* O157 from food samples. *Epidemiology and Infection,* **113**(1), pp. 31-39.

WU, M., STOCKLEY, P.G. and MARTIN, W.J., 2002. An improved Western blotting technique effectively reduces background. *Electrophoresis,* **23**(15), pp. 2373-2376.

YANG, H., ZHANG, S., CHEN, X., ZHUANG, Z., XU, J. and WANG, X., 2004. Magnetite-Containing Spherical Silica Nanoparticles for Biocatalysis and Bioseparations. *Anal. Chem.,* **76**, pp. 1316-1321.

YANG, H., QU, L., WIMBROW, A.N., JIANG, X. and SUN, Y., 2007. Rapid detection of Listeria monocytogenes by nanoparticle-based immunomagnetic separation and real-time PCR. *International journal of food microbiology,* **118**(2), pp. 132-138.

YANG, L., ZHANG, X., YE, M., JIANG, J., YANG, R., FU, T., CHEN, Y., WANG, K., LIU, C. and TAN, W., 2011. Aptamer-conjugated nanomaterials and their applications. *Advanced Drug Delivery Reviews,* **63**(14–15), pp. 1361-1370.

YOZA, B., ARAKAKI, A., MARUYAMA, K., TAKEYAMA, H. and MATSUNAGA, T., 2003. Fully automated DNA extraction from blood using magnetic particles modified with a hyperbranched polyamidoamine dendrimer. *Bioscience and Bioengineering*, **95**(1), pp. 21-26.

YU, Y., OUYANG, C., GAO, Y., SI, Z., CHEN, W., WANG, Z. and XUE, G., 2005. Synthesis and characterization of carbon nanotube/polypyrrole coreshell nanocomposites via in situ inverse microemulsion. *Journal of Polymer Science Part A: Polymer Chemistry,* **43**(23), pp. 6105-6115.

ZHAO, X., BAGWE, R.P. and TAN, W., 2004a. Development of Organic-Dye-Doped Silica Nanoparticles in a Reverse Microemulsion. *Advanced Materials,* **16**(2), pp. 173-176.

ZHAO, X., HILLIARD, L.R., MECHERY, S.J., WANG, Y., BAGWE, R.P., JIN, S. and TAN, W., 2004b. A rapid bioassay for single bacterial cell quantitation using bioconjugated nanoparticles. *Proceedings of the National Academy of Sciences of the United States of America,* **101**(42), pp. 15027-15032.

ZHOU, J., CHILDS, R.F. and MIKA, A.M., 2005. Pore-filled nanofiltration membranes based on poly(2-acrylamido-2-methylpropanesulfonic acid) gels. *Journal of Membrane Science,* **254**(1-2), pp. 89-99.

ZHU, P., SHELTON, D.R., LI, S., ADAMS, D.L., KARNS, J.S., AMSTUTZ, P. and TANG, C., 2011. Detection of E. coli O157:H7 by immunomagnetic separation coupled with fluorescence immunoassay. *Biosensors and Bioelectronics,* **30**(1), pp. 337-341.